DTIC FILE COPY

(4)

Applied Research Laboratory

AD-A209 410

Technical Report

A RAYTRACING APPROACH TO UNDERWATER REVERBERATION MODELING

by

Anthony C. Arruda III
Michael W. Roeckel
Joseph Wakeley

DTIC
ELECTE
JUN 2 3 1989
S E D

PENNSTATE

This document has been approved for public release and sale; its distribution is unlimited.

Reproduced From
Best Available Copy

The Pennsylvania State University
APPLIED RESEARCH LABORATORY
P. O. Box 30
State College, PA 16804

A RAYTRACING APPROACH TO UNDERWATER REVERBERATION MODELING

by

Anthony C. Arruda III
Michael W. Roeckel
Joseph Wakeley

Technical Report No. TR 89-002
June 1989

DTIC
ELECTE
JUN 23 1989
S D
E S

Supported by:
Naval Sea Systems Command

L. R. Hettche, Director
Applied Research Laboratory

Approved for public release; distribution unlimited

89 6 22 031

UNCLASSIFIED
SECURITY CLASSIFICATION OF THIS PAGE

REPORT DOCUMENTATION PAGE

1a REPORT SECURITY CLASSIFICATION Unclassified	1b. RESTRICTIVE MARKINGS
2a SECURITY CLASSIFICATION AUTHORITY	3. DISTRIBUTION/AVAILABILITY OF REPORT Approved for public release; distribution unlimited.
2b. DECLASSIFICATION/DOWNGRADING SCHEDULE	
4 PERFORMING ORGANIZATION REPORT NUMBER(S) TR-89-002	5. MONITORING ORGANIZATION REPORT NUMBER(S)
6a NAME OF PERFORMING ORGANIZATION Applied Research Laboratory The Pennsylvania State University 6b OFFICE SYMBOL (If applicable) ARL	7a. NAME OF MONITORING ORGANIZATION
6c ADDRESS (City, State, and ZIP Code) P.O. Box 30 State College, PA 16804	7b. ADDRESS (City, State, and ZIP Code)
8a. NAME OF FUNDING/SPONSORING ORGANIZATION Space&Naval Warfare Systems Command SPAWAR 8b. OFFICE SYMBOL (If applicable)	9. PROCUREMENT INSTRUMENT IDENTIFICATION NUMBER
8c ADDRESS (City, State, and ZIP Code) Department of the Navy Washington, DC 20363	10. SOURCE OF FUNDING NUMBERS PROGRAM ELEMENT NO. / PROJECT NO. / TASK NO. / WORK UNIT ACCESSION NO.

11 TITLE (Include Security Classification)
A Raytracing Approach to Underwater Reverberation Modeling

12 PERSONAL AUTHOR(S)
A. C. Arruda III, M.W. Roeckel, J. Wakeley

13a TYPE OF REPORT	13b TIME COVERED	14. DATE OF REPORT (Year, Month, Day)	15. PAGE COUNT
M.S. Thesis	FROM ____ TO ____		177

16 SUPPLEMENTARY NOTATION

17 COSATI CODES		
FIELD	GROUP	SUB-GROUP

18. SUBJECT TERMS (Continue on reverse if necessary and identify by block number)
Multiple boundary returns, non-isovelocity, time-varying, underwater reverberation, frequency spectra, acoustic beam, backscattering, reflection loss, absorption

19 ABSTRACT (Continue on reverse if necessary and identify by block number)

In this study, the effects of multiple boundary returns and non-isovelocity conditions were incorporated into a time-varying representation of underwater reverberation measured at the moving source. ~~Most of~~ the research ~~in this work~~ focused on the development of the time-varying power gain and frequency spectra of scattering functions, which have been shown to characterize the reverberation from an underwater environment. A sound velocity profile, which may consist of up to fifty depth-velocity point pairs, has been introduced. The ocean has been assumed to be horizontally stratified, and each stratification to be represented by a constant velocity gradient. Acoustic beam effects, backscattering coefficients, reflection loss factors, and a varying absorption coefficient have been considered. All reverberant returns have been assumed to arrive at the receiver along the same raypath that was traversed from the source to the backscattering element.

20 DISTRIBUTION/AVAILABILITY OF ABSTRACT ☒ UNCLASSIFIED/UNLIMITED ☐ SAME AS RPT. ☐ DTIC USERS	21. ABSTRACT SECURITY CLASSIFICATION Unclassified
22a NAME OF RESPONSIBLE INDIVIDUAL	22b. TELEPHONE (Include Area Code) (814) 865-6344 22c. OFFICE SYMBOL

DD FORM 1473, 84 MAR 83 APR edition may be used until exhausted. All other editions are obsolete.

SECURITY CLASSIFICATION OF THIS PAGE
UNCLASSIFIED

19 ABSTRACT - Continued

Two examples are presented for comparison of the spectra and total power levels of the modified scattering function with those of the original model. One ~~example~~ focuses on the inclusion of multiple boundary returns only. The total power curve from the revised model was observed to decay more slowly than that of the original model because of the added boundary retruns. The other ~~example~~ emphasizes the propagation effects of a non-isovelocity profile. In this scenario, the emergence of a surface shadow zone was observed, as well as the formation of a caustic near the axis of source motion.

ABSTRACT

In this study, the effects of multiple boundary returns and non-isovelocity conditions were incorporated into a time-varying representation of underwater reverberation measured at the moving source. Most of the research in this work focused on the development of the time-varying power gain and frequency spectra of scattering functions, which have been shown to characterize the reverberation from an underwater environment. A sound velocity profile, which may consist of up to fifty depth-velocity point pairs, has been introduced. The ocean has been assumed to be horizontally stratified, and each stratification to be represented by a constant velocity gradient. Acoustic beam effects, backscattering coefficients, reflection loss factors, and a varying absorption coefficient have been considered. All reverberant returns have been assumed to arrive at the receiver along the same raypath that was traversed from the source to the backscattering element.

Two examples are presented for comparison of the spectra and total power levels of the modified scattering function with those of the original model. One example focuses on the inclusion of multiple boundary returns only. The total power curve from the revised model was observed to decay more slowly than that of the original model because of the added boundary returns. The other example emphasizes the propagation effects of a non-isovelocity profile. In this scenario, the emergence of a surface shadow zone was observed, as well as the formation of a caustic near the axis of source motion.

DTIC
COPY
INSPECTED
6

Accession For
NTIS GRA&I [X]
DTIC TAB [ ]
Unannounced [ ]
Justification
By
Distribution/
Availability Codes
Dist | Avail and/or Special
A-1

TABLE OF CONTENTS

TABLE OF CONTENTS (continued)

TABLE OF CONTENTS (continued)

TABLE OF CONTENTS (continued)

TABLE OF CONTENTS (continued)

LIST OF FIGURES

LIST OF FIGURES (Continued)

LIST OF FIGURES (Continued)

LIST OF FIGURES (Continued)

NOMENCLATURE

A	area
$\hat{A}_{i,j}$	attenuation factor
a	Snell's law constant
AL	absorption loss
b	velocity gradient
$\tilde{b}(\lambda_i)$	complex Gaussian weighting variable
$\tilde{b}_R(\lambda)$	sample function from a zero-mean Gaussian process
$\tilde{b}(t-\frac{\lambda}{2},\ \lambda)$	time-varying impulse response function
BA	beam attenuation
BSL	backscattering level
c, V	speed of sound
c_o	arbitrary reference phase speed
E_t	source energy level
e	exponential
$\vec{e}_{bi}$	unit vector difference of incident and scattered waves
f	frequency
f_D	Doppler-shifted frequency
f_T	transmitted frequency
$\tilde{f}(t)$	transmitted waveform
h	height
I	acoustic intensity

I_o	reference acoustic intensity, 1 W/m^2
i	grid row summation index
j	grid column summation index
K	state number index
KA	number of times a ray passes above the source
KB, KL	number of times a ray passes below the source
KD	number of times a ray passes between the source and receiver
$\tilde{K}_{\tilde{b}}(t-u,\ \lambda)$	covariance function
L	length; also, ray separation
$n(x,\ y,\ z)$	refractive index
$\vec{n}_i$	unit vector of incident wave
$\vec{n}_s$	unit vector of scattered wave
P	pressure amplitude
$p(x)$	probability density function
$p(x,\ y,\ z,\ t)$	pressure function
R	distance from source to scatterer
R_o	reference distance, 1 m.
r	radial arm from vertical axis of source to receiver
S	salinity in parts per thousand
$\tilde{S}_{\tilde{b}}(f,\ \lambda)$	backscattering function
$\hat{\tilde{S}}_{\tilde{b}_{i,j}}(f,\ \lambda)$	incremental scattering function
$\tilde{s}(t)$	backscattered waveform
SL	spreading loss

t	time
T	temperature in degrees Celsius
u	velocity
$\vec{V}_s$	velocity vector of scatterer
v	velocity
w	width of grid cell
w_f	transformed final depth variable
w_i	transformed initial depth variable
z	actual depth variable
z_f	final depth
z_i	initial depth

Greek Letter Symbols

α	absorption coefficient
Γ	distance function
γ	cone angle
$\Delta\gamma$	bistatic deflected angle
ς	backscattering function
θ	azimuthal angle
λ	time delay variable
μ	mean value
π	constant, ≈ 3.14159265
Π	power
ρ	density
σ	standard deviation
σ_{bs}	backscattering cross section
τ	pulse duration
ϕ	elevation angle
ω	angular frequency

Chapter 1
INTRODUCTION

1.1. Statement of the Problem

The purpose of this study is to incorporate the effects of multiple boundary returns and non-isovelocity conditions into a time-varying representation of underwater acoustic reverberation measured from a moving source. The reverberation model used as a foundation for this study is outlined by Hodgkiss [1]. The model was originally developed by C. L. Ackerman and R. L. Kesser at the Applied Research Laboratory of The Pennsylvania State University.

Reverberation can be described as a lingering of sound energy in a space after some sound has been generated. In the ocean, once a sound has been transmitted, there are various ways in which the energy may return to a receiver situated at the source location. The ocean environment scatters sound in all directions, including back toward the direction from which the sound originated. The scattering is due to discontinuities and inhomogeneities within the ocean. Scattering functions may be used to describe the backscattered energy levels as a function of time and frequency for different portions of the ocean. The scattering function is dependent on the medium's scattering strength, i.e., its ability to scatter sound.

If acoustic beam patterns are introduced for source and receiver transducers, and acoustic spreading and absorption are considered, a scattering function of the ocean may be determined. The scattering function represents a complex, time-varying filter, through which a transmitted waveform may be passed to yield the reverberation power level and spectrum versus time at a receiver.

The original model for predicting reverberation, which has been modified in this effort, has two limitations. First, no boundary reflections are allowed.

The ocean surface and bottom both reflect sound forward and scatter it in all directions in addition to scattering the sound backward toward the source. Secondly, the speed of sound is assumed to be constant throughout the ocean. In the real ocean, the speed of sound varies from point to point, especially over longer distances.

1.2. Importance of the Problem

The air-water interface, which is referred to as the surface of the ocean, is an excellent reflector of sound. A pressure-release type boundary condition exists and, due to the high impedance mismatch between the water and the air, the impinging energy has a difficult time penetrating the boundary. The consequence is that most of the energy remains contained in the ocean, either through scattering or reflection.

The ocean bottom is a more complex boundary than the surface. In some instances, the bottom may be made of rock. In other cases, it may vary with depth from soft mud to harder clay. In any event, reflection does occur when sound impinges upon the ocean bottom. The actual amount of reflection depends highly on the composition of the bottom. Reflections from the surface and the bottom can play an important role in the model, as sound, which is backscattered after the occurrence of reflections, may contribute significantly to the received reverberation.

In the actual ocean, the speed of sound is by no means constant. Over somewhat short distances, a constant speed of sound may be a good assumption. However, the variation in the sound velocity is dependent upon such factors as temperature, pressure, and salinity. These parameters do change with distance, mostly with depth. Therefore, a non-isovelocity medium would be a better assumption in a realistic model of the ocean.

There are many physical phenomena which become prevalent in a non-isovelocity environment. With a varying speed of sound, spherical spreading may no longer be assumed. Acoustic waves are refracted and their paths are no longer straight lines. Channels, regions in which a portion of the acoustic energy becomes trapped between two horizontal planes, may exist. The decay of the sound pressure level over distance becomes much less in a channel than in a spherical-spreading situation. Convergence zones also may be formed in a non-isovelocity environment. These are regions in which the sound pressure level is greater than that predicted by spherical spreading. In contrast, shadow zone regions in which the sound pressure level drops drastically over distance, could be formed in an environment with a varying sound velocity. All of these factors add to the complexity of predicting underwater reverberation levels and spectral content.

1.3. Generalized Approach

The reverberation model to be modified, REVMOD (REVerberation MODel), consists of a series of five FORTRAN computer programs. In the third program of the series, SCATTER, a scattering function at a particular distance is determined. The effects that the sea has on a transmitted signal are described by the scattering function [1]. The carrier frequency and pulse length are necessary parameters, but the signal envelope and source level are not required in this section of REVMOD. This study focuses on the modification of SCATTER.

In SCATTER, the ocean is divided into a spherical grid of cells at a given distance from the source. This grid has a thickness proportional to the pulse length. Each cell contributes only one type of reverberation, either surface, volume, or bottom as in Figure 1.1. In Figure 1.1, six rows of cells are shown. The top and bottom rows consist of surface and bottom cells, respectively. These

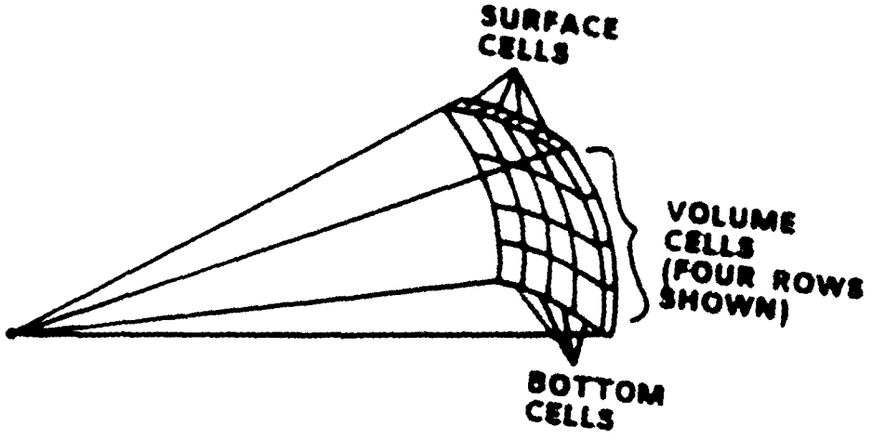

Figure 1.1 *Illustration of a portion of a grid of cells.*

cells are two-dimensional, and are therefore represented as areas. The middle four rows are volume cells, which are three dimensional. The type of reverberation depends on where the cell lies in the ocean, whether it is on the surface, in the volume, or on the bottom. The grid cells are processed individually for their contributions to the total power gain of the reverberation. The term "power gain" is used because the actual reverberation power level is not determined until a transmitted energy level is specified. This energy level is not necessary in the determination of the reverberation power gain. For each cell, a backscattering cross-section is determined, a frequency shift due to the velocities of both the source and the scatterer is introduced, and a spreading of frequency due to an assumed Gaussian distribution of random velocity at the scatterer is calculated. Acoustical spreading and absorption are considered, as well as the directivities of the source and the receiver. The contributions from all cells are summed to obtain the power gain and scattering function spectrum at a given distance.

When a non-isovelocity environment and multiple forward reflections are considered, straight-line propagation and spherical spreading of the acoustic energy no longer results. In order to solve the problem of non-spherical spreading, the concept of surfaces of constant time is introduced. With straight-line propagation and no boundary reflections, the surface of constant time is a sphere. If a grid similar to the spherical grid in SCATTER is to be utilized, a surface of constant time, over which a new grid is set up, must be defined. Figure 1.2 illustrates a series of constant time contours, having a total vertical angular span of sixty degrees, and centered at zero degrees. The source is at a depth of fifty feet. The second contour in this series shows a surface reflection. The eighth shows a bottom reflection and the ninth shows a surface-bottom reflection. Once this new grid has been established, other ways of determining the backscattering cross section, Doppler shift and frequency spreading must be formulated. See

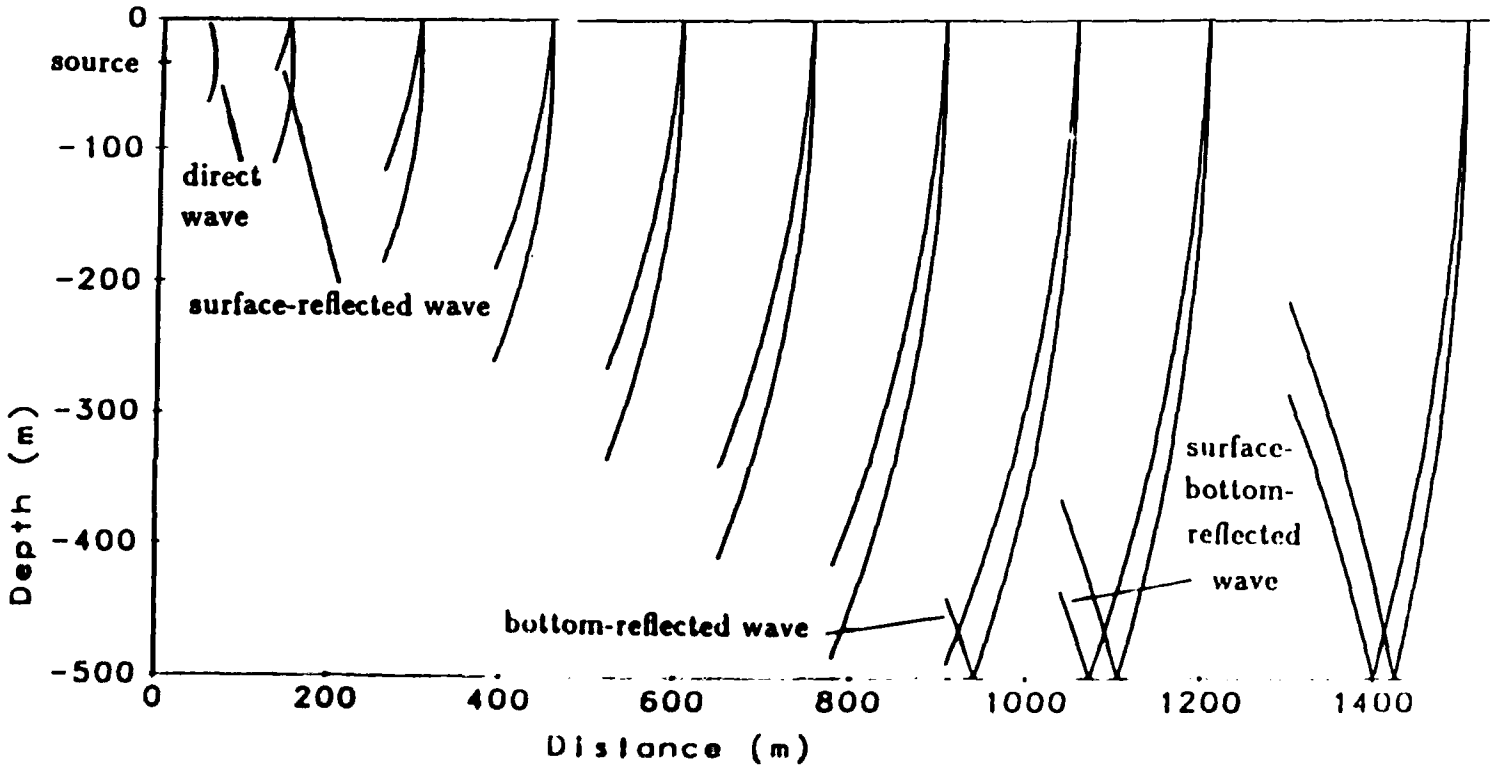

Figure 1.2 **A series of constant time contours**

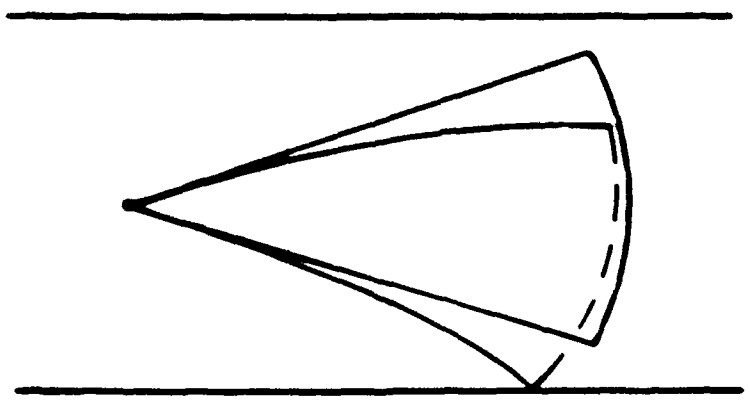

Figure 1.3 Comparison of a spherically spreading wavefront to a downwardly refracting wavefront.

Figure 1.3 for a comparison of a section of a spherically spreading wavefront for isovelocity propagation, the solid curve, to the same section of a downwardly refracting wavefront, the dashed curve, which is due to a decreasing sound velocity with depth.

Since SCATTER uses a constant speed of sound and straight line propagation, the angle at which a ray impinges upon a scatterer is the same as the transmitted angle. This is the angle used for Doppler shift calculations. In the non-isovelocity case, the angle at the scatterer is, in general, different from the transmitted angle. Knowledge of this angle is very important when the scatterer is moving with some velocity. This velocity might be due to an underwater current, to surface waves moving with the wind, or to random scatterer motion.

Spreading loss, also, must be carefully considered in the modification of this reverberation model. In SCATTER, the inverse square law predicts the *two*-way spherical-spreading loss as being proportional to R^{-4}, where R is the distance to the scatterer. This spreading loss is constant for all grid cells. When a non-isovelocity environment is present, some grid cells may encounter a focusing of sound and others a diverging of sound. An alternate method for determining the spreading loss at each cell has been used.

A series of raytracing subroutines has been written to perform the various tasks necessary to construct a new grid over a constant time surface. These subroutines also compute the information needed to determine the backscattering cross-section, Doppler shift, frequency spreading, spreading loss and absorption loss for each cell.

Whereas REVMOD does not allow for surface or bottom reflections, the revised model does. Each ray is traced for a predetermined length of time. The rays leading to a particular grid cell may undergo any number of surface and bottom reflections. These reflections are assumed to be specular in nature. The

numbers of surface and bottom reflections are determined for each grid cell. Angularly independent loss factors for the surface and bottom have been made input variables to the new program so that each cell may be weighted by a reflection loss parameter not previously used in REVMOD.

The input section of the REVMOD series, INPUT, has undergone minor changes to permit sound velocity profile and other pertinent raytracing input data. Once the new constant time grid has been established and the scattering function determined in SCATTER, the remainder of the REVMOD series of programs operates as always, except that the modified scattering function is incorporated.

Chapter 2

UNDERWATER ACOUSTICS

2.1. Reverberation

2.1.1. Introduction

An underwater acoustical environment is very much different than an ideal free-space acoustical environment. When sound is transmitted into the ocean from an underwater source, the energy encounters various inhomogeneities in the medium. In the volume of the ocean, these appear as marine life, such as zooplankton, passively floating animal life, and fish. Near the surface, the air-water interface, there are tiny air bubbles and a rough boundary. The bottom of the sea is not smooth either, but rather is made up of peaks and valleys. These discontinuities cause portions of the transmitted energy to be scattered in many directions. Some of this scattered energy makes its way back to the receiver, which is at the source location, and is observed as reverberation. The reverberation level at any given time after the sound has been transmitted is dependent upon many factors in addition to those mentioned previously. Included are the transmission loss due to spreading and absorption, reflection loss, the directivity of both the source and the receiver, and the abilities of the surface, volume, and bottom to scatter sound back to the receiver. This scattering of sound back in the direction from which the sound was incident upon a scatterer is referred to as backscattering.

2.1.2. Backscattering Cross Section

A measure of a body's ability to scatter sound along the same path back to the receiver at the source location is called the backscattering cross section. The backscattering cross section, σ_{bs}, is directly related to the cross-sectional area (for either the surface or bottom), or the volume of the scatterer, A, as well as

the backscattering function, ς_{bs} [2].

$$\sigma_{bs} \equiv \varsigma_{bs} \cdot A. \tag{2.1}$$

The backscattering function relates the backscattered intensity to the intensity incident upon a scatterer. The scatterers of concern are either surface, volume, or bottom cells. In an isovelocity environment, the areas and volumes of these cells are easily computed geometrically. The amount of symmetry involved leads to a small number of calculations required to define the areas or volumes of all grid cells. When raytracing is involved, however, the calculation of the back-scattering area or volume becomes much more complicated geometrically. Although, in any one horizontal row, the size of the grid cells is constant, the grid cells may vary in size within a vertical column for non-isovelocity conditions. Thus, many more calculations are involved.

For the determination of the backscattering volume of ocean for a cell at a particular distance, a pair of rays, $O - A$ and $O - B$ in Figure 2.1, defining the top and bottom of the cell, are traced for a given amount of time, t. An identical pair, $O - C$ and $O - D$, are traced for a time corresponding to the back of the scattering volume, $t + \triangle t$, where $\triangle t$ is to be determined with knowledge of the pulse length. The endpoints of these four rays define an area in a vertical plane, $A - C - D - B$. The scattering volume is found by multiplying this area by the product of an azimuthal angular increment, $\triangle\theta$, and a radius, r, equal to $ct\cos\phi$, to the cell, where ϕ is the elevation angle. See Figure 2.1 for an example of a backscattering volume cell.

A special case arises when a volume cell is at the surface or bottom of the ocean. In the general case, shown in Figure 2.2, part of the cell has just undergone a reflection from a boundary and the rest of the cell is just approaching that boundary. For this case, the cell is split in two because the portion of the cell

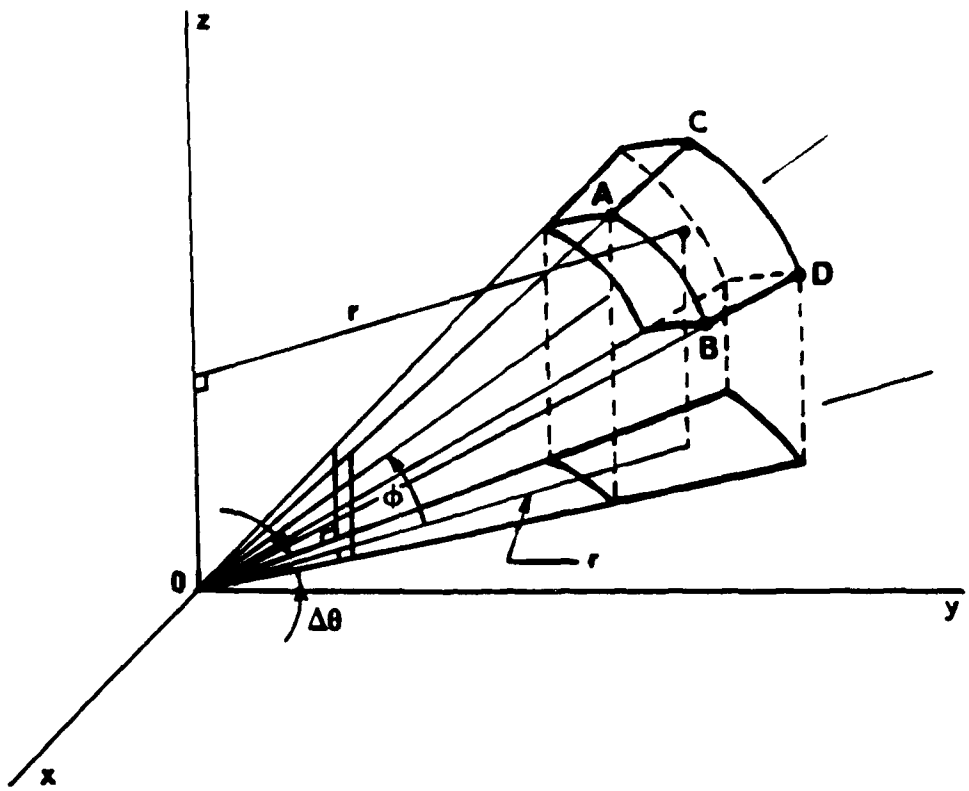

Figure 2.1 **Scattering volume element.**

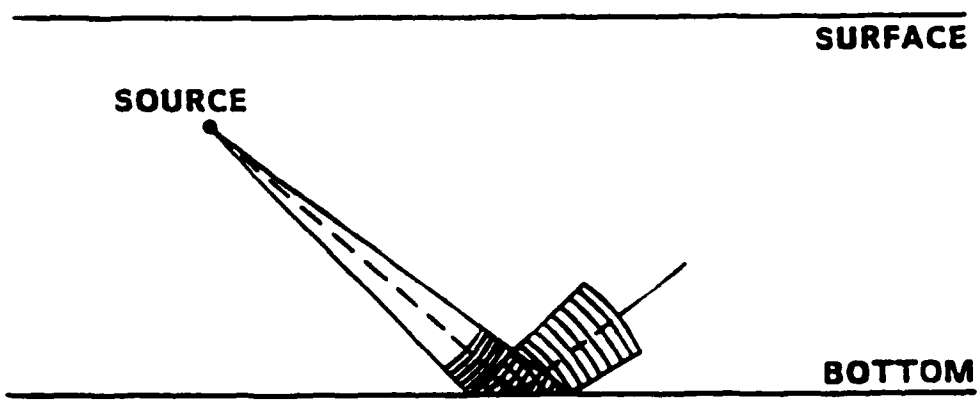

Figure 2.2 Volume element split at a boundary.

after the reflection would have undergone a boundary forward scattering loss not realized by the first portion of the cell. This splitting of the cell is done by locating the centerline of the cell and dividing it where it impinges upon the boundary. Each portion of the volume cell is processed separately for its contribution to the reverberation, and weighted according to its fraction of the total cell volume.

Often, the predominant reverberant returns come from the ocean's surface and bottom as opposed to the volume. Therefore, it is very important to be able to determine the areas of the surface and bottom that are ensonified at a particular time. At any one time, there may be many different patches of surface and bottom being ensonified due to different raypaths with different numbers of reflections. This is illustrated in Figure 2.3 by two constant time contours, one at the front and one at the back of the scattering volume. The contours are defined over a vertical span of $\Delta\phi$. The heavy lines at the surface and the bottom represent regions of boundary ensonification. One area of the surface has been ensonified after the occurrence of a bottom reflection.

2.1.3. Scatterer Depth

The backscattering cross section, as in Equation 2.1, cannot be determined unless the area (in the case of either the surface or the bottom) or the volume of the scatterer is known. For a volume element of the ocean, the A in Equation 2.1 actually represents a volume, and ς_{bs} has units of dB/m^3. Otherwise, for ocean surface or bottom elements, the A represents an area. Whenever a pulse of sound is transmitted, the ensonified portion of the medium appears as a shell with a thickness, $c\tau$, where c is the speed of sound and τ is the duration of the pulse. In the case of an isovelocity medium, the ensonified region assumes the geometry of a spherical shell. The thickness corresponds to the physical length of

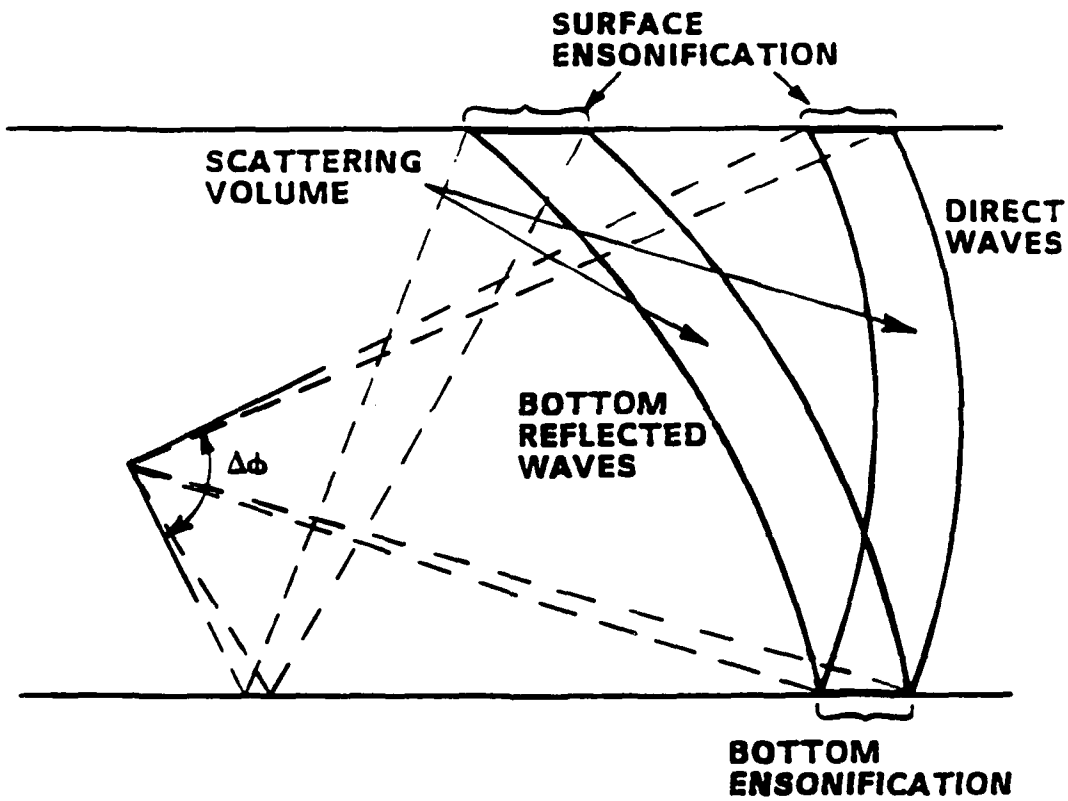

Figure 2.3 Constant time contours at the front and back of the scattering volume over the transmitted span of angles, $\Delta\phi$.

the pulse in the medium. The depth used for the thickness of a scattering element in REVMOD, however, is not the same as the actual ensonified thickness as the pulse travels outward. It turns out to be one half of this thickness as discussed below.

The reverberation observed at the receiver at a particular time, t, after the trailing edge of a pulse has been transmitted, is the net result of all energy reaching the receiver at that time. The trailing edge of a pulse is transmitted one pulse length, τ, later than the leading edge of the pulse. In order for the backscattered energy from the leading edge of the pulse to arrive at the receiver at the same time as the backscattered energy from the trailing edge of the pulse, the leading edge must travel for a longer period of time. The time at which the trailing edge of the pulse is being backscattered is $\frac{t}{2}$, which is half of the round trip time. Since, at the instant the trailing edge is being transmitted, the leading edge has already been traveling for one pulse length, this leading edge has an additional "τ" added to the total travel time, t as is shown in Figure 2.4. Therefore, the point at which the leading edge, line B-B' in the figure, is backscattered, such that it reaches the receiver at the same time as the trailing edge, line A-A', is $\frac{t+\tau}{2}$. The difference in these travel times is

$$\frac{t+\tau}{2} - \frac{t}{2} = \frac{\tau}{2}. \tag{2.2}$$

Any energy received as reverberation at time t may have been backscattered at any time between $\frac{t}{2}$ and $\frac{t+\tau}{2}$. These limits define the scattering depth, or shell thickness, in time as $\frac{\tau}{2}$.

In an isovelocity environment, the actual depth of a scattering element, in units of distance, is $\frac{c\tau}{2}$, where c is the constant sound speed in the medium. When the speed of sound is not a constant, the scatterer depth varies throughout the medium. The length of the pulse, in time, however, remains constant. Thus, it

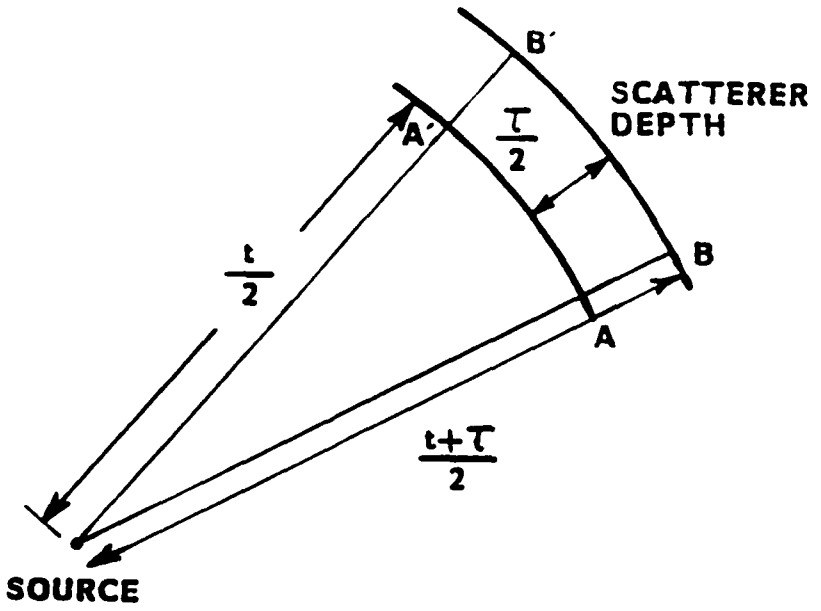

Figure 2.4 Illustration of the scatterer depth for a receiver observation time, t.

is necessary, when non-isovelocity raytracing is involved, for the scattering depth to be visualized as a time difference, $\frac{\tau}{2}$, rather than a physical distance.

2.1.4. Mathematical Description of Reverberation

Underwater reverberation may be assumed, as a first approximation, to be the result of acoustic backscatter from various discontinuities in the oceanic environment. Hodgkiss [1] has described the ocean as a linear, random, time-varying filter, through which a transmitted waveform, $\tilde{f}(t)$, must pass before it is received at the source location as reverberation. Random variables are used because there is seldom enough detailed information on the acoustic scattering environment to use a deterministic description. In this section, the concept of a scattering function is developed. The scattering function describes how the energy from a transmitted pulse is statistically redistributed over frequency and time [3].

Van Trees [4] has shown how a finite length scatterer may be modeled as a multi-element reflector. The scatterer, of length L in time, is broken down into increments of length $\Delta\lambda$ as is shown in Figure 2.5. The total return from this scatterer may be expressed as a summation of returns from all increments.

$$\tilde{s}(t) = \sqrt{E_t} \sum_{i=0}^{N} \tilde{b}(\lambda_i)\tilde{f}(t-\lambda_i)\Delta\lambda, \tag{2.3}$$

where $\tilde{s}(t)$ is the backscattered waveform, E_t is the source energy level, $\tilde{f}(t)$ is the transmitted waveform, and $\tilde{b}(\lambda_i)$ is a complex Gaussian weighting variable. As the size of the increment tends toward zero, the summation becomes an integral [4].

$$\tilde{s}(t) = \sqrt{E_t} \int_{L_0}^{L_1} \tilde{f}(t-\lambda)\tilde{b}_R(\lambda)d\lambda \tag{2.4}$$

In Equation 2.4, $\tilde{b}_R(\lambda)$ is a sample function from a zero-mean complex Gaussian process.

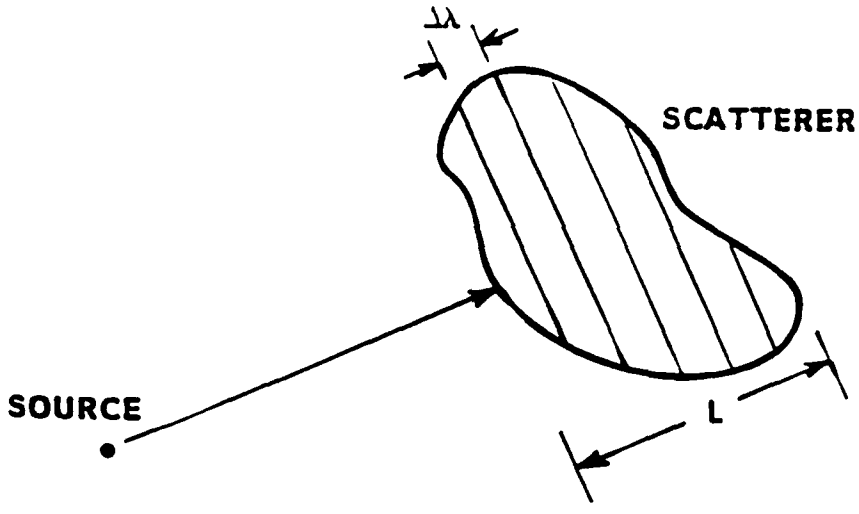

Figure 2.5 Geometry of a scattering element.

Hodgkiss has used this theory to model reverberation as a result of the acoustic backscatter, $\tilde{s}(t)$, from the ocean. He has implemented a random, time-varying, complex, impulse response of a filter, $\tilde{b}(t-\frac{\lambda}{2},\lambda)$, and has obtained the following [1]:

$$\tilde{s}(t) = \sqrt{E_t} \int_{-\infty}^{+\infty} \tilde{f}(t-\lambda)\tilde{b}(t-\frac{\lambda}{2},\lambda)d\lambda \; . \tag{2.5}$$

Here, λ is a time delay variable which corresponds to distance. The time variation of the impulse response function has a covariance function of the form

$$\tilde{K}_{\tilde{b}}(t-u,\lambda). \tag{2.6}$$

Since $\tilde{b}(t-\frac{\lambda}{2},\lambda)$ has been assumed to be a zero-mean process, the covariance function is equal to the correlation function [5]. A spectral density function is obtained through the Fourier transform of the correlation function [5]. Hodgkiss has described the scattering function as the Fourier transform of the covariance function associated with the impulse response of the filter [1].

$$\tilde{S}_{\tilde{b}}(f,\lambda) = \int_{-\infty}^{+\infty} \tilde{K}_{\tilde{b}}(\tau,\lambda)e^{-j2\pi f\tau}d\tau \tag{2.7}$$

The scattering function describes not only the attenuation due to propagation losses and source and receiver directivities, but also the redistribution in frequency due to scatterer motion.

2.1.5. Computer Modeling of Reverberation

In section 2.1.4, a mathematical description of reverberation was discussed in which the ocean was approximated as a complex, time-varying filter through which a transmitted signal must pass in order to be received as reverberation. The time-varying impulse response of the filter, $\tilde{b}(t-\frac{\lambda}{2},\lambda)$, would be difficult, if not impossible, to predict in the computer modeling of a realistic oceanic environment. However, the concept of the scattering function, $\tilde{S}_{\tilde{b}}(f,\lambda)$, may

quite easily be used to develop a practical model for reverberation. Hodgkiss has shown how the fundamental laws of acoustics, as well as some geometric considerations, can be used to construct, piece by piece, a scattering function of the ocean.

At any distance, the ocean may be divided into a number of sections, or cells, each contributing to the total scattering function for that distance. It is convenient to divide an isovelocity environment into rows and columns falling on the surface of a sphere with a radius equal to the scatterer distance from the source. Therefore, a particular cell may be referred to as being located in the i^{th} row and the j^{th} column for each distance. An incremental scattering function, for each cell, in which both Doppler spreading and frequency shifting are taken into account, is produced. The incremental scattering functions each contribute to the total scattering function.

Doppler shift for a source moving with some velocity, v, at an angle, γ, with respect to the scatterer, is calculated through the use of the Equation [6]:

$$f_D = f_T(1 + \frac{2v\cos\gamma}{c}) \tag{2.8}$$

where f_D is the Doppler shifted frequency, f_T is the transmitted frequency, and c is the speed of sound, which has thus far been assumed to be constant throughout the ocean. See Appendix $A.1$ for a derivation. An additional Doppler shift arises due to a cell moving with a mean velocity, u, at an angle, γ, with respect to the source. The equation governing this case turns out to be identical to Equation (2.8), except that v in Equation (2.8) is replaced by u. See Appendix $A.2$ for a derivation. The net Doppler-shifted component is the summation of the Doppler due to a moving source and the Doppler due to a moving scatterer.

The Doppler shifting discussed to this point pertains only to the monostatic case, in which the sound is received at the same location from which it originated. The question has arisen as to whether a specular forward reflection from a moving scatterer would contribute a component of Doppler shift. Pierce [7] has shown how sound scattered in any direction, not necessarily backward, is influenced by the Doppler effect. A situation in which the sound is not backscattered, but is scattered in some other direction, may be referred to as a bistatic case because, in general, an observation point from which the Doppler shift is realized, is not located at the source. The geometry for a case of bistatic scatter is shown in Figure 2.6. $\vec{V}_s$ is the velocity vector of the scatterer, and $\vec{n}_i$ and $\vec{n}_s$ are unit vectors in the directions of the incident and scattered waves respectively. The vector, $\vec{e}_{bi}$, is the unit vector in the direction $\vec{n}_s - \vec{n}_i$. Pierce's equations may be rearranged to show that

$$f_D = f_T(1 - \frac{\vec{V}_s}{c} \bullet \vec{e}_{bi}\, 2\sin\frac{1}{2}\triangle\gamma). \tag{2.9}$$

In Equation 2.9, c is the speed of sound at the scatterer and $\triangle\gamma$ is the deflection angle between $\vec{n}_i$ and $\vec{n}_s$. If the bistatic reflection were to be in the form of a specular reflection, and the velocity vector, $\vec{V}_s$, were assumed to lie in the x-y plane, then the vectors, $\vec{V}_s$ and $\vec{e}_{bi}$, would be orthogonal and the dot product of the two would equal zero. Figure 2.7 illustrates this case. Therefore, in the case of a forward specular reflection from a scatterer moving horizontally, such as the surface of the ocean, no frequency shifting would result.

Frequency spreading for a scattering element of the ocean is a result of variations in the scatterer speed from the mean value. The scatterer speed distribution has been assumed to be a zero-mean Gaussian probability density function, which is characterized by its standard deviation, σ. The Gaussian probability density function, which is used to closely approximate many random

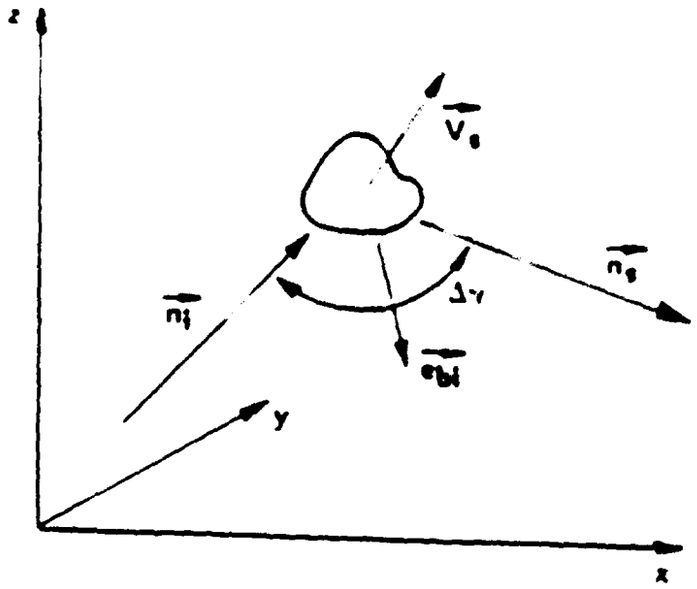

Figure 2.6 Geometry for Doppler shift resulting from bistatic scattering.

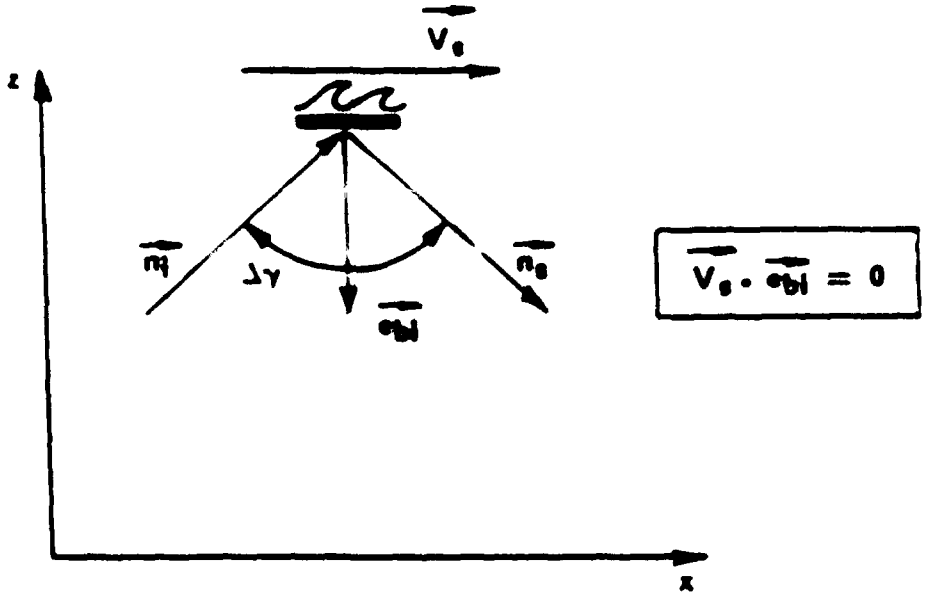

Figure 2.7 A specular surface reflection produces no Doppler because of the orthogonal vectors, $\vec{V}_s$ and $\vec{e}_{bi}$.

phenomena, may be expressed as [5],

$$p(x) = \frac{1}{\sigma\sqrt{2\pi}} e^{-(x-\mu)^2/2\sigma^2}, \tag{2.10}$$

where x, the scatterer speed, is the random variable, σ is the standard deviation, and μ is the mean scatterer speed which has been assumed equal to zero for spectral spreading considerations. The random spectral spreading is directly related to the random scatterer motion through the Doppler equation shown previously. Both spectral spreading and Doppler shifting comprise the incremental scattering function for each cell.

The previously mentioned redistribution of frequency between the time of transmitting and receiving, for each ocean element, is referred to as the incremental scattering function, $\hat{\tilde{S}}_{\tilde{b}i,j}(f,\lambda)$ [1]. Incremental scattering functions must be calculated for each cell and weighted by an attenuation factor, $\hat{A}_{i,j}$, before being summed to obtain the composite scattering function. The attenuation for each scattering element is comprised of absorption loss, spreading loss, and the directivities of the source and receiver. The backscattering strength has been assumed to be independent of the angle of incidence. Hodgkiss has not considered either surface or bottom forward reflections in his model, thus, no energy is assumed to be lost due to interactions with these boundaries. The backscattering strength of each cell is also taken into account in the attenuation factor through the backscattering coefficient. The total scattering function for the ocean, then, may be expressed as a summation of all incremental scattering functions, each weighted by a corresponding attenuation factor [1].

$$\tilde{S}_{\tilde{b}}(f,\lambda) = \sum_{i,j} \hat{A}_{i,j} \hat{\tilde{S}}_{\tilde{b}i,j}(f,\lambda) \tag{2.11}$$

The total backscattered power levels may thus be expressed as a summation of

the attenuation factors [1].

$$\tilde{K}_{\tilde{b}}(0,\lambda) = \sum_{i,j} \hat{A}_{i,j} \tag{2.12}$$

Equation 2.12 is used to determine the total power gain versus time for a particular scenario. The scattering level for each cell, $BSL_{i,j}$, is computed by first finding the volume of the cell, or the area of the cell if it falls on the surface or the bottom, and then multiplying by an appropriate backscattering coefficient, in units of either dB/m^3 or dB/m^2, depending on the type of cell being processed. Absorption loss and spreading loss factors are included in the attenuation factor equation as are weighting factors corresponding to the source and receiver directivities [1]. The attenuation factors may be expressed as follows.

$$10 \log \hat{A}_{i,j} = BSL_{i,j}\ (dB) \ - \ AL_{i,j}\ (dB) \ - \ SL_{i,j}\ (dB) \ - \ BA_{i,j}\ (dB), \tag{2.13}$$

where BSL is the backscattering level, AL and SL are absorption and spreading loss, respectively, and BA is the combined transmit and receive beam pattern weighting. Equation 2.13 makes up part of the SONAR (SOund NAvigation Ranging) equation [1]. The complete SONAR equation includes additional terms related to the transmitter and receiver, such as sensitivities, transmitted power level and the ambient noise in the ocean. These factors are out of the scope of this effort and are irrelevant to the scattering function determination.

2.2. Sound Propagation: Raytracing

When acoustic waves travel from one fluid to another with a different speed of sound, c, at some angle other than normal, the waves are bent, or refracted. The sound propagates through the second medium at a different angle than it did through the first. If a number of fluids with varying speeds of sound are layered, a wave will refract through each layer. Tracing a wave through such a varying medium can be made much easier by the use of ray theory as opposed to

wave theory. Sound rays are defined as lines which are everywhere perpendicular to acoustic wavefronts, i.e., areas of constant phase [6]. Ray theory is not an exact replacement for wave theory, but is a good approximation under certain conditions.

2.2.1. The Eikonal Equation

Kinsler, Frey, Coppens, and Sanders [6] provide a derivation of the Eikonal equation by assuming a solution of the following form to the wave equation:

$$p(x,y,z,t) = P(x,y,z)e^{j\omega[t-\Gamma(x,y,z)/c_o]} \tag{2.14}$$

where P is pressure, Γ is distance, and c_o is a constant value of phase speed. The speed of sound, c, is assumed to be a function of x, y, and z. Areas over which $\Gamma = constant$ are surfaces of constant phase. $\nabla\Gamma$ is always perpendicular to these constant phase surfaces [6]. The operator, ∇, is defined as

$$\nabla = \frac{\partial}{\partial x}\hat{i} + \frac{\partial}{\partial y}\hat{j} + \frac{\partial}{\partial z}\hat{k}\,.$$

Likewise, the operator, ∇^2, is defined as

$$\nabla^2 = \frac{\partial^2}{\partial x^2} + \frac{\partial^2}{\partial y^2} + \frac{\partial^2}{\partial z^2}\,.$$

When the trial solution is substituted into the wave equation, the result is

$$\frac{\nabla^2 P}{P} - \left(\frac{\omega}{c_o}\right)^2 \nabla\Gamma\cdot\nabla\Gamma + \left(\frac{\omega}{c}\right)^2 - j\frac{\omega}{c_o}\left(2\frac{\nabla P}{P}\cdot\nabla\Gamma + \nabla^2\Gamma\right) = 0. \tag{2.15}$$

All terms, except for the second and third, can be considered very small if both P and $\nabla\Gamma$ are slowly varying. Neglecting them yields the Eikonal equation:

$$\nabla\Gamma\cdot\nabla\Gamma \doteq n^2 \tag{2.16}$$

where

$$n(x,y,z) = \frac{c_o}{c(x,y,z)} \tag{2.17}$$

is the refractive index and c_o is an arbitrary reference phase speed. There are two conditions necessary for Equation 2.15 to reduce to Equation 2.16. The first is that the amplitude of the wave must not change appreciably over distances comparable to a wavelength. The second is that the speed of sound must not change appreciably over distances comparable to a wavelength. The solution of the Eikonal equation for Γ yields the path that the acoustic energy follows.

2.2.2. Snell's Law

As a ray passes from one medium into another, the angle of refraction is determined by both the angle of incidence and the speeds of sound of the two layers. This relation is given by Snell's Law [2]:

$$\frac{\sin\phi_1}{c_1} = \frac{\sin\phi_2}{c_2}. \tag{2.18}$$

In Equation 2.18, c_1 is the speed of sound in the first medium, and c_2 is the speed of sound in the second medium. Likewise, ϕ_1 and ϕ_2 are the angles of the rays in the first and second media, respectively. See Figure 2.8 for an illustration of a refracting ray and the corresponding wavefronts. For the case shown, $c_1 > c_2$. Snell's Law also applies in a multi-layered medium. As the layer thickness becomes infinitesimal, the speed of sound becomes a continuous function of depth. The angle, ϕ, at a depth, z, of a ray beginning at an angle, ϕ_i, and depth, z_i, can be determined by

$$\frac{\sin\phi}{c(z)} = \frac{\sin\phi_i}{c(z_i)} = a \tag{2.19}$$

where a is the Snell's Law constant of the ray. The angles are always measured between the ray and the axis normal to the layers.

Clay and Medwin [2] show that if the medium is divided into horizontal stratifications of constant velocity gradient, dc/dz, then the following expressions

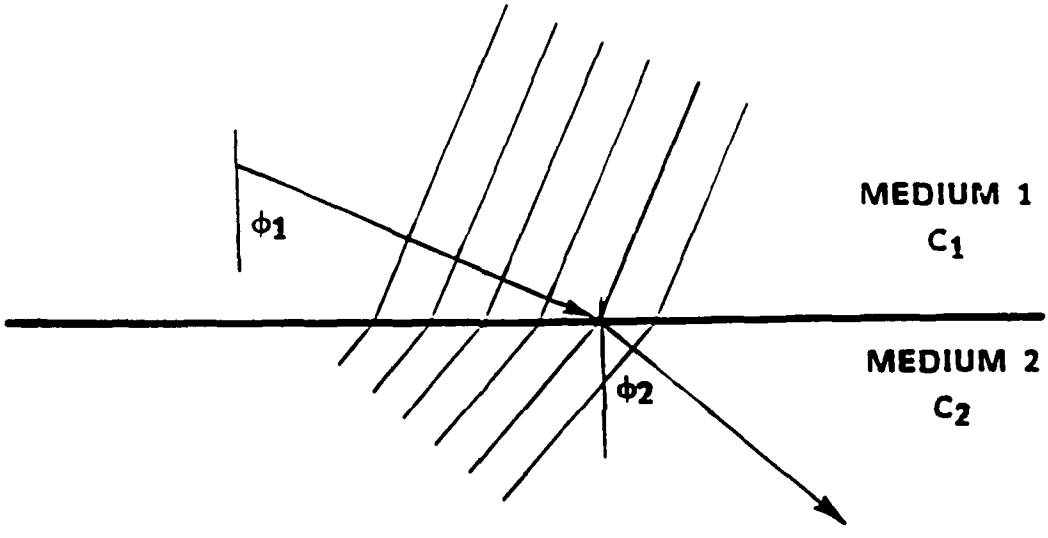

Figure 2.8 Refracting ray and wavefronts. ($c_1 > c_2$).

for time and distance may be obtained:

$$t_f - t_i = \frac{1}{b}\log_e \frac{w_f(1+\cos\phi_i)}{w_i(1+\cos\phi_f)} \tag{2.20}$$

$$r_f - r_i = \frac{1}{ab}(\cos\phi_i - \cos\phi_f) \tag{2.21}$$

Where

t_i = initial time of a ray in a layer,

t_f = final time of the ray in the same layer,

r_i = initial horizontal distance of a ray in a layer,

r_f = final horizontal distance of the ray in the same layer,

b = sound velocity gradient in layer,

a = Snell's Law constant for the ray,

ϕ_i = initial angle,

ϕ_f = final angle,

w_i = transformed initial depth variable,

w_f = transformed final depth variable.

The transformed depths are as follows:

$$w_i = z_i - z_1 + \frac{c(z_1)}{b} \tag{2.22}$$

$$w_f = z_f - z_1 + \frac{c(z_1)}{b} \tag{2.23}$$

where $c(z_1)$ is an arbitrary reference speed of sound at depth z_1. These equations are valid for travel times and distances through one particular layer. A ray must, therefore, be traced through one layer at a time. The rays which travel through constant velocity gradient layers follow the arcs of circles [8]. The radius of the circle is equal to $(ab)^{-1}$ and is constant for a particular ray in a particular layer.

2.2.3. Sound Velocity Profile

Due to the tendency of less dense water to rise above more dense water, the ocean may be modeled as a horizontally stratified medium. Therefore, the speed of sound may be considered to vary only with depth. This might not be true in some situations, especially over long distances. However, this is the assumption used in the development of the raytracing algorithms for the modification of the isovelocity reverberation model. A plot of the speed of sound versus depth is referred to as a sound velocity profile.

The speed of sound is usually measured by the use of either a velocimeter or a bathythermograph. A velocimeter is an acoustical device for measuring the actual sound speed. Urick [9] gives a brief description of Tschiegg and Hays' [10] original velocimeter. The bathythermograph measures the temperature as a function of depth [9]. With some knowledge of or an assumption of the salinity, and a calculation of the pressure, the temperature may be used to determine the speed of sound through Wilson's equation [11].

$$V = 1449.22 + \Delta V_T + \Delta V_P + \Delta V_S + \Delta V_{STP} \tag{2.24}$$

where

$$\Delta V_T = 4.5721T - 4.4532 \times 10^{-2}T^2 - 2.604 \times 10^{-4}T^3 + 7.9851 \times 10^{-6}T^4,$$

$$\Delta V_P = 1.60272 \times 10^{-1}P + 1.0268 \times 10^{-5}P^2 + 3.5216 \times 10^{-9}P^3,$$
$$-3.3603 \times 10^{-12}P^4,$$

$$\Delta V_S = 1.39799(S-35) + 1.69202 \times 10^{-3}(S-35)^2,$$

and

$$\begin{aligned}\Delta V_{STP} = (S-35)&(-1.1244 \times 10^{-2}T + 7.7711 \times 10^{-7}T^2 + 7.7016 \times 10^{-5}P \\ &-1.2943 \times 10^{-7}P^2 + 3.1580 \times 10^{-8}PT + 1.5790 \times 10^{-9}PT^2) \\ &+P(-1.8607 \times 10^{-4}T + 7.4812 \times 10^{-6}T^2 + 4.5283 \times 10^{-8}T^3) \\ &+P^2(-2.5294 \times 10^{-7}T + 1.8563 \times 10^{-9}T^2) + P^3(-1.9646 \times 10^{-10}T).\end{aligned}$$

A similar formulation was made earlier by Wilson [12] for a limited range of salinity ($33ppt < S < 37ppt$). Here, *ppt* stands for parts per thousand. Wilson had later revised that formulation to obtain Equation 2.24, which is valid in the range of $0 < S < 37ppt$. Equation 2.24 is also valid for the temperature range of $-4°C < T < 30°C$ and the pressure range of $1kg/cm^2 < P < 1000kg/cm^2$ [11]. Actually, the units given for pressure are incorrect. A factor for the acceleration due to gravity, g, is missing. If g is assumed to be equal to $9.81m/s^2$, then the range of pressures for which Equation 2.24 is valid is $9.81 \times 10^4 Pa < P < 9.81 \times 10^7 Pa$. The temperature, pressure, and salinity ranges of validity may be expanded slightly, introducing only a small amount of error [13].

It can be seen, then, that the speed of sound increases with an increase in all three parameters – temperature, pressure, and salinity. The sound velocity profile, thus, changes with temperature, pressure, and salinity. At any given location, the sound velocity profile varies with time both throughout the day and with the seasons [9].

2.2.4. Ray Diagrams

Raytracing plots, or ray diagrams, may be used as helpful visual aids in understanding the behavior of acoustic fields. A ray diagram is a set of rays, usually angularly equispaced at the source, which are plotted with depth as a function of the horizontally traveled distance. Differences in intensity levels at different points in the medium may be observed by comparing the spacing of adjacent rays at some distance away from the source. Shadow zones, regions where there is very little acoustic intensity, and caustics, regions of very concentrated intensity, may easily be located in raytracing plots. Figure 2.9 shows a ray diagram which is characteristic of an isovelocity environment. The rays have been plotted at 1.0° increments for the range of $-5.0° < \phi < +5.0°$,

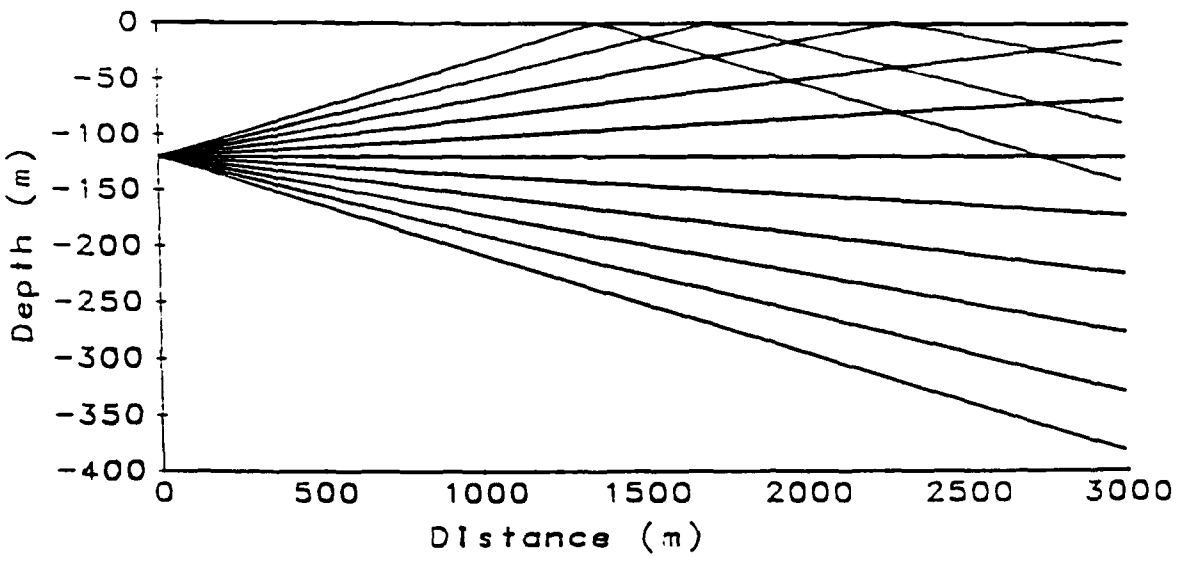

Figure 2.9 **Isovelocity ray diagram.**

where ϕ is the vertical angle, in degrees, of the rays at the source. The angle, ϕ, is measured from the horizontal plane in which the source lies. Positive angles are assumed in the upward direction from this plane and negative angles are assumed in the downward direction. All rays are straight lines, which should be expected, as no refraction occurs in an isovelocity environment. Because the ray spacing is constant at any particular distance, the intensity is uniform at all points in the medium at any fixed distance from the source.

In Figure 2.10, a non-isovelocity sound velocity profile was assumed. This profile is shown in Figure 2.11. The rays that have been traced are the same as those that appear in Figure 2.9. It is evident in this diagram that, in any particular region, the spacing between the rays is not constant. This is an indication that the intensity is not constant for all points at the same travel time from the source. In region *A*, the rays are closely spaced, indicating a relatively high intensity, whereas, in region *B*, the rays are separated, indicating a lower intensity. It can also be seen in Figure 2.10 that some of the sound rays beginning upward from the source, refract away from the surface, as opposed to the ones that reflect from the surface in Figure 2.9.

An alternate way of examining the behavior of sound through raytracing is to construct the actual wavefronts at different points in time after the sound has been transmitted. This can be done by tracing a series of rays, each for the same amount of time, and retaining only the final point of each ray. These points represent one instant in time, thus, they may be connected to form a wavefront. A series of these wavefronts may be plotted to illustrate how the acoustic waves travel over time. Shadow zones and the general refraction of sound may be observed rather easily with this type of plot, although, there is no major advantage over the ray diagrams. Figure 2.12 shows a series of wavefronts superimposed on the associated ray diagram. An isovelocity scenario was used

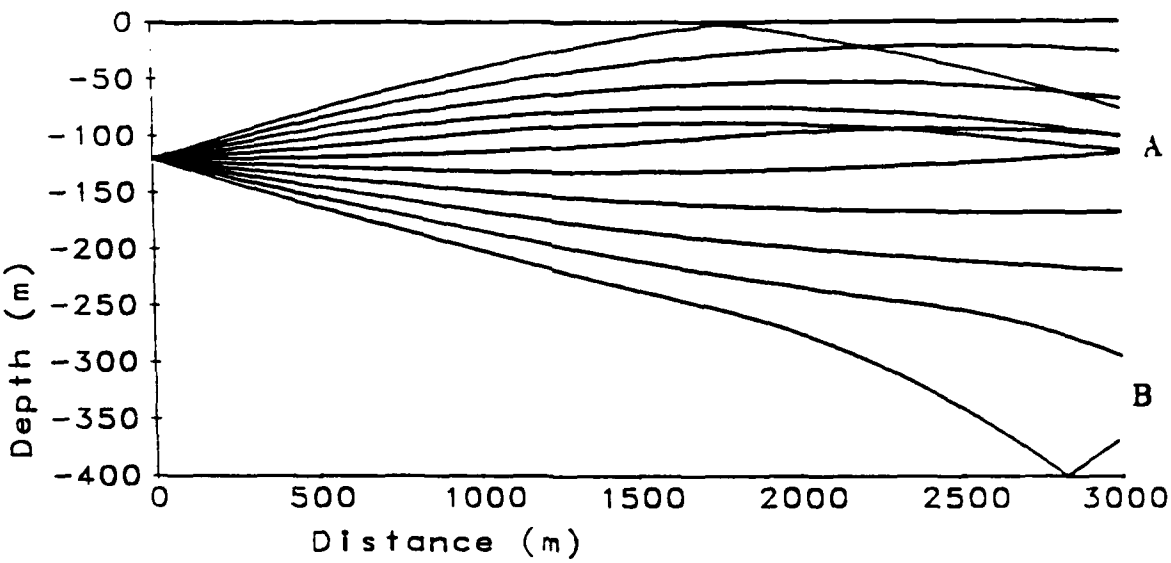

Figure 2.10 Ray diagram illustrating regions of varying intensity for a non-isovelocity case.

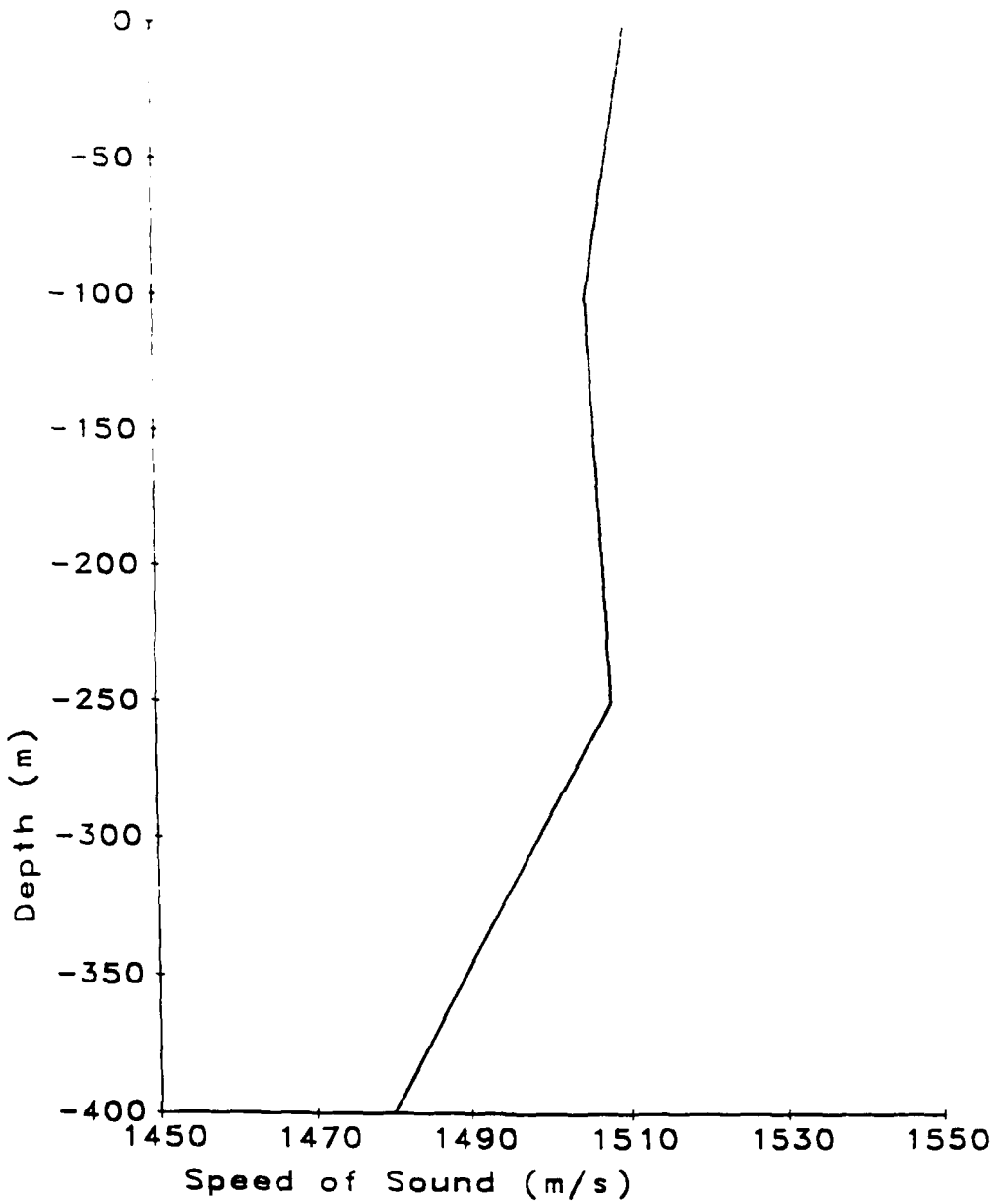

Figure 2.11 Sound velocity profile used for the raytracing plot in Figure 2.10.

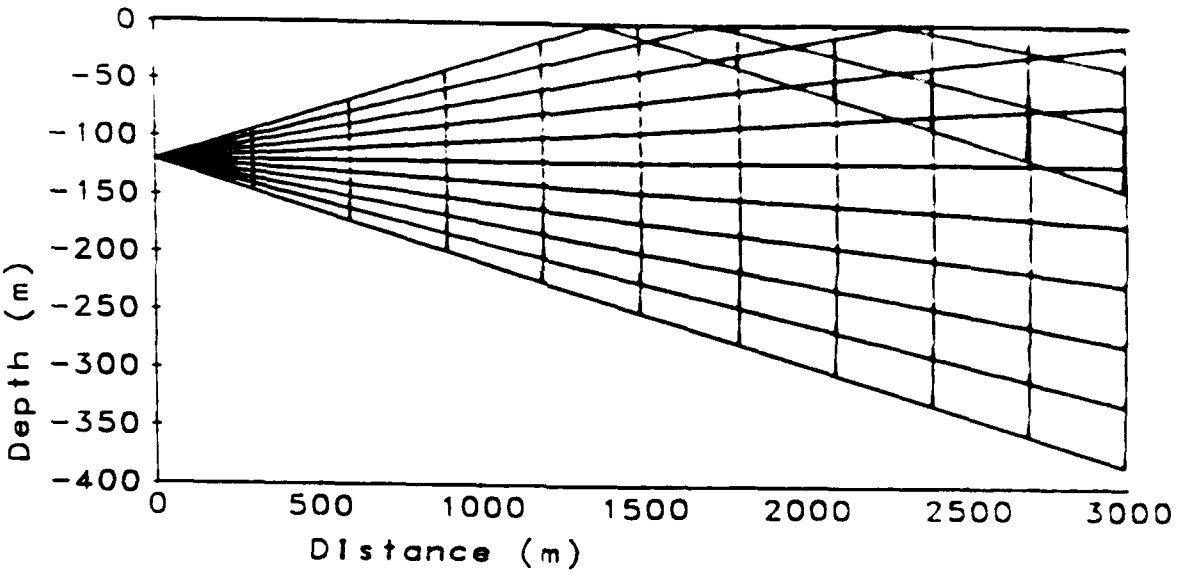

Figure 2.12 Wavefronts superimposed on a ray diagram for the isovelocity case.

and the rays were traced from $-5.0° < \phi < +5.0°$ at 1.0° increments. It can be seen that the wave has undergone a surface reflection, after which a reflected wavefront has appeared. Because of the different scaling on the x and y axes, the wavefronts do not appear to be curved as they are.

In Figure 2.13, a decreasing speed of sound with depth has been assumed, and the z axis has been contracted. The wavefronts have been plotted from $-10.0° < \phi < +10.0°$, as well as the ray, at approximately 8.0°, that grazes the surface. The formation of a surface reflection and a shadow zone are both illustrated in this figure.

2.2.5. Ray State Numbers

Due to Snell's law and the assumption of a horizontally stratified medium, any ray beginning at an angle above the horizontal will eventually return to the source depth at the same angle below the horizontal. The ray may either reflect specularly from the surface of the ocean or it may refract downward, i.e., turn before coming into contact with the surface. The same principle of symmetry applies for rays beginning downward from the source which either reflect or refract upward, back to the source depth. An ocean bottom with a constant depth has been assumed. See Figure 2.14 for examples of raytracing symmetry. All ray segments labeled A, have identical travel times and distances. The same applies to the travel times and distances for the segments labeled, B.

As an aid to the discussion of different ray paths from a source to a scatterer, the concept of ray state numbers will be introduced. Let the ocean be divided into three layers, the first being the region between the bottom and the source; the second, that between the source and the scatterer; and the third, that between the scatterer and the ocean surface. It may be assumed that the source is always below the scatterer for purposes of labeling individual raypaths. Acoustic

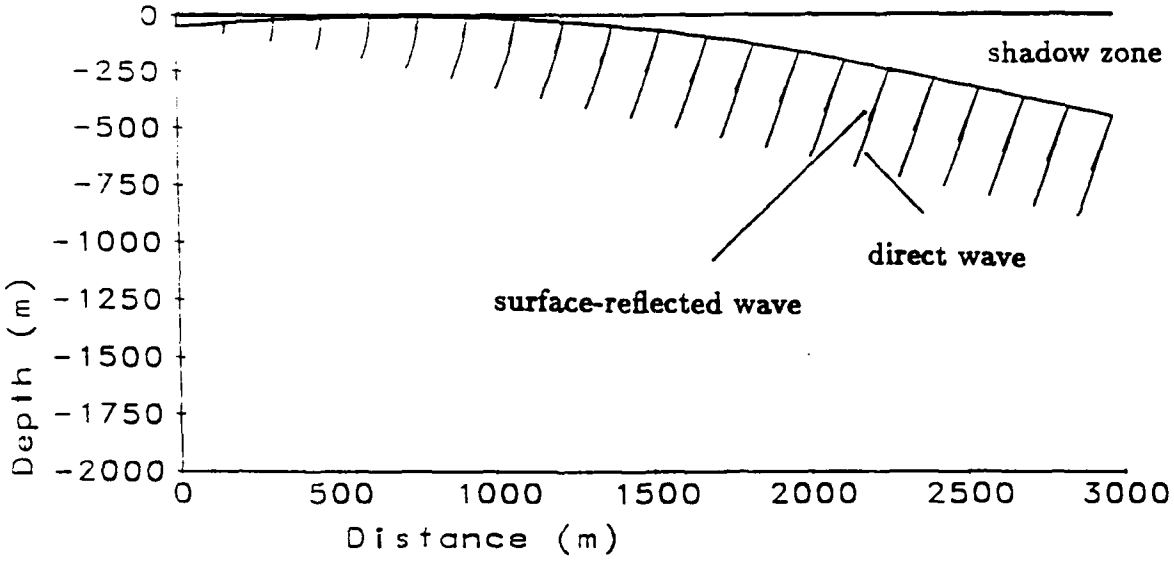

Figure 2.13 A negative velocity gradient produces downwardly refracting waves. A shadow zone is formed at the surface.

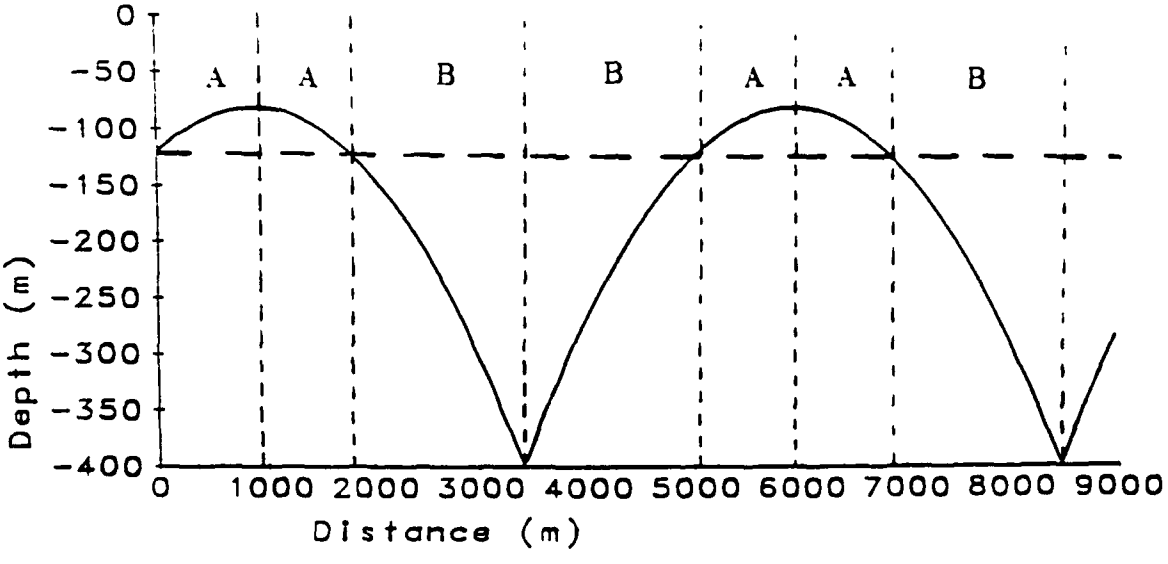

Figure 2.14 **Raytracing symmetry.**

reciprocity dictates that the roles of the source and the receiver, i.e., scatterer, may be interchanged.

Roeckel [14] has developed a method of ordering rays according to the number of times they pass through the region between the source and the scatterer. This number of passes is denoted by the state number, KD. Since all rays begin at the source and end at the scatterer, KD must always be an odd number. Each class of ray solutions is represented by the index, K, such that

$$KD = 2K - 1. \tag{2.25}$$

Two other state numbers, KL and KA, have also been defined. The number of times a ray passes through the region below the source is represented by KL. Likewise, the number of times a ray passes through the region above the source is represented by KA. KL and KA are each related to K in one of two ways, depending on the actual raypath.

$$KL = 2K \ \ or \ \ 2(K-1). \tag{2.26}$$

$$KA = 2K \ \ or \ \ 2(K-1). \tag{2.27}$$

See Appendix B for the class of rays for $K = 1$. For any index, K, a particular ray is uniquely defined by a set of state numbers, KD, KL, and KA.

2.2.6. Final Position and Angle of Ray

The final position and the final angle of a ray from the source after a certain length of time are important parameters to be determined. The final position of a ray will allow for the calculation of the grid cell thickness, as well as the ensonified volume or area of any grid cell. The final angle of the ray at the scattering element will determine the amount of Doppler shift contributed by that element.

The procedure used to calculate the final position of a ray, given a total travel time, t, consists of two basic steps. First, the layer in which the ray ends after time, t, has passed is found. Then, the actual position of the ray within this layer is determined. In order for this to be done, an equation which yields a final depth given an initial angle, depth and time must be developed. This can be achieved by beginning with Clay and Medwin's [2] alternate expression for the time traveled in a layer:

$$t_f - t_i = \frac{1}{b}\log_e \frac{w_f[1 + (1 - a^2b^2w_i^2)^{1/2}]}{w_i[1 + (1 - a^2b^2w_f^2)^{1/2}]} . \tag{2.28}$$

Rearranging, and solving for w_f, the transformed depth variable, the following result is obtained:

$$w_f = 2\frac{\left[\frac{1+\cos\phi_i}{w_i \exp(b\triangle t)}\right]}{\left[\frac{1+\cos\phi_i}{w_i \exp(b\triangle t)}\right]^2 + a^2b^2} . \tag{2.29}$$

The final depth of the ray in the layer is obtained by transforming w_f back to the actual depth, z_f.

$$z_f = w_f + z_1 - \frac{c(z_1)}{b} \tag{2.30}$$

Since these equations are valid for only one layer at a time, it is necessary to find the layer in which the solution lies before calculating the exact final position of the ray. Once a final depth, z_f, is obtained, the final angle and horizontally traveled distance follow through the use of Snell's law and Equation 2.21, respectively.

The total distance traveled along the ray is needed for the determination of the absorption loss. Since linear velocity gradient segments are used in the sound velocity profile, the path of any ray through any layer will always follow the arc of a circle, as was mentioned earlier. The arclength is simply the angle, ψ, times the radius, $(ab)^{-1}$. See Figure 2.15 for the geometry used in determining the arclength of a ray passing through any one layer. From Figure 2.15, it can be

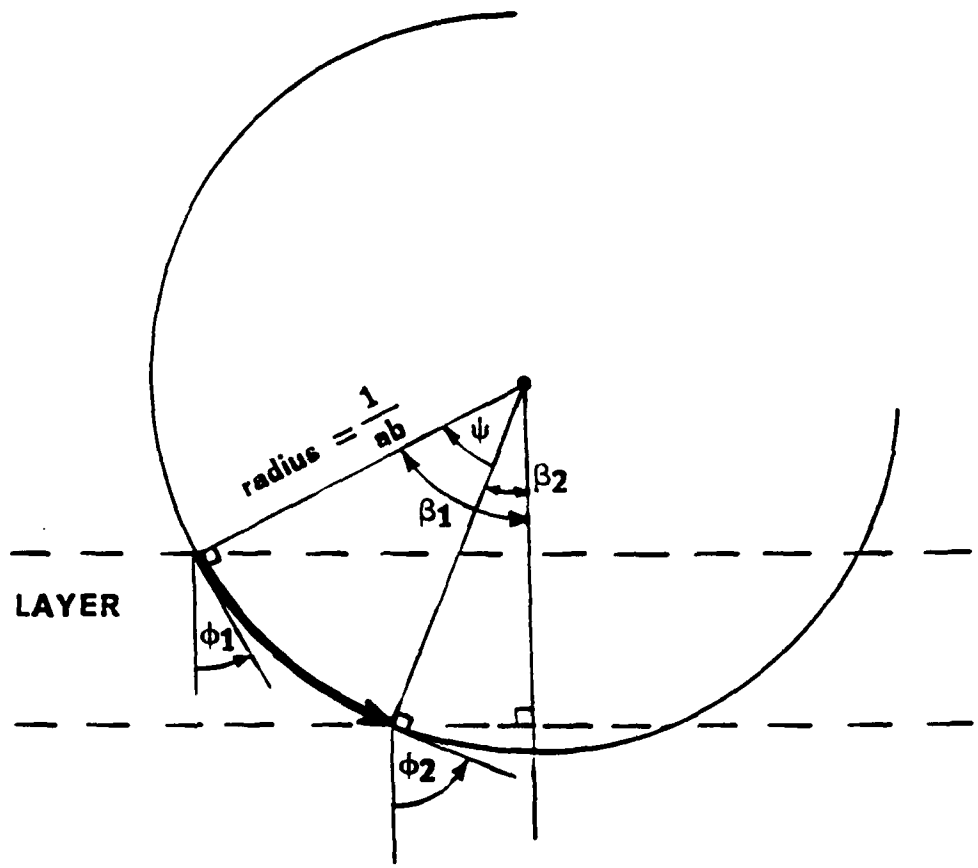

Figure 2.15 Geometry for the arclength determination.

seen that

$$\beta_1 = \frac{\pi}{2} - \phi_1,$$

$$\beta_2 = \frac{\pi}{2} - \phi_2,$$

thus,

$$\psi = \beta_1 - \beta_2 = \phi_2 - \phi_1,$$

and finally,

$$ARCLENGTH_i = \frac{\phi_{2i} - \phi_{1i}}{ab_i} \tag{2.31}$$

where the subscript i denotes layer i and all angles are in radians. As a ray is traced through various layers along its path from source to scatterer, the total horizontal distance and arclength may be incrementally obtained through the use of Equations 2.21 and 2.31 for each layer.

2.2.7. Critical Angles

A critical angle is defined here as an angle at the source, such that the corresponding ray reaches a turning point at a depth at which the gradient of the speed of sound changes. This is any depth dividing two constant velocity gradient bands in the ocean. A turning point is defined as a depth at which a ray changes vertical direction from downward to upward or from upward to downward. These critical angles are essential for classifying different types of ray paths. All rays which fall between two adjacent critical angles will behave similarly and will travel together in a group.

The only depth at which a ray will, or can, turn is one at which the speed of sound is greater than or equal to the speed of sound at the source. This can be demonstrated by the use of Snell's law and the fact that when a ray turns, its direction is horizontal, or ninety degrees with a reference of zero degrees being

straight downward:

$$\frac{\sin\phi_c}{c_{source}} = \frac{\sin 90}{c_{turn}} = \frac{1}{c_{turn}}. \tag{2.32}$$

Therefore,

$$\phi_c = \sin^{-1}\left(\frac{c_{source}}{c_{turn}}\right). \tag{2.33}$$

Thus, a critical angle, ϕ_c, can only exist when the speed of sound at the turning point is greater than or equal to that at the source.

Since a ray beginning at some angle below the source will eventually be directed at an equal angle above the source and vice versa, every critical angle has a mirror-image angle, which is also critical, associated with it. See Figure 2.16 for examples of rays at critical angles. Note that all points on the sound velocity profile with a speed of sound greater than the speed of sound at the source depth will yield a critical angle both above and below horizontal.

2.2.8. Losses

Along its path from the source to the scatterer and back to the receiver, the transmitted energy encounters three types of attenuation, or transmission loss (TL); spreading loss, absorption loss, and reflection loss. Non-isovelocity propagation can have a great influence on these loss mechanisms. In a non-isovelocity environment, not only does the absorption coefficient vary with depth, but the spreading loss, to the scatterer and back, is no longer R^{-4}. Reflection losses due to interaction with the surface and the bottom are also affected by ray bending. Under certain conditions, the sound velocity profile may cause the acoustic energy to be refracted away from the surface or bottom in which case no reflection loss would occur.

The acoustic intensity at a field point in a non-isovelocity environment may be approximated through the use of ray theory. Depending on the sound velocity profile, the source location and the field point, the rays may either converge or

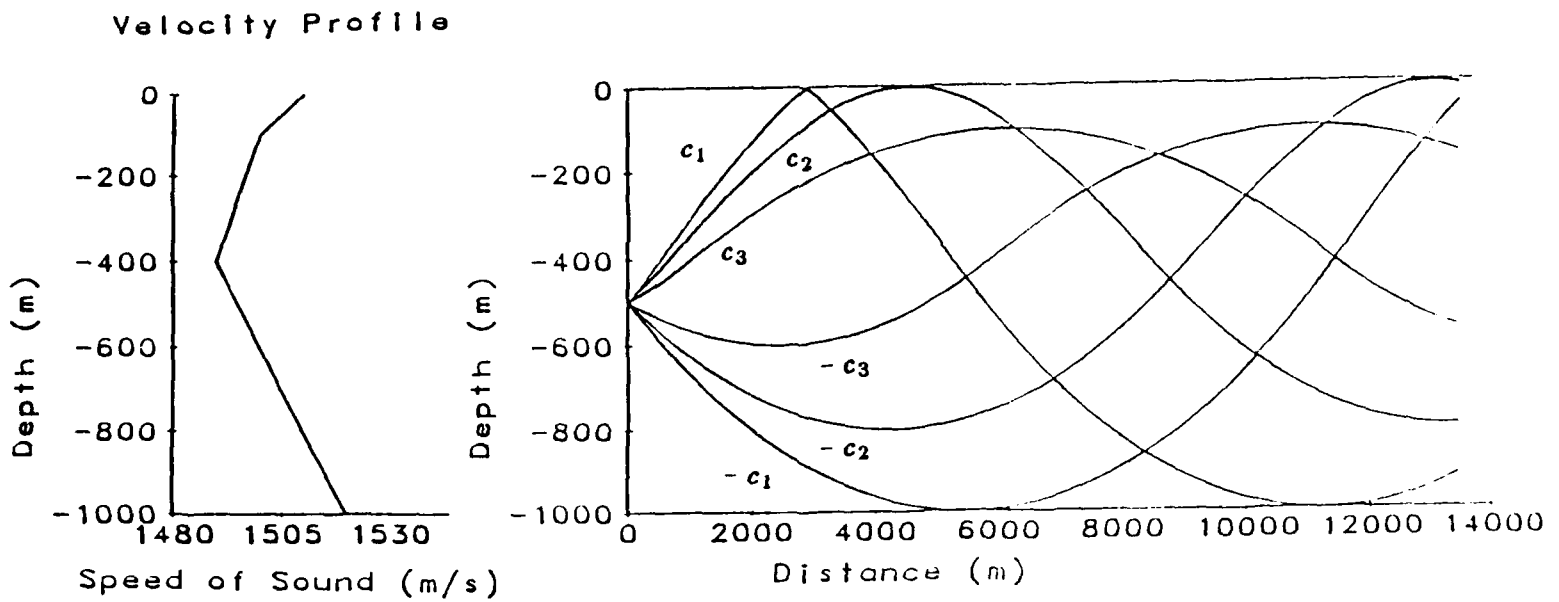

Figure 2.16 **Rays traced at critical angles.**

diverge. Clay and Medwin [2] show that the separation distance of closely spaced rays in the vicinity of an observation point can be used to estimate the pressure at that point from an omnidirectional source. This pressure may be expressed in the form:

$$P^2 = P_o^2 \frac{R_o^2 \triangle\phi}{rL} \frac{\rho c}{\rho_o c_o} \sin\phi_o \tag{2.34}$$

where,

$$P_o^2 = \frac{\rho_o c_o \Pi}{4\pi R_o^2}.$$

See Figure 2.17 for an illustration of the geometry. In Equation 2.34, $\phi = 0$ corresponds to an angle straight downward, and $\triangle\phi$ must be in radians. The transmission loss due to spreading is defined [2] as

$$TL_{(dB)} = -10\log_{10}\left(\frac{P^2}{P_o^2}\right). \tag{2.35}$$

In terms of acoustic intensity, this may be represented as

$$TL_{(dB)} = -10\log_{10}\left(\frac{I}{I_o}\right). \tag{2.36}$$

The expression for the squared pressure at a field point (Equation 2.34) includes a term which is the ratio of the density at the field point to that at the source. Since the density changes just a fraction of a percent with significant changes in temperature, pressure, and salinity [15], the minute change in density can be neglected in the pressure calculations. Clay and Medwin [2] point out that L in Figure 2.17 may be estimated from the angle, ϕ_o, at the receiver and numerical values of h if the rays are not converging or diverging rapidly. This relation is given as

$$L = |h\sin\phi|. \tag{2.37}$$

If two closely spaced rays are traced for the same amount of time, the straight-line separation of the rays may be solved exactly. Since the two rays are traced for

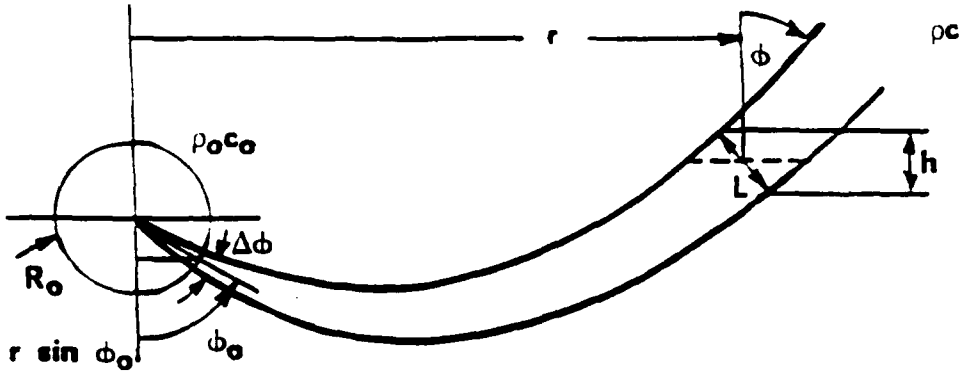

Figure 2.17 Geometry for the determination of the ray separation, *L*.

exactly the same length of time, the endpoints of these rays are points which are in phase on the same wavefront. These points, (x_1, z_1) and (x_2, z_2), are therefore connected to determine the ray separation, L.

$$L = \sqrt{(x_2 - x_1)^2 + (z_2 - z_1)^2} \tag{2.38}$$

The ratio of P^2 to P_o^2 as in Equation 2.35 may finally be expressed as

$$\frac{P^2}{P_o^2} = \frac{c \sin \phi_o \triangle \phi}{c_o r L}. \tag{2.39}$$

This equation is only practical when used in volume cell spreading loss calculations. For closely spaced rays ending at a boundary, either the surface or the bottom, with a slight difference in travel time, L must be approximated as

$$L = \triangle r |\cos \phi| \tag{2.40}$$

where ϕ is the angle at the boundary and $\triangle r$ is the horizontal separation of the two rays [2]. The geometry for rays ending at a boundary is shown in Figure 2.18. Equation 2.40 may be substituted into 2.39 to obtain

$$\frac{P^2}{P_o^2} = \frac{c \sin \phi_o \triangle \phi}{c_o r \triangle r |\cos \phi|} \tag{2.41}$$

which is valid for the determination of spreading loss between two rays at a boundary.

Since acoustic reciprocity holds true for a non-isovelocity environment [7,16], the two-way transmission loss due to spreading may simply be expressed as twice the one-way spreading loss (in dB) [2]. This, of course, assumes that the path out to the field point is the same as the return path. If the path to the scatterer were different from the return path, then the spreading loss associated with each path would have to be determined individually.

Absorption loss in a horizontally stratified medium may not be assumed to be constant for all raypaths at a given travel time. In fact, the absorption coefficient,

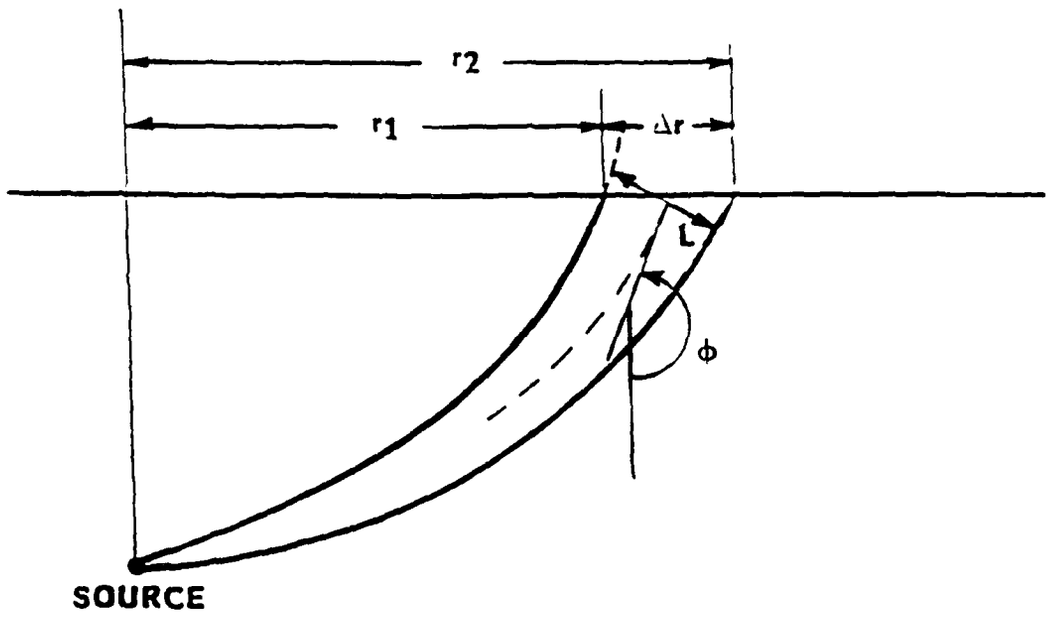

Figure 2.18 Geometry for the determination of the ray separation at a boundary.

α, varies with temperature, salinity, and pressure throughout the medium. In fresh water, the absorption coefficient is dependent on the shear viscosity, μ_s, and the volume viscosity, μ_v, of the water as well as on the square of the frequency. The fresh water absorption coefficient, α_F may be expressed as follows [17]:

$$\alpha_F = \frac{8\pi^2}{3\rho c^3}\left(\mu_s + \frac{3}{4}\mu_v\right) f^2. \tag{2.42}$$

In sea water, however, frequencies below about $100kHz$ are predominantly absorbed through an ionic relaxation process. This molecular dissociation-reassociation process occurs with fluctuations of pressure as an acoustic disturbance passes. A finite length of time, the relaxation time, is required for this process to occur [9]. The reciprocal of the relaxation time is referred to as the relaxation frequency [9]. Although the most abundant salt found in sea water is sodium chloride, it is the magnesium sulfate, $MgSO_4$, which is the principle cause of absorption in the range from about $10kHz$ to $100kHz$ [18]. The relaxation frequency for $MgSO_4$ may be expressed as [18]

$$f_{(MgSO_4)} = 1.55 \times 10^7 (T + 273.1) \exp[-3052/(T + 273.1)] Hz. \tag{2.43}$$

Boric acid, $B(OH)_3$, dominates the absorption below about $10kHz$, with a relaxation frequency in the $1kHz$ region [18] which may be expressed as

$$f_{(B(OH)_3)} = 1.32 \times 10^3 (T + 273.1) \exp[-1700/(T + 273.1)] Hz. \tag{2.44}$$

Both the relaxation processes and the shear and volume viscosities must be considered in order to obtain the absorption coefficients for frequencies up to at least $100kHz$.

Fisher and Simmons [18] developed an equation for the absorption coefficient in sea water which is dependent on temperature, pressure, and salinity. The effects of the relaxation processes of $MgSO_4$ and $B(OH)_3$ were considered, as

well as the fresh water absorption contribution. The salinity was assumed to be 35 parts per thousand (ppt) and the pH to be 8.0. The results of this work are as follows:

$$\alpha = 8.686[A_1 f_1 f^2/(f_1^2 + f^2) + A_2 P_2 f_2 f^2/(f_2^2 + f^2) + A_3 P_3 f^2] dB/m. \quad (2.45)$$

Where,

$$A_1 = (1.03 \times 10^{-8} + 2.36 \times 10^{-10} T - 5.22 \times 10^{-12} T^2) sec/m,$$

$$A_2 = (5.62 \times 10^{-8} + 7.52 \times 10^{-10} T) sec/m,$$

$$A_3 = (55.9 - 2.37T + 4.77 \times 10^{-2} T^2 - 3.48 \times 10^{-4} T^3) \times 10^{-15} sec^2/m,$$

$$P_2 = 1 - 10.3 \times 10^{-4} P + 3.7 \times 10^{-7} P^2,$$

and,

$$P_3 = 1 - 3.84 \times 10^{-4} P + 7.57 \times 10^{-8} P^2,$$

for, f measured in Hz, T in degrees Celsius, and P in atmospheres. The frequencies, f_1 and f_2, are relaxation frequencies of boric acid and magnesium sulfate, respectively.

In a non-isovelocity environment, the absorption coefficient varies continuously with depth. If an average absorption coefficient is assumed constant throughout each constant velocity gradient layer, then the absorption loss along a ray in any layer would be calculated by a multiplication of the length of the ray segment (arclength of a circular path) by the average absorption coefficient (dB/m) in that layer.

$$ABSORPTION\ \ LOSS_{(dB)} = PATHLENGTH \times \alpha \quad (2.46)$$

The total absorption loss at the end of a ray is a summation of the losses (in dB) in all layers through which the ray passes.

When acoustic energy reflects from a boundary, such as the ocean surface or bottom, additional transmission losses arise. From the surface, very little

energy is actually transmitted through to the air above, as a pressure-release type boundary condition exists. The impedance mismatch at the water-air interface causes the sound to remain contained in the ocean. In addition to being an excellent reflector of sound, the ocean surface is a tremendous scatterer of sound because of its roughness and trapped air bubbles or biological life just below it. The acoustic energy impinging upon the surface is actually scattered in all directions. This scattering is a very complex function of wave height, wind speed, rain, grazing angle, and frequency [19,20]. An additional attenuation process at the surface is acoustic absorption due to tiny resonant air bubbles near the surface. High concentrations of trapped bubbles occur near the surface due to environmental conditions [21]. A relatively high amount of absorption results from small (compared to a wavelength) bubbles because of the isothermal conditions that arise; there may be significant heat transfer from the bubble to the surrounding water. Sound propagation is usually assumed to be an adiabatic process, one in which no heat transfer occurs. In the case of small resonant bubbles, however, heat will transfer from the air to the water, thus yielding energy absorption [2]. Some scattering results from the presence of bubbles, but, the absorbed energy is much greater than the scattered energy [21].The sound energy that continues forward after a specular reflection is lower than the incident energy primarily as a result of the energy "lost" to scattering.

Bottom reflections behave quite differently than surface reflections. In many cases, the bottom type changes gradually with depth. The impedance also changes gradually from that of the ocean water. Thus, some of the impinging energy is free to be transmitted into the bottom and to be attenuated due to absorption. The incident sound, however, may additionally be scattered in all directions as well as reflected forward. In other cases, the bottom may be very hard, such as rock. In this event, little energy would penetrate and be absorbed

by the bottom. Rather, the majority of incident energy would reflect forward. The reflection, absorption, and scattering from the bottom are dependent on the bottom type, density, speed of sound, grazing angle, and frequency. Considerable work has been done on the formulation of expressions for bottom scattering [22,23,24,25]; however, there is still a substantial amount of research to be done in this field.

Chapter 3

THE INCORPORATION OF RAYTRACING AND MULTIPLE BOUNDARY RETURNS INTO AN ISOVELOCITY MODEL

3.1. Isovelocity Reverberation Model

A computer model for predicting the power level and spectral characteristics of reverberation has been developed [1,26,27]. Effects due to environmental conditions, source and receiver beam patterns, and a transmitted waveform are taken into account. Although reverberation from the surface, volume, and bottom are considered in the model, no forward reflections are allowed. Thus, whenever any portion of the transmitted energy impinges upon either the surface or the bottom, energy is assumed to be backscattered only; i.e., forward-reflecting energy is neglected. Forward-reflected sound, however, may be very significant. For instance, a smooth surface, hard bottom, and shallow water might all account for significant reverberant returns after reflections occur.

Also assumed in this model is an isovelocity profile; i.e., the speed of sound has been assumed to be constant everywhere throughout the medium. The geometry of the problem has been greatly simplified through this assumption. Refraction of sound is non-existent under isovelocity conditions, and the acoustic energy spreads out spherically from the source. The isovelocity approximation, however, may not be a good one, especially over long distances or around regions in which strong thermal or salinity gradients exist.

3.1.1. Introduction to REVMOD

The base isovelocity reverberation model to be modified, REVMOD (REVerberation MODel) [1,26,27], is a package consisting of five FORTRAN computer programs. In this model, the ocean is divided into a finite number of cells, N, at a distance from the source which is half of the round-trip distance from

the source back to the receiver. These cells are the scatterers whose reverberant returns are summed to obtain a composite reverberant spectrum or a total power level. For each distance of interest, a scattering function is accumulated. This scattering function is then convolved with the power spectrum of the transmitted waveform [1,4] to obtain the total reverberation power spectrum at any distance. See Figure 3.1 for a flow diagram of how REVMOD computes the reverberation power level and spectrum. The purpose of this study is to incorporate raytracing and multiple boundary returns into the model. The section which produces the scattering function, SCATTER, is of primary interest. Following is a brief description of each of the programs that make up the unmodified version of REVMOD, a synopsis of the major reverberation modeling program, SCATTER, a discussion of the capabilities of REVMOD and some sample output.

In the first program section of the REVMOD series, BEAMS, files containing desired transmitting and receiving beam patterns for later use in the reverberation model are created. Both beams are assumed to be circularly symmetric. Beam pattern weightings, normalized to one at zero degrees, are input from zero to ninety degrees. Each beam may be pointed in an arbitrary direction through the specification of a beam vector, (θ, ϕ), where θ is an azimuthal angle and ϕ is an elevation angle. An option has also been made available for the utilization of two-dimensional beam patterns, but the option is not exercised in this study.

All of the information needed for the scattering function calculations is accepted in the input program of REVMOD, INPUT. Included as input data are the source speed and depth, the environmental conditions of the ocean, the pulse length and frequency, the acoustic beam patterns, and the grid cell dimensions. See Appendix C for a complete list of the INPUT variables.

The scattering function of the ocean for a specified distance, or series of distances is computed in the third program, SCATTER. In this program, a grid is

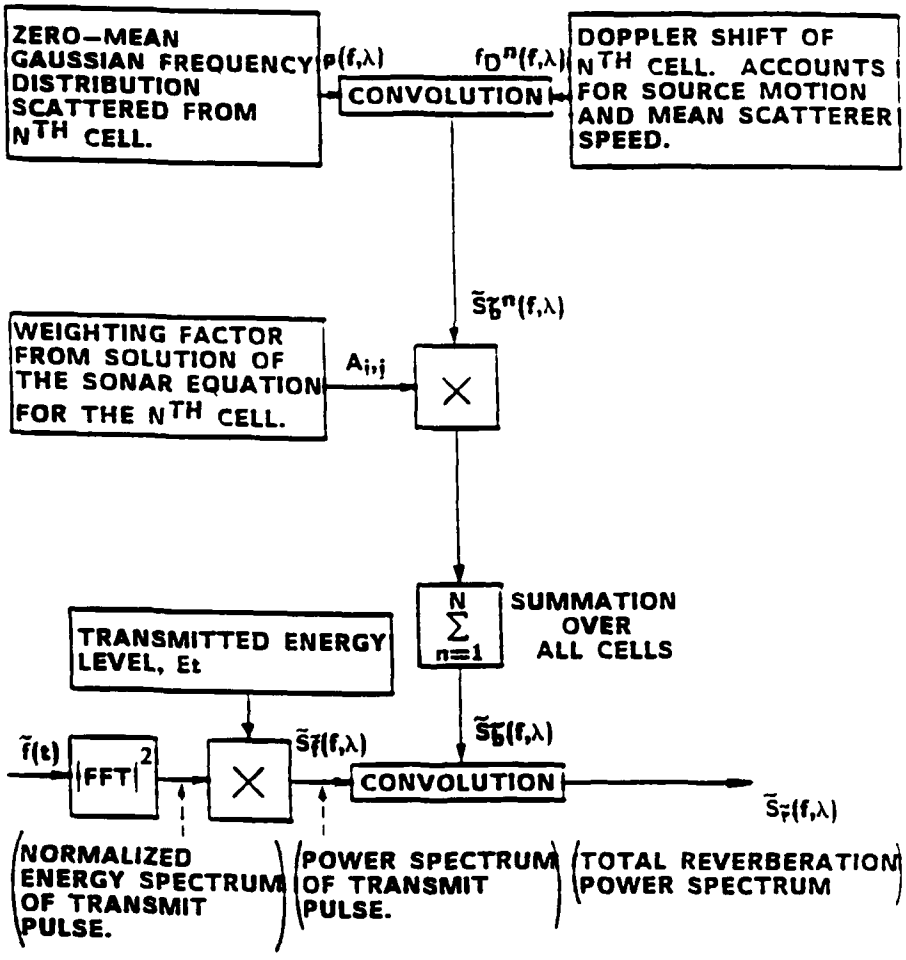

Figure 3.1 REVMOD flow diagram.

used to divide the ensonified boundaries and volume of the ocean into cells. Each cell is individually processed for its contributions to the backscattered spectrum or power gain. Taken into account are spectral spreading and shifting, and attenuation factors resulting from the environmental conditions, the geometry, and the beam patterns. The SONAR (SOund NAvigation Ranging) equation is solved for each cell to determine the relative backscattering level [26]. The actual transmitted power level is not needed at this time as it is assumed that the scattering function is independent of the source level. In addition to calculating the total spectrum, SCATTER has the capability of separating the surface, volume, and bottom contributions so that each may be studied individually.

Until this point in the reverberation model, the source level and signal envelope have not been of concern. The scattering function which characterizes the ocean environment is independent of these parameters. In the fourth program of the REVMOD series, TRANSMIT, the normalized energy spectrum of the transmit pulse is convolved with the scattering function produced by SCATTER to obtain the reverberation power spectrum at the receiver [26].

3.1.2. Description of SCATTER

The incorporation of raytracing and multiple boundary returns into REVMOD involved a rewriting of program SCATTER. Although some SCATTER subroutines have been kept intact, many have been altered or excluded altogether. In this section, the functions of all pertinent SCATTER subroutines, as they existed before any changes had been made, are described. It will serve as a reference later when the raytracing and multiple boundary return algorithms are discussed. A flow diagram for SCATTER is shown in Figure 3.2*a*.

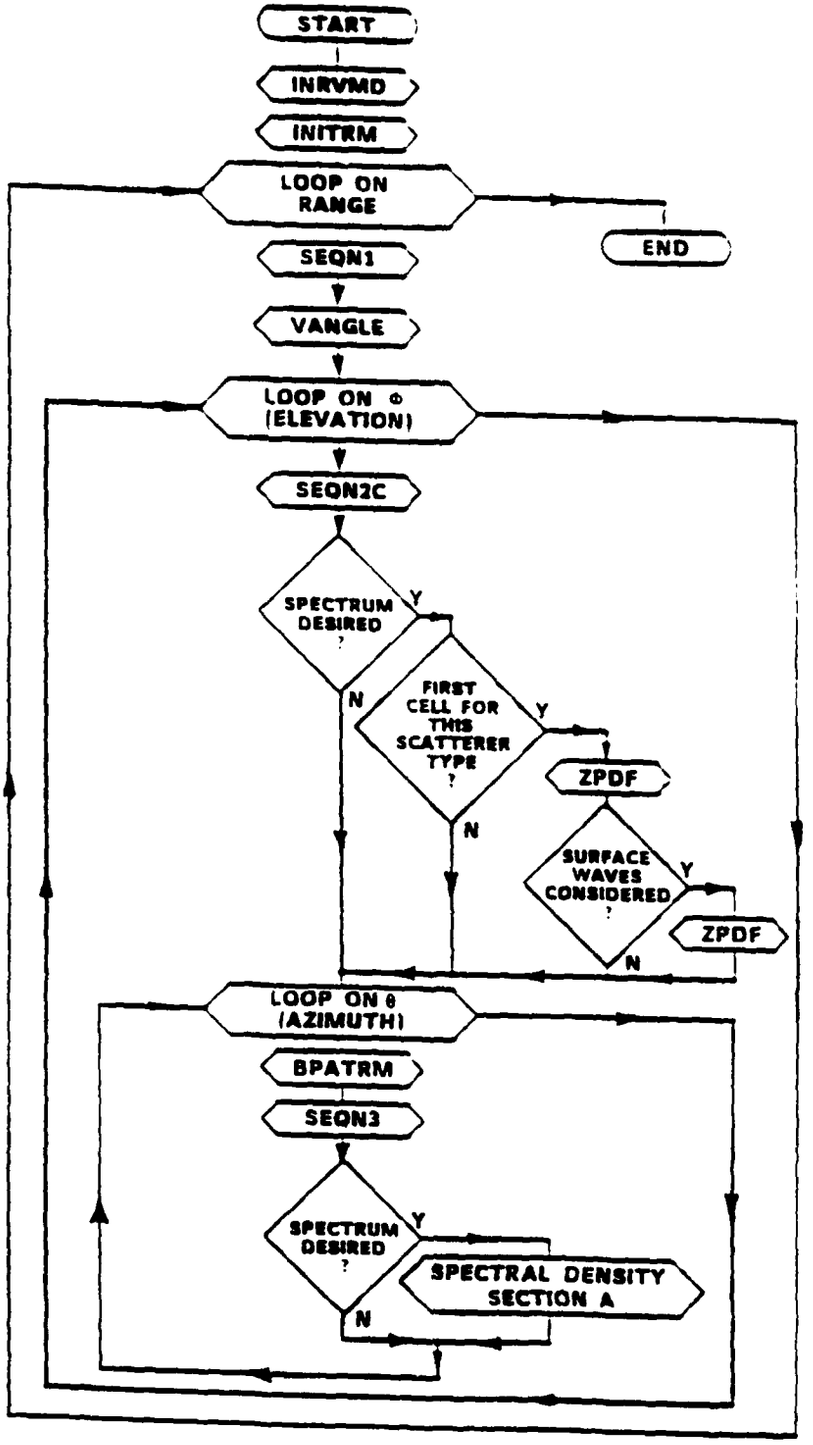

a. Main program.

Figure 3.2 Flow diagram for SCATTER.

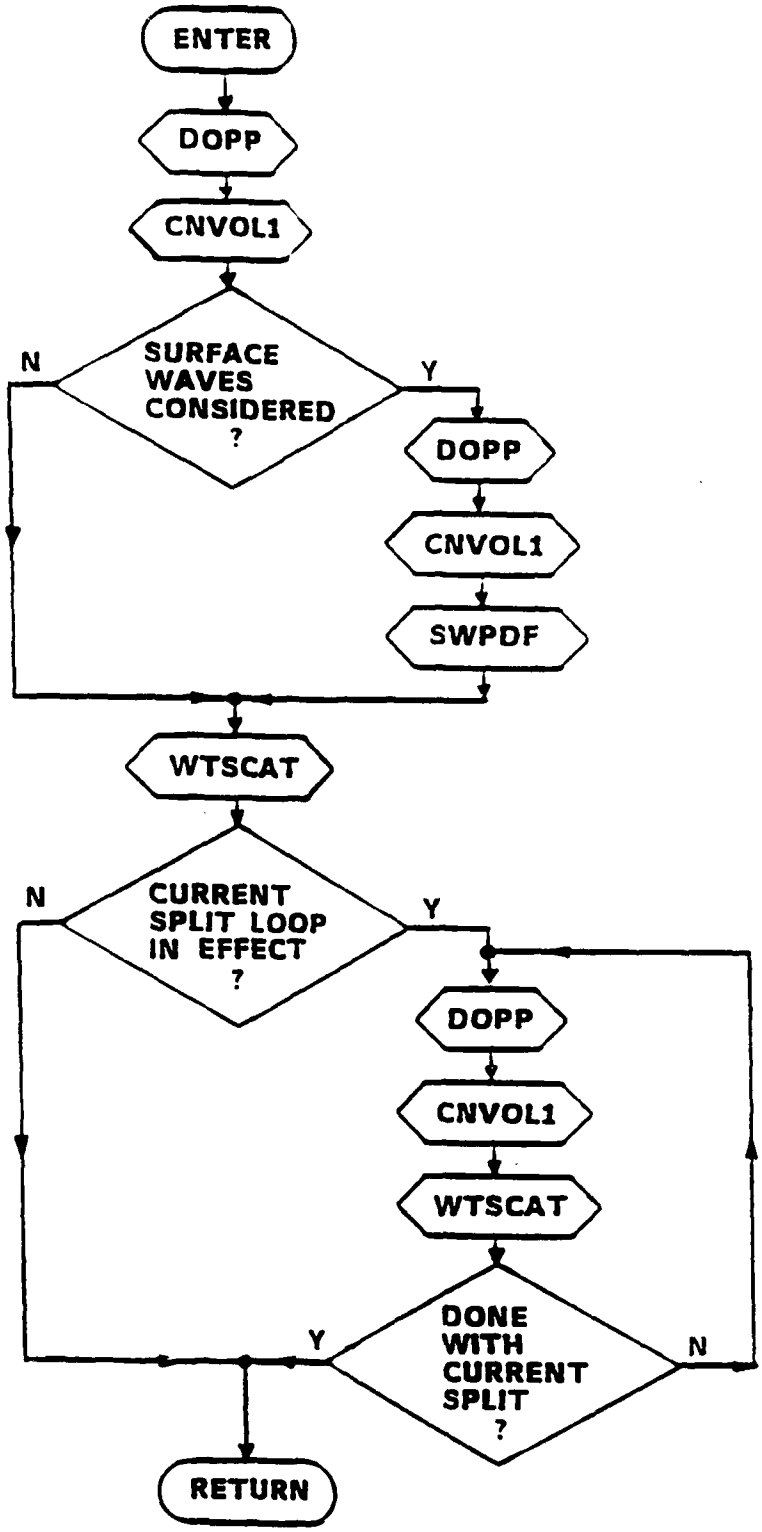

b. Spectral density section *A*.

Figure 3.2 Continued.

The section of this flow diagram which determines the spectral density is shown in Figure 3.2*b*. All of the subroutines which appear in Figures 3.2*a* and 3.2*b* are discussed either in this section or in Appendix *D*.

Provided in Appendix *D*.1 is a brief description of the initialization subroutines found in SCATTER. Once all input parameters are initialized, the SONAR equation is solved in three steps. First, subroutine SEQN1 is called once for each distance, at which time a partial SONAR equation solution is calculated. Determined in SEQN1, is the two-way transmission loss, which, in this isovelocity model, is the same for all cells at one distance, regardless of the scattering mechanism, surface, volume, or bottom. Only absorption and spreading losses are considered in this section.

Secondly, in subroutine SEQN2, a partial SONAR equation for each type of reverberation, only one type per cell, is calculated. See Appendix *D*.2 for a brief outline of how the different reverberation types are distinguished. SEQN2 is called once for each row of cells as the backscattering mechanism, surface, volume, or bottom, is constant throughout any one row. In SEQN2, a backscattering coefficient is multiplied by the ensonified area of the scatterer to obtain the relative backscattered intensity level. If a volume cell is being processed, the backscattering coefficient is multiplied by the volume of the scattering element. The partial SONAR equation computed in SEQN2 is multiplied by the value computed in SEQN1 to obtain a new partial SONAR equation value.

Finally, the SONAR equation is completed for each cell in subroutine SEQN3. Here, the partial SONAR equation from SEQN2, which accounts for spreading, absorption, and backscattering level, is multiplied by the composite beam pattern attenuation. Both transmitting and receiving beam patterns are taken into account. See Appendix *D*.3 for a description of subroutine BPATRM, in which the beam attenuations are interpolated. Once SEQN3 has been called for a cell,

that cell's contribution to the power gain is complete. However, if a reverberation spectrum is desired, some additional operations must be performed on that cell. See Appendix *D*.4 for the descriptions of subroutines ZPDF, DOPP, CNVOL1, SWPDF, WTSCAT, and RINIT2 and RINIT3. These include operations which determine the Doppler shift due to source motion, current layers and wind speed, and the spectral spreading due to random scatterer motion.

3.1.3. Capabilities and Output from SCATTER

Program SCATTER has been designed to produce two types of output. The first type is a plot of the power gain of the scattering function versus time. The variation in the received reverberation level with time may be examined through this feature. Plots of this type are illustrated in Figure 3.3. The individual contributions to the scattering function from the surface, volume, and bottom are shown in addition to the combined total. The scenario corresponding to the plot in Figure 3.3 is shown in Figure 3.4. The input data used may be found in Appendix *E*.1. The first surface return is marked by point *S* in Figures 3.3 and 3.4. It is seen to appear at a time of 0.40 seconds after transmitting. The first bottom return is, likewise, marked by point *B* in Figures 3.3 and 3.4. This return is seen first at a time of 0.27 seconds after transmitting. Factors such as the scattering strengths, absorption coefficient, and beam patterns are not necessary to be known in the understanding of this introductory example. However, a major role is played by these factors in the shaping of the general curves of Figure 3.3.

The second type of output that SCATTER has been designed to yield is the spectral density of the scattering function for one time. The spreading and shifting in frequency of the transmitted signal is dependent on both source and scatterer motion. The source motion has been assumed to be a constant velocity

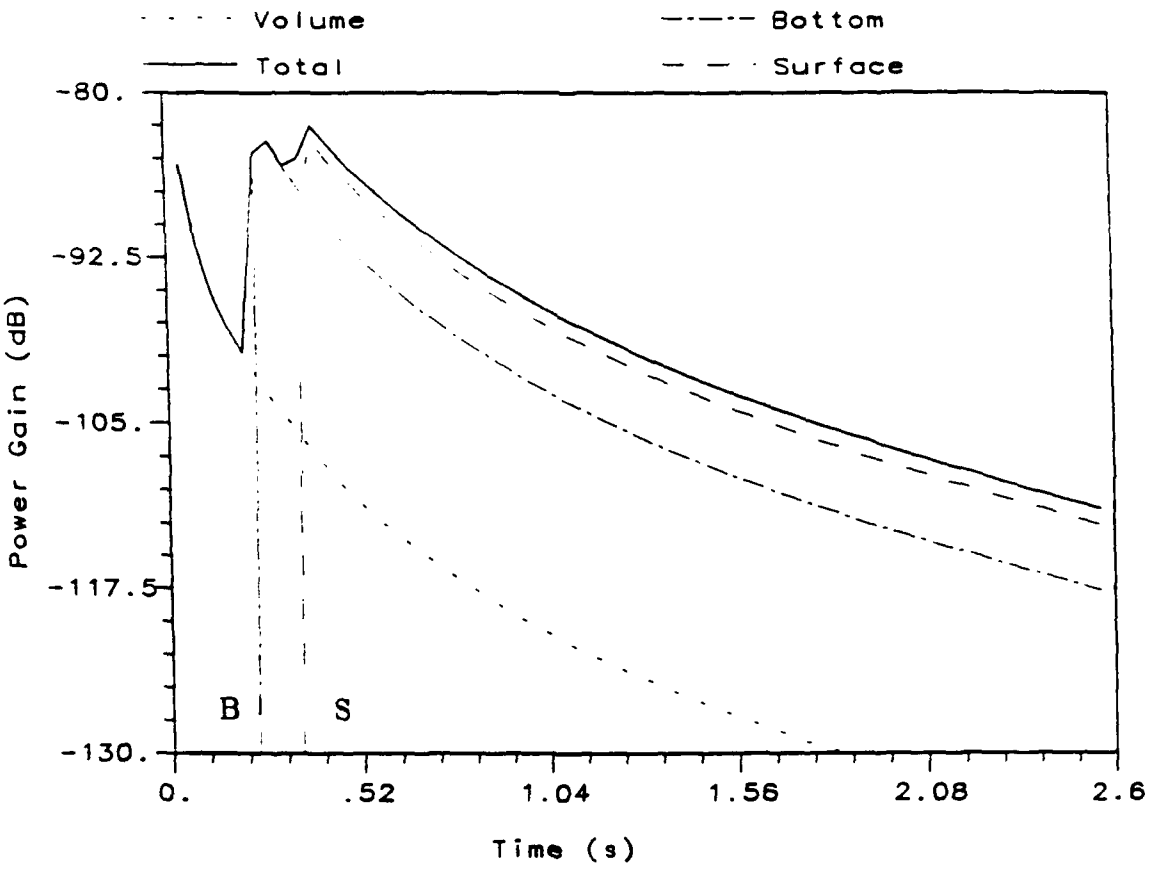

Figure 3.3 Output from SCATTER. Power gain versus time plots for the surface, volume, bottom and combined total. Ocean depth: 500 m.

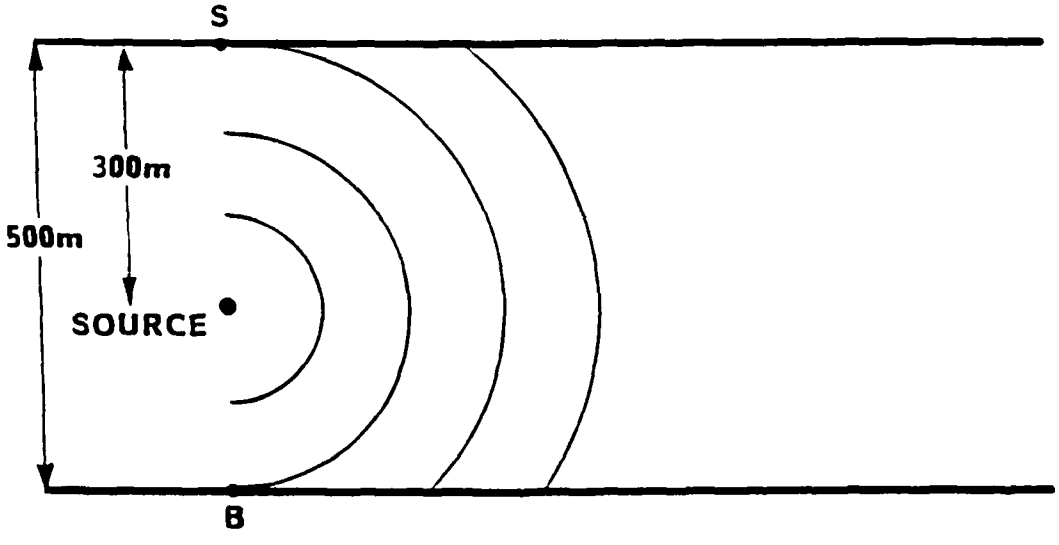

Figure 3.4 A series of time increments illustrates the first bottom return, point B, and the first surface return, point S.

in the horizontal plane. The scatterer motion is modeled as two components, a zero-mean Gaussian velocity distribution and an average velocity vector. The former is the cause for a spreading of frequency about some transmitted frequency. This is actually modeled as a random Doppler shifting. The latter, along with the source motion, is the cause of the mean Doppler shifting of the transmitted signal. Some basic scattering functions are shown in Figure 3.5. The velocity for the source was chosen to be 5 m/s and the elapsed time from transmitting to receiving was set as 0.48 seconds. Aside from the fact that the source has been assigned a velocity, the scenario used for Figure 3.5 is identical to that shown in Figure 3.4. The inputs are shown in Appendix $E.2$. The acoustic beams used in these examples are omni-directional in the vertical, ϕ, direction and ten degrees wide in the horizontal, θ, direction with no sidelobes present. These beams have been chosen to place an emphasis on the effects from the surface and bottom returns, and thus, to best illustrate the differences of the modified scattering function from those of the original model.

Before a discussion of the significance of Figure 3.5, a brief explanation of the Doppler-shifting mechanisms is necessary. In SCATTER, a frequency offset has been introduced, such that a stationary scatterer, which lies in line with the vector of source motion, produces zero Doppler shift. This frequency offset has an effect on each cell. The cells which lie ninety degrees off of the source motion axis account for the greatest amount of Doppler shift due to the offset, although their motion with respect to the source is minimal. This shift occurs in the negative Doppler region as a result of the frequency offset. When the source is stationary, no frequency offset is introduced and the Doppler from each cell is related only to the motion of the cell with respect to the stationary source. In Figure 3.5, both a spreading and shifting of frequency can be observed. The frequency spreading that is present in all cells is due to the standard deviation

of the scatterer speed distributions. The shifting here is a result of the source motion only. All scattering elements have a mean velocity of zero.

Figure 3.5 shows a single surface return, a single bottom return and a volume reverberation return. The surface return is the more negatively Doppler shifted one, as the grazing angle at the surface is greater than the grazing angle at the bottom. The volume return in Figure 3.5 mainly underlies the surface and the bottom contributions. However, some positive frequency spreading from the volume may be observed. This is due to the random motion of those volume elements which lie on, or very close to, the axis of source motion.

3.2. Modified Reverberation Model

A modified version of SCATTER has been written to construct a scattering function for a non-isovelocity environment in which reflections may occur at the boundaries. This new program, called RAYSCT (RAYtracing version of SCaTter), has been designed to use the same approach as SCATTER in producing a scattering function. The concept of a grid of cells is maintained, as well as the program's ability to separate the surface, volume, and bottom contributions to reverberation from one another. The scattering function, which is produced in RAYSCT, is compatible with the TRANSMIT section of the REVMOD series. In other words, the output scattering function from RAYSCT may be convolved with the power spectrum of any of the transmit signal types found in TRANSMIT to obtain the total reverberation power spectrum.

3.2.1. Considerations for the Non-isovelocity Model

Although the general format for the determination of the scattering function has remained unchanged, there have been many aspects of the problem which had to have been considered carefully. For one, the grid cells in the modified model are not consistent in size. They are also summed over a contour of constant time

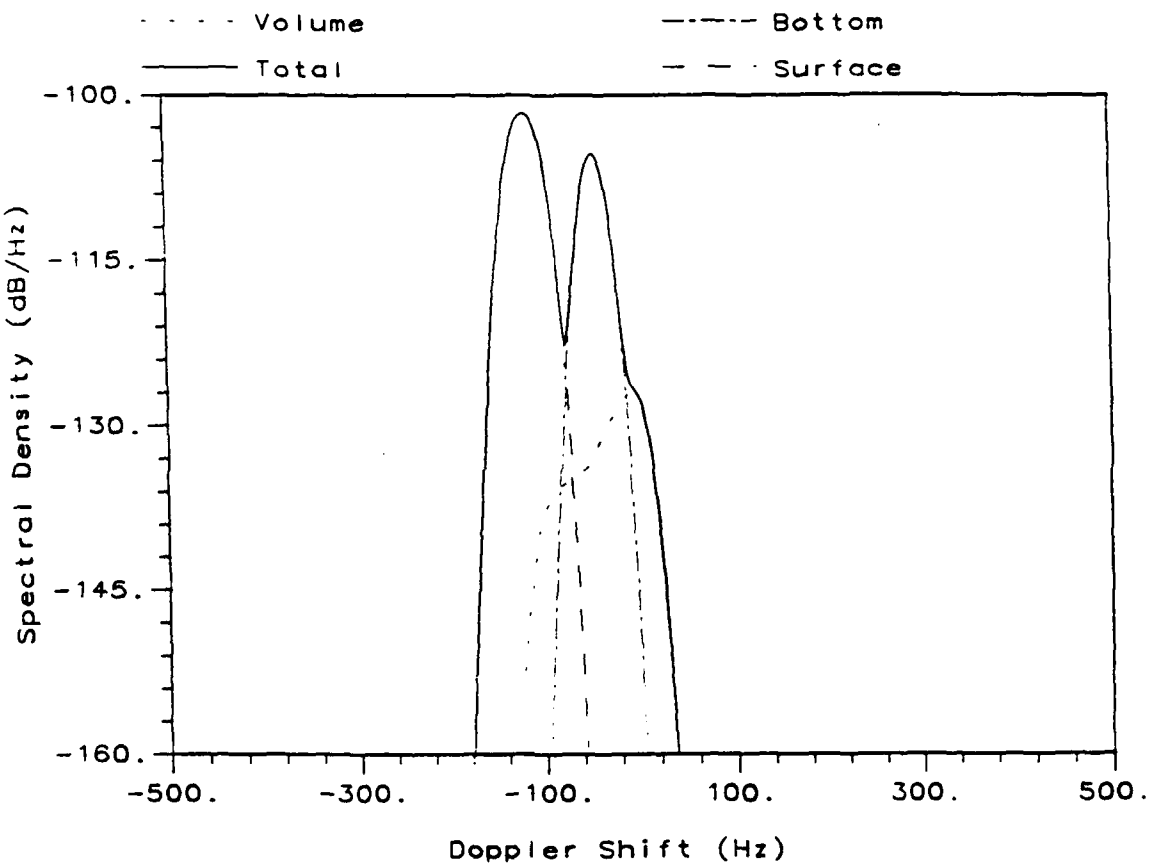

Figure 3.5 Output from SCATTER. Surface, volume, bottom and total contributions to the scattering function spectrum at a time of 0.48 s.

as opposed to the spherical contour of constant distance found in SCATTER. Another complication is that the cells, which fall on the surface and bottom boundaries at a certain time, are not as clearly defined due to both the non-isovelocity environment and the allowance of reflections. In fact, there may be a number of different patches of the surface and bottom which are ensonified simultaneously. Also, as opposed to the isovelocity model, SCATTER, every single cell is a volume reverberation cell, which may or may not ensonify a boundary as well. Additionally, there are some complicated Doppler situations which may arise due to varying speeds of sound throughout the medium. Furthermore, the backscattered Gaussian frequency distribution is varied from cell to cell due to the differences in sound speed. Finally, as reflections were not permitted in SCATTER, a procedure for subtracting energy which is lost to interactions with the surface and bottom boundaries had to be developed. Each of these factors plays an important role in the development of the modified scattering function program, RAYSCT.

The grid of cells in RAYSCT was not able to be defined as uniformly as it had been in SCATTER. The critical angles that were defined in Chapter 2 are used to define different sectors of which the entire grid is made. Figure 3.6 illustrates a set of critical angles being used to divide the ensonified medium into what may be defined as critical sectors. In RAYSCT, these sectors are each subdivided into equal vertical angular increments, such that the sector contains the smallest whole number of increments which are, in size, less than or equal to a predetermined maximum grid cell height. For example, if a critical sector were to have a vertical spread of 11°, and the maximum grid cell height allowed by a user was 2°, then the sector would be subdivided into 6 cells, each having a vertical spread of 1.83°. Five subdivisions would have caused the cells to be too large and seven would have been more than were necessary. Since the critical

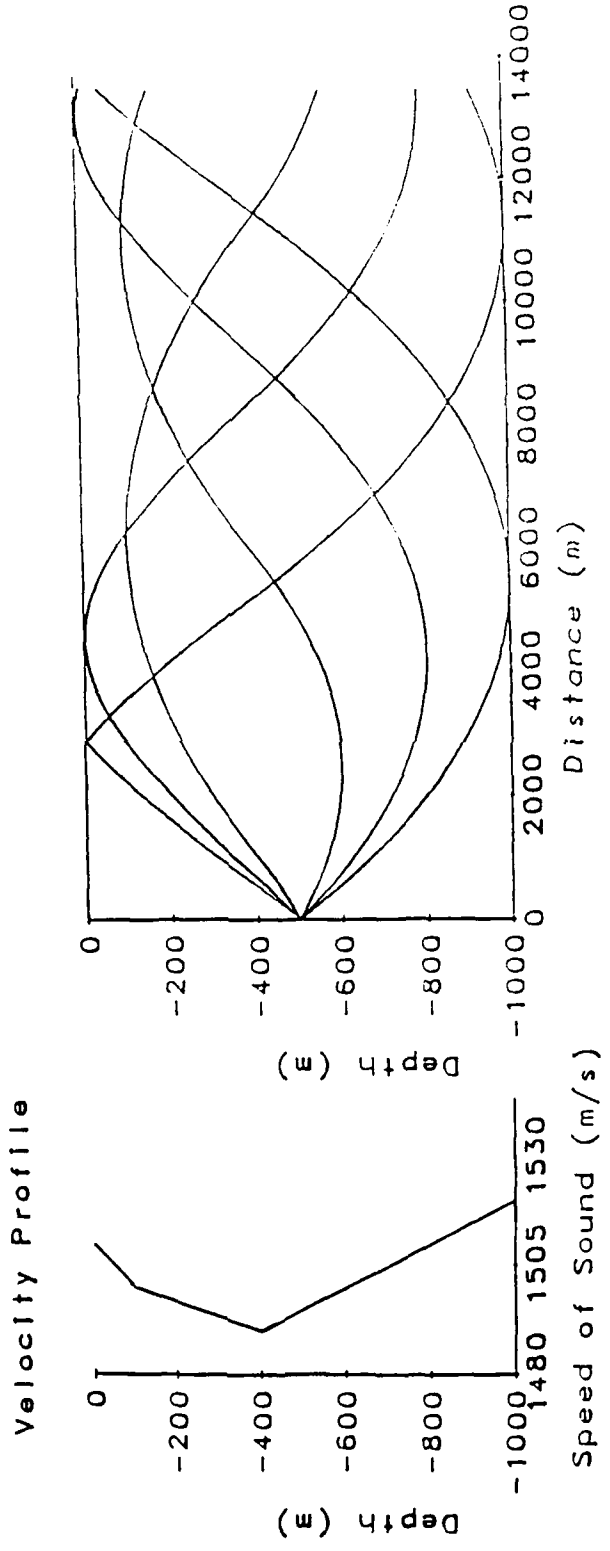

Figure 3.6 Critical sectors.

sectors may vary in size, the cells in one critical sector would not necessarily be the same size as the cells in another critical sector. No additional problems are brought about in the event of differently sized cells because the backscattered level from each cell is dependent on the angular separation of the rays to that cell.

In program SCATTER, the ensonified medium is divided into three regions; surface, volume, and bottom. In general, the cells with the greatest elevation are considered to yield surface reverberation. The middle region is comprised of cells which yield volume reverberation and cells with the least elevation yield bottom reverberation. Figure 3.7 is a general case of a grid of cells. All three types of reverberation, however, might not exist simultaneously at certain times. In Figure 3.7, the boundaries dividing each type of cell are well defined. In a non-isovelocity environment, the regions of boundary ensonification are not as well defined. Once multiple boundary returns are allowed via reflections, there might be any number of groups of cells which ensonify the surface or the bottom at the same instant. Figure 2.3 is an example of different regions of each boundary being ensonified simultaneously. Also, a reverberant return from a boundary at one time may vanish completely at some later time due to effects from the sound velocity profile. Figure 3.8 illustrates how the acoustic energy is refracted downward and away from the surface by a negative velocity gradient, such that, at the longer time, the direct ray path from the source to the surface has vanished.

Another matter which was considered in the modification of the scattering function computing program is the fact that all boundary cells, those falling on either the surface or the bottom, will yield two types of reverberation. One type is from the particular boundary of concern and the other is volume reverberation. In Figure 3.9, all surface cells are accompanied by a fraction of a volume cell. The additional volume cell fractions, which are crossed out in Figure 3.9, are not

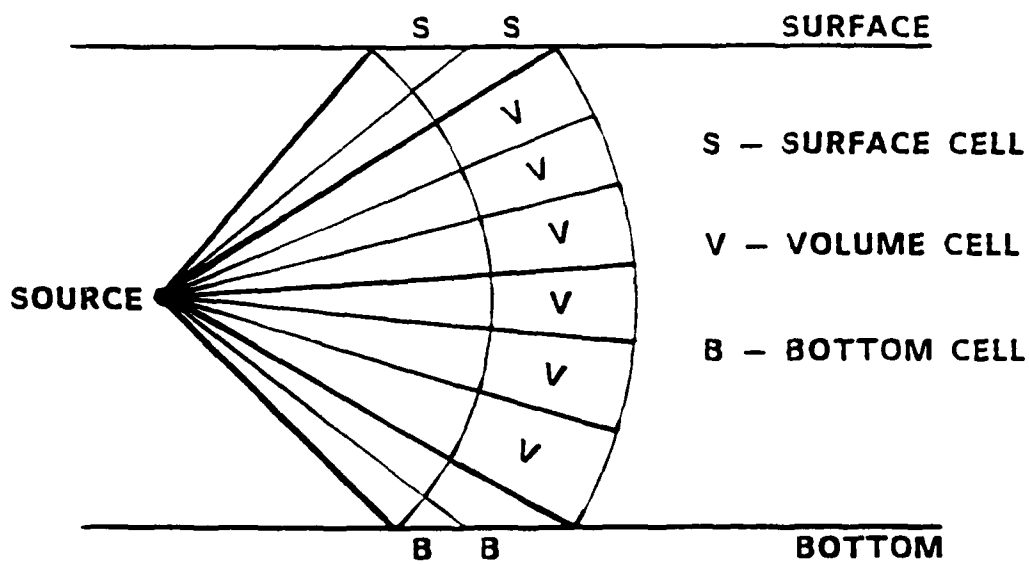

Figure 3.7 Differentiation between surface, volume, and bottom cells. Isovelocity environment, reflections are disallowed.

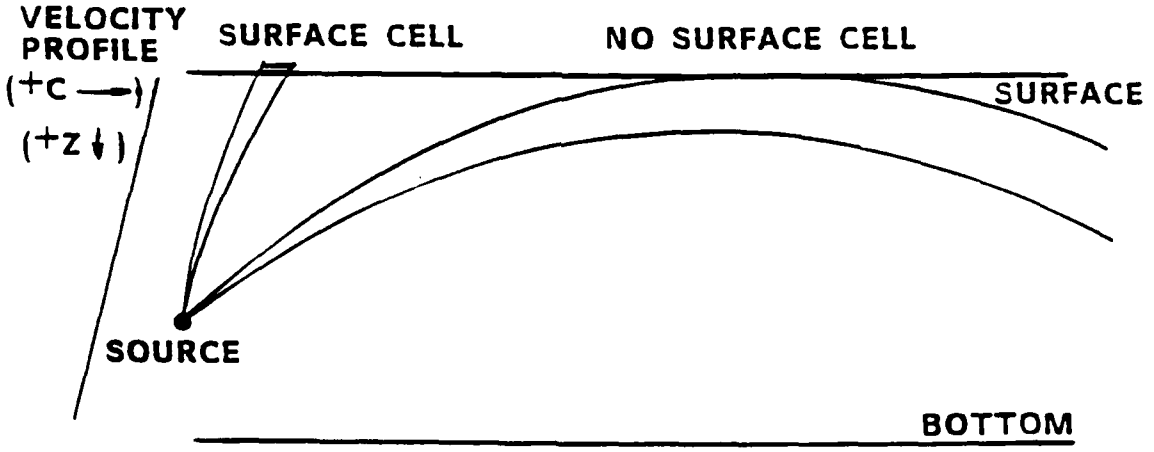

Figure 3.8 A direct surface return vanishes at some later time in the presence of a negative velocity gradient.

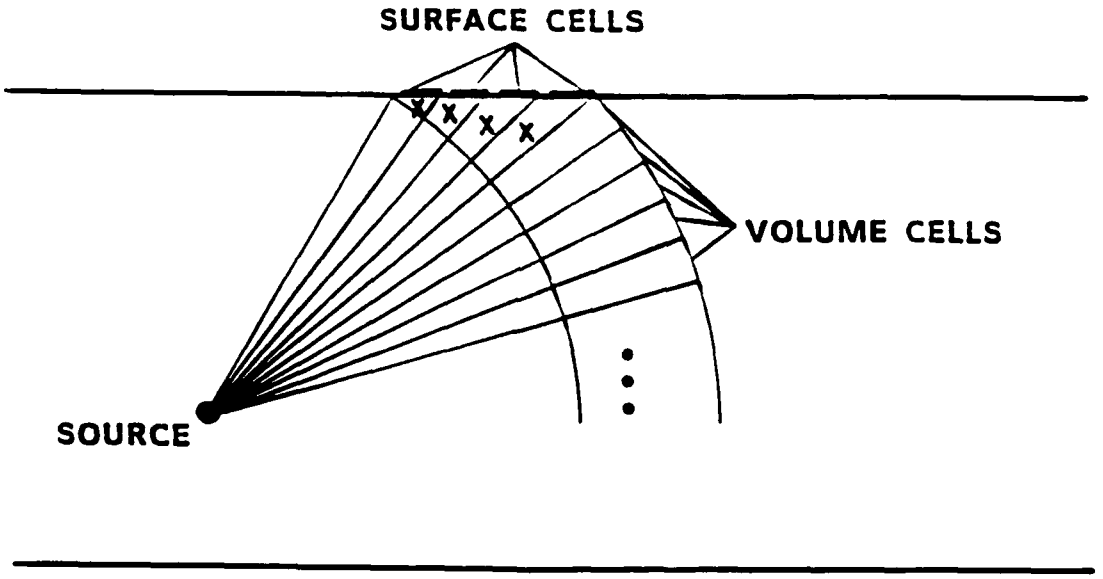

Figure 3.9 Cells marked with an "X" have been assumed to yield no volume reverberation in SCATTER.

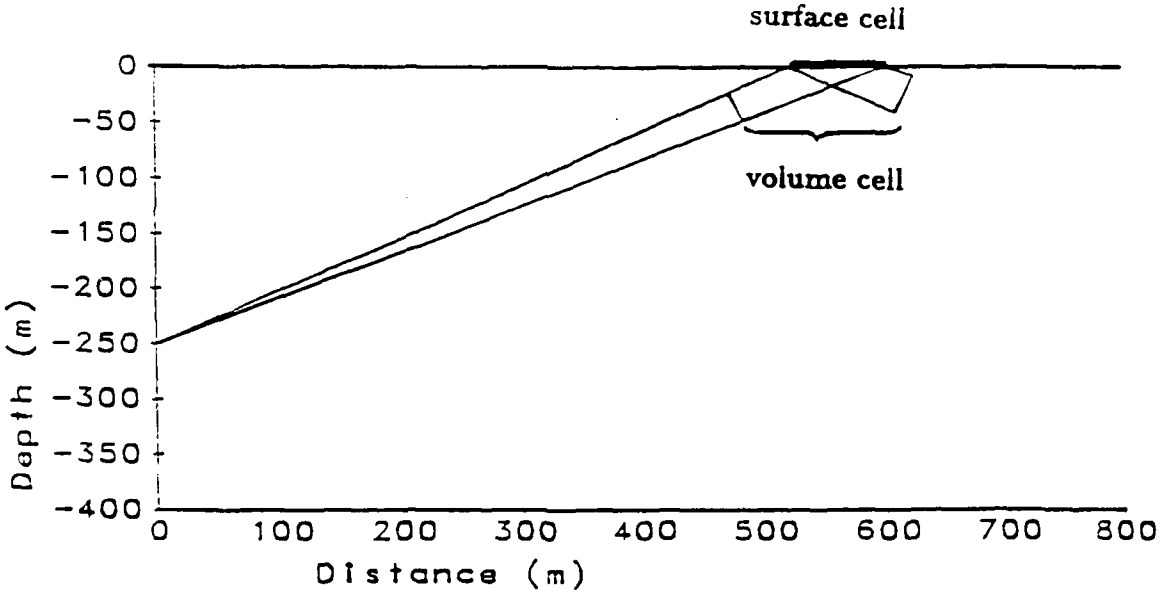

Figure 3.10 **A surface reverberation cell is located inside a volume reverberation cell.**

taken into account in SCATTER. Each cell has been assumed to yield one type of reverberation only. However, in program RAYSCT, the fractions of volume cells which fall both before and after a boundary return have been considered. Figure 3.10 illustrates a surface cell that is located inside a volume cell. Each part of the volume cell must be weighted differently, not only because of the differences in size, but because the portion after the reflection would have lost some additional energy due to the interaction with the surface.

In order for a cell to be divided at a boundary, at least two ray segment lengths must be known. First, the total grid cell depth in meters should be found. This is determined by subtracting the ray to the center elevation of the front of the cell from the ray to the center elevation of the back of the cell. Next, the length of either portion of the divided cell must be determined. For this dimension to be found, however, the length of the ray from the source to the boundary must first be determined. For use in RAYSCT, a set of ray state numbers similar to those suggested by Roeckel [14] in section 2.2.5 have been developed. KA has been designated as the number of times a ray passes through the region above the source and KB has been designated as the number of times a ray passes through the region below the source.

A raytracing scheme has been employed such that, if an initial angle, ϕ_i, were given, the time, t_A, for the ray to travel from the source to the surface, or until a turning point above the source is reached, could be calculated. If this ray were to continue, it would reflect from the surface, or turn, and eventually pass through the depth of the source at an angle of $-\phi_i$ due to symmetry. Thus, the raytracing scheme would also calculate the time, t_B, of the ray, transmitted at $-\phi_i$, to travel from the source to the bottom, or until it reaches a turning point below the source. If these partial travel times, as well as the state numbers, KA and KB, are known, then the time for the ray to arrive at the boundary may be

determined.

$$t_{BOUNDARY} = KA \times t_A \ + \ KB \times t_B. \tag{3.1}$$

Figure 3.11 shows a ray from the source to the surface after one surface and one bottom reflection. For this case, KA is equal to 3 and KB is equal to 2. If the travel times t_A and t_B were known, the time for the ray to come into contact with the surface the second time would be

$$t_{SURFACE} = 3 \times t_A + 2 \times t_B \ .$$

Once the time for the ray to travel to the boundary, $t_{BOUNDARY}$, is known, the distance along the ray from the source to the boundary is determined by actually tracing the ray for this amount of time and accumulating the ray segment lengths through each layer.

Figure 3.12 shows the case of a volume reverberation cell which is split by a surface reflection. In Figure 3.12, the total cell length is represented by ray segment $\overline{AC}$, where

$$\overline{AC} = \overline{SC} - \overline{SA}. \tag{3.2}$$

Since $\overline{SB}$ is known through the $t_{BOUNDARY}$ calculation,

$$\overline{AB} = \overline{SB} - \overline{SA}. \tag{3.3}$$

Similarly,

$$\overline{BC} = \overline{SC} - \overline{SB}. \tag{3.4}$$

With all ray segments known, the weighting factor, W_1, for the portion of the cell before the reflection in Figure 3.12 would be

$$W_1 = \frac{\overline{AB}}{\overline{AC}}. \tag{3.5}$$

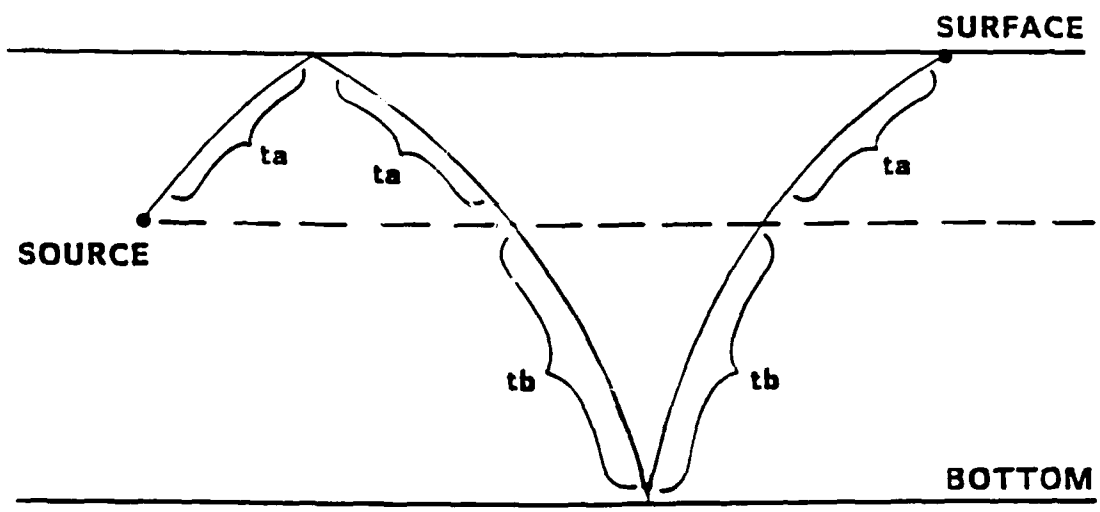

Figure 3.11 Illustration of a ray ending at the surface of the ocean. The ray state numbers are, $KA = 3$ and $KB = 2$.

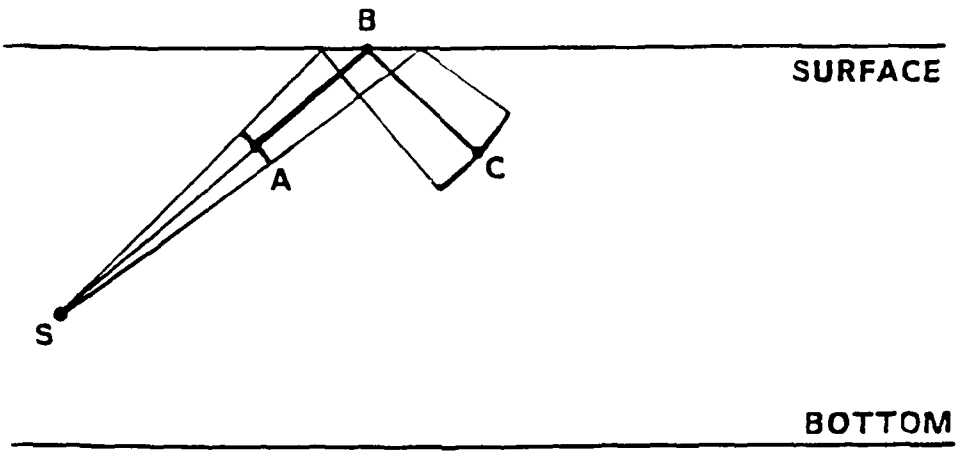

Figure 3.12 Geometry for the division of a volume cell at the surface.

It follows that the weighting factor, W_2, for the portion of the cell after the reflection would be

$$W_2 = \frac{\overline{BC}}{\overline{AC}}, \tag{3.6}$$

such that

$$W_1 + W_2 = 1.0. \tag{3.7}$$

Thus, energy is neither added to nor subtracted from the cell as it is divided and its parts processed individually.

There is a problem which may arise in the determination of whether a volume cell is split by a boundary reflection. A part of the cell may have undergone a reflection, but the center ray of that cell might not yet have reached the boundary. Figure 3.13 illustrates this case. If this volume cell were to be processed as was just outlined, the entire cell would be weighted uniformly, as the center ray has not reflected at the boundary. To avoid this potential trouble spot, an additional set of angles, which will be referred to as surface and bottom-solution sector angles, have been added to the list of critical angles. Included in this set are all angles ending at either boundary at a time corresponding to either the front or the back of the scattering volume. In Figure 3.14, a scattering volume is shown to contact the surface by a direct path from the source. A surface-solution sector is defined by the two rays shown. This solution sector may be made up of many grid cells. Surface reverberation is represented by all cells falling between the two rays in Figure 3.14. Each of these cells, though, is also a volume reverberation cell which is divided at the surface. No cell which lies outside the surface-solution sector touches the surface at any time. With the solution sector defined as such, the center ray of any volume cell which falls entirely within the surface-solution sector, is reflected from the surface, thus, making it impossible for the situation shown in Figure 3.13 to exist. A volume cell which has been split by the surface is

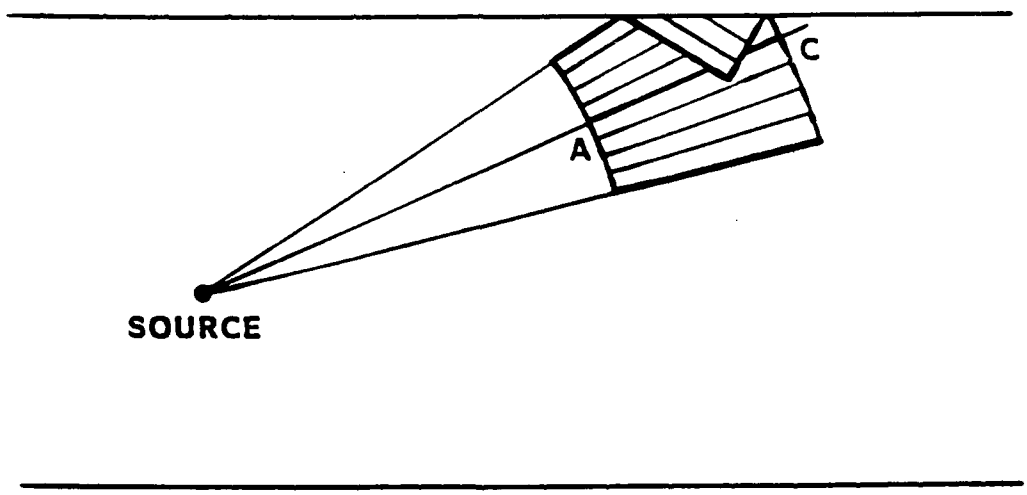

Figure 3.13 Partial reflection of a volume cell. In this case, the center ray of the cell, $\overline{AC}$, may not be used to indicate whether a reflection has occurred.

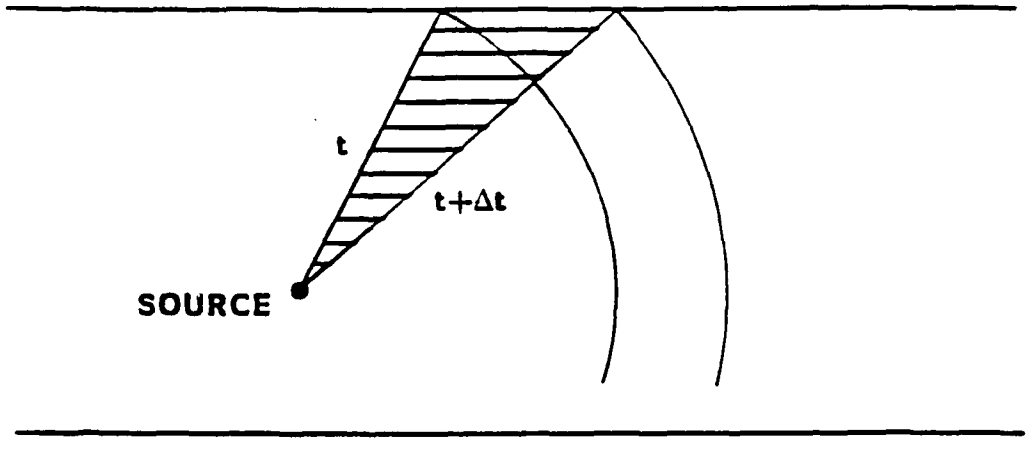

Figure 3.14 **The shaded area is a surface solution sector.**

illustrated in Figure 3.15. Examples of volume cells which fall outside the surface-solution sector are shown in Figures 3.16 and 3.17. An additional surface-solution sector is produced each time a surface reflection occurs. Existing in the same manner as surface-solution sectors, of course, are bottom-solution sectors.

In RAYSCT, a complete set of boundary-solution angles, resulting from all surface and bottom reflections, is accumulated and added to the list of critical angles. However, after the reverberation at one time has been computed, and the next time increment is considered, all of the boundary-solution angles change. The angles intersecting the surface and bottom are generally more shallow for a longer time interval between transmitting and receiving. Thus, a new set of boundary-solution angles must be determined for each time increment. The list of critical angles, to which these are added, however, remains constant. Their only dependencies are on the source location and the sound velocity profile.

When a non-isovelocity environment is present, the Doppler shift component for a moving scatterer is not determined by using the same parameters that are used for a moving source. The speed of sound, as well as the angle of the ray, may vary from the source location to the scatterer location. It turns out, however, that, due to Snell's law, the effect of a different angle at the scatterer is negated by the effect of a different speed of sound, with a reference to the transmitted angle and the speed of sound at the source. Appendix *F* offers a more detailed explanation. Hence, in the case of a monostatic return, the speed of sound and transmitted angle at the source may actually be used along with the velocity of a scatterer to determine the Doppler shift caused by that scatterer. In RAYSCT, the speed of sound and incident angle at the scatterer have been used, first, so that the option of implementing bistatic scatter to the problem may be left open for future research, and secondly, simply because the parameters needed were readily accessible from the raytracing programs.

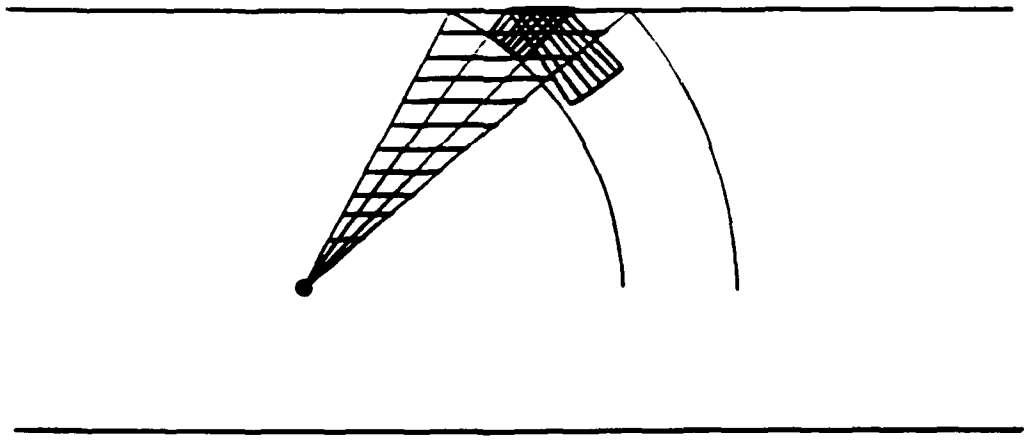

Figure 3.15 The volume cell shown falls within the surface-solution sector.

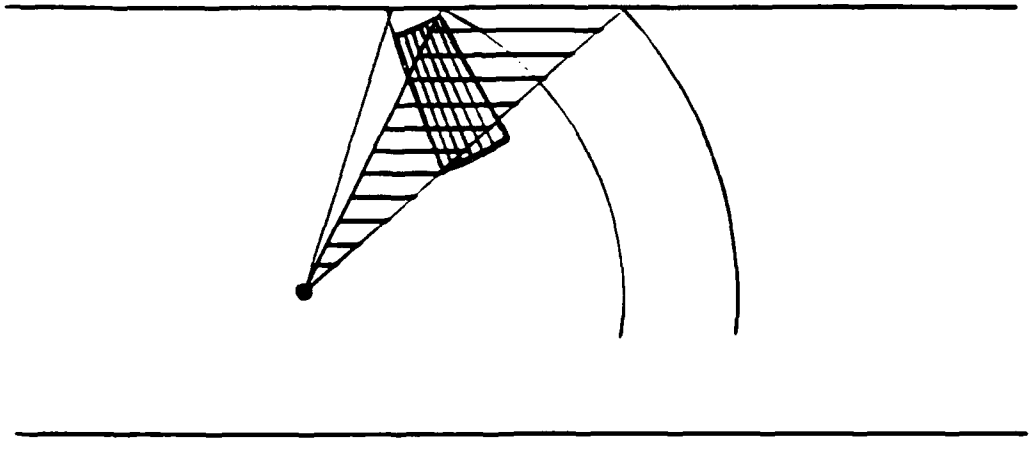

Figure 3.16 The volume cell shown falls above the surface-solution sector.

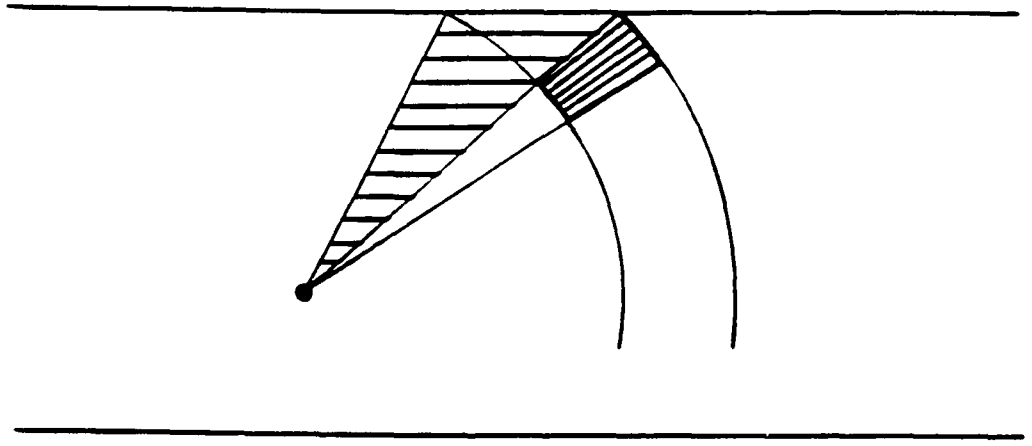

Figure 3.17 The volume cell shown falls below the surface-solution sector.

A similar case has arisen concerning the backscattered Gaussian frequency distribution for each cell. Although all cells of the same type, surface, volume, or bottom, have been assumed to have the same random velocity distribution, the Gaussian frequency distributions, which are a direct result of the velocity distribution, may vary from cell to cell. This is due to the varying speed of sound throughout the medium. The Gaussian frequency distribution is calculated as a random Doppler shifting through the use of the Gaussian scatterer speed distribution, the transmitted frequency, and the speed of sound at the cell. Since, in RAYSCT, the speed of sound at the scatterer may vary, so may the Gaussian frequency distribution. This distribution is calculated once for each horizontal row of cells in RAYSCT. Actually, because the speed of sound is constant everywhere along the surface and the bottom, only volume cells can have a varying Gaussian frequency distribution.

Since reflections are not permitted in the isovelocity reverberation model, some assumptions had to be made in its modification. First, specular reflections were assumed, in which the angle of incidence is equal to the angle of reflection. It was assumed that no frequency spreading occurs during a reflection; the only frequency spreading allowed is that which occurs during the backscattering process. Another assumption that was made is that losses due to surface and bottom reflections are independent of both frequency and grazing angle. The incorporation of complicated reflection loss functions into RAYSCT in the future is anticipated. The code has been written for the program to conveniently accept these functions. At the present, though, two loss factors, one for the surface and one for the bottom, are used as input variables to the modified program.

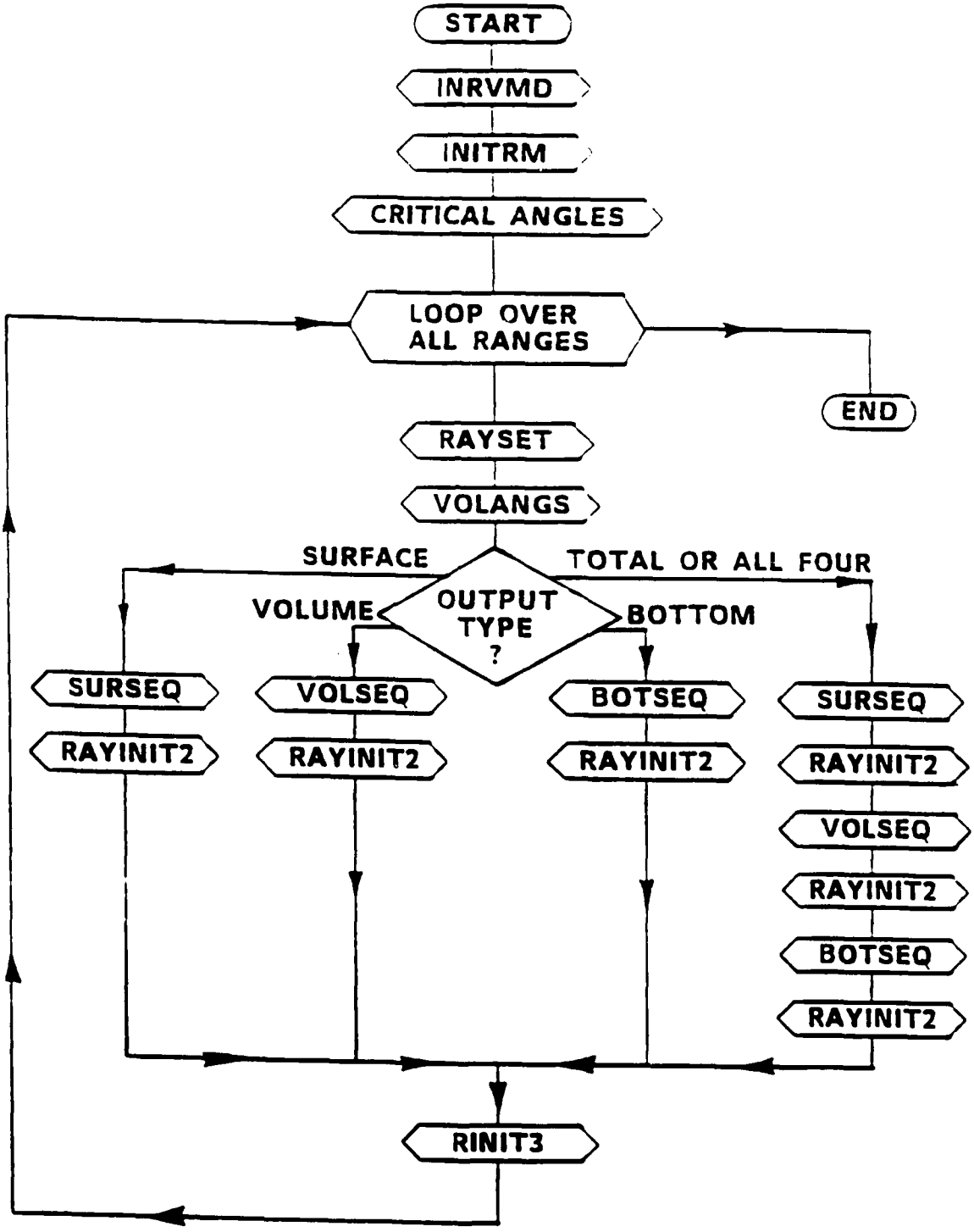

Figure 3.18 **Program RAYSCT.**

3.2.2. Modified Algorithm for the Scattering Function Calculation

Several raytracing subroutines have been written for the modified version of the scattering function program, RAYSCT. Figure 3.18 is a flowchart of the basic operation of this program. A hierarchy diagram of the subroutines called from RAYSCT to produce the modified scattering function is shown in Appendix *G*. Some of these routines had been found originally in SCATTER, some are based on subroutines from SCATTER, and some are new raytracing subroutines written primarily for the modification of SCATTER. The asterisks in Appendix *G* signify subroutines from SCATTER which were left unchanged in the modified program. In this section, the functions of the new subroutines which appear in RAYSCT are discussed.

The input to the new program, RAYSCT, is quite similar to the input for the original program, SCATTER. However, there are some important differences. Program RAYSCT accepts a sound velocity profile (SVP), instead of a constant speed of sound. This SVP consists of up to fifty depth-velocity point pairs. The ocean depth need not be input since it is predetermined by the maximum depth of the SVP. An absorption coefficient is calculated for each constant velocity gradient layer in the SVP. Power loss factors for surface and bottom reflections are added to the list of input variables. The total spread in elevation of the grid is always assumed to be one hundred eighty degrees. An upper limit on the vertical cell size is an input variable as the vertical cell size may vary. Finally, the input variables for distances in meters have been changed to times in seconds where appropriate.

Several of the raytracing routines, which had been written for the modified program, initialize certain parameters. These parameters are used to set up a new grid for the incremental scattering function accumulation. In the subroutine

CRITICAL_ANGLES (Appendix *H*.1), a complete set of critical angles between plus and minus ninety degrees, with a reference of zero degrees as horizontal, are calculated. These are used to define the critical sectors, regions throughout which all rays behave similarly. The critical sectors are actually formed in RAYSET (Appendix *H*.2) from the list of critical angles. In the subroutine RAYBOUND (Appendix *H*.3), these critical sectors are searched for all sets of rays which hit a surface or bottom boundary within the scattering volume. Each set of rays determined in RAYBOUND is designated as either a surface or a bottom-solution sector. Subroutines TIMEBOUND, BROKEN, ITERATION, and SOLBND (Appendices *H*.4, *H*.5, *H*.6, and *H*.7 respectively) are each called to iterate upon a solution for the angle of the ray which reaches a particular boundary at a specified time. In the last subroutine of the set up procedure, VOLANGS (Appendix *H*.8), a list of volume angles is compiled by the addition of all surface and bottom-solution angles to the set of critical angles. These angles are called volume angles because they are used to divide the ensonified volume into sectors. The sectors are later subdivided into vertical grid cells.

Once all of the sectors have been defined for a particular time, the scattering function accumulations are begun. Whereas one loop to sweep through all cells from the surface to the bottom is used in SCATTER, three different subroutines are called to perform this function in RAYSCT. These subroutines are called SURSEQ (SURface Sonar EQuation), VOLSEQ (VOLume Sonar EQuation), and BOTSEQ (BOTtom Sonar EQuation). Flowcharts for these subroutines are located in Appendices *H*.9, *H*.11, and *H*.12 respectively. Appendix *H*.10 is a flowchart for SPECTRAL DENSITY SECTION B, which is referred to in Appendix *H*.9.

In the subroutine SURSEQ, every surface-solution sector is processed individually. Each sector is divided into equal-sized vertical angular increments

which are smaller than or equal to an input maximum vertical cell size. The horizontal angular cell size, $\triangle\theta$, is constant for all cells at all times and is an input variable to the program. The non-isovelocity environment has no effect on the angular horizontal grid cell size since the speed of sound has been assumed to be a function of depth only. In general, a different-sized patch of surface area is ensonified by each surface reverberation cell. Subroutine TIMEBOUND is used to trace the upper and lower bounding rays of the cell to the surface, thus determining the length of the ensonified patch. The width of the patch, w, is determined through the use of the azimuthal angular increment, $\triangle\theta$, and the radial arm, r, from the vertical axis through the source to the center of the scattering element.

$$w = r\triangle\theta. \tag{3.8}$$

Figure 3.19 displays the geometry used in the determination of the grid cell width and a general illustration of a surface reverberation cell. Once the ensonified area (length times width) of the surface has been determined, the spectrum and relative power gain of the scattering function are computed through the same process used in SCATTER. The subroutine used for calculating Doppler shift in SCATTER has been modified to accept different angles and speeds of sound which occur at different scattering elements. The new subroutine is called RAYDOP and a subroutine is shown in Appendix *H*.13. After all surface-solution sectors have been processed, the volume and bottom sectors are processed in a like manner.

Subroutine VOLSEQ is used to determine the scattering function for all volume cells. The sectors formed from the volume angles are each divided into cells as was done in SURSEQ. In the determination of the backscattering level for each volume cell, a backscattering coefficient is multiplied by the volume of

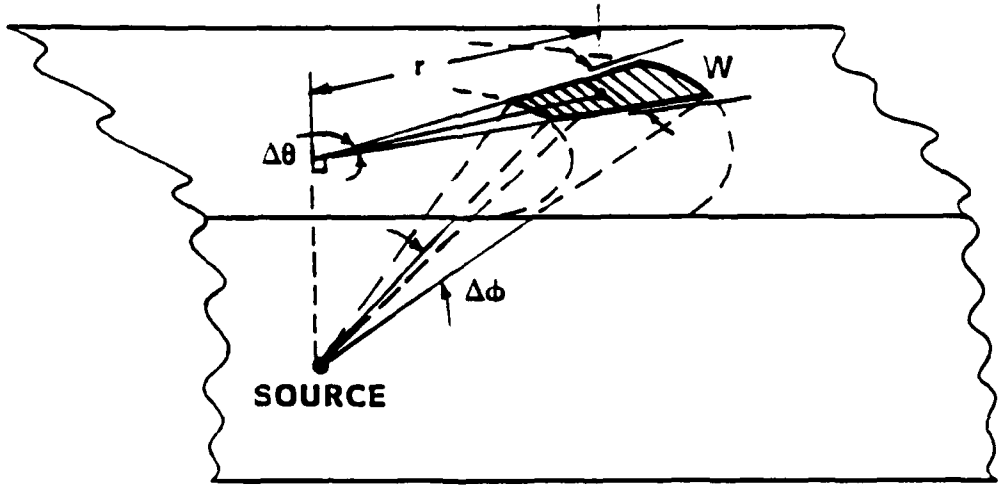

Figure 3.19 Surface reverberation cell.

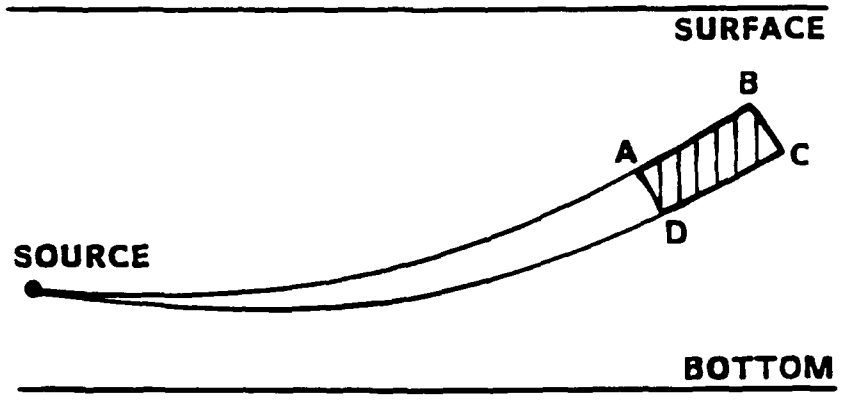

Figure 3.20 Vertical wall of a volume reverberation cell.

each cell. This volume is determined by tracing rays to points A, B, C, and D as shown in Figure 3.20. Subroutine RAYSPOT (Appendix H.14), which utilizes subroutines TURN and PIECES (Appendices H.15 and H.16), is used to trace the four rays. These four points form a vertical wall of the cell, which, when multiplied by the cell width, yields the volume of the cell. The width of the volume cells is determined in the same manner as the width of the surface cells, by the product of the radial arm, r, to the center of the cell, and the azimuthal incremental angle, $\triangle\theta$. An algorithm for dividing a volume cell at a boundary, if necessary, is also implemented in VOLSEQ.

In the final SONAR equation subroutine, BOTSEQ, all of the bottom-solution sectors are processed for their contributions to the scattering function. The same procedure that is used in SURSEQ is followed in BOTSEQ, with one exception. In SURSEQ, the surface wave speed is used to obtain an additional Doppler shift component. This component cannot exist for the bottom of the ocean as the bottom is assumed stationary. Otherwise, through the use of the bottom-solution sectors and all additional bottom-related parameters, the contribution by the ocean bottom to the scattering function is determined in an algorithm similar to that in SURSEQ.

Once the scattering function for each type of reverberation has been calculated, the components due to the surface, volume, and bottom are combined to yield the total scattering function. It may be specified beforehand, however, that only one type of reverberation is to be processed. In distinguishing the different types of reverberation, the convention that is used in the isovelocity model, SCATTER, is maintained. The type of reverberation is dictated by the type of element actually doing the backscattering. Surface reverberation has been assumed to be the compilation of all returns which are backscattered from the surface, even though a certain number of returns may have reflected from

the bottom several times. Likewise, bottom reverberation is comprised of all of the backscattered energy from the bottom. All of the remaining reverberation is, therefore, due to volume backscattering.

3.2.3. Capabilities and Output from RAYSCT

The revised reverberation modeling program, RAYSCT, has been written to perform the same functions as SCATTER. These are to produce either a power gain versus time plot or a spectral density plot for the scattering function. However, many more physical factors have been taken into account in the revised model than in the original. A sound velocity profile, with the capability of handling up to fifty constant velocity gradient segments, has been introduced. A different absorption coefficient is represented in each of these segments. Also, multiple forward reflections are allowed, along with associated loss factors for surface and bottom reflections. These additions provide a simulation of more realistic underwater environments.

The output from RAYSCT is in the same format as the output from SCATTER as described in section 3.1.3. Therefore, sample plots have not been included in this section. The analysis of the revised model has been reserved for Chapter 4.

Chapter 4

COMPARISON OF REVERBERATION MODELS

4.1. Introduction

The results presented here are comparisons of the spectral densities and power gains of scattering functions produced by the original model, SCATTER, and the revised model, RAYSCT. Because of the very large number of parameters which govern the output from these models, as many as possible have been kept constant, limiting the number of comparisons made. There are many features of the original model which have been left unchanged in the revised model: thus, it was not necessary to dwell upon them. In this section, the presence of multiple boundary returns has been analyzed with respect to the original model. Additionally, the effects of different sound velocity profiles have been compared to the isovelocity case.

The raypaths for all surface and bottom returns in this chapter are referenced by the state numbers, KA and KB. KA has been defined as the number of times a ray passes through the region between the source and the surface, and KB as the number of times a ray passes through the region between the source and the bottom. The state numbers that correspond to a particular return define the raypath to that boundary from the source, and not from the source to the boundary and back. For example, if a bottom return has occurred after a surface reflection, the path to the boundary would have gone from the source to the surface and then to the bottom. This path is represented by the state numbers, $KA = 2$, and $KB = 1$, and is denoted by "$(2-1)$". The state number corresponding to the region above the source, KA, is always listed first.

4.2. Description of the Different Scenarios Used

The only input variables to the new model that differ from those of the original model are the surface and bottom reflection loss factors. For the scenarios chosen as examples, four parameters were varied. These include the source depth, the ocean depth, the elapsed time between transmitting and receiving, and the sound velocity profile. Lists of the input variables for all examples to be shown appear in Appendix *E*. For these examples, the source depth may be either one hundred or three hundred meters below the surface, and the ocean depth, either five hundred or two thousand meters. An isovelocity profile is used for some examples and a sound velocity profile consisting of both a negative gradient layer and a positive gradient layer is used for others.

Two types of environments were chosen to be used for comparison. The first is a somewhat shallow ocean with an isovelocity profile. It will serve to show the results of the inclusion of multiple boundary returns. In the second example, the ocean has been set quite a bit deeper and a sound velocity profile consisting of a decreasing speed of sound with depth, followed by an increasing speed of sound with depth, has been used. Although the example shows some effects of multiple boundary returns, the main emphasis should be placed on the effects of the sound velocity profile.

4.3. Discussion of Results

4.3.1. Multiple Boundary Returns

A scenario which includes a moving source has been shown to best illustrate the effects of the surface and bottom boundary returns. Therefore, the examples that were chosen for the comparison of the multiple boundary return model to the single boundary return model include a moving source.

The first scenario used for comparison is identical to that used for Figures 3.3 and 3.5. The ocean is 500 meters deep and the source is moving with a velocity of 5 meters per second at a depth of 300 meters below the surface. The speed of sound is a constant 1500 meters per second. The purpose of this first example is to compare a multiple boundary return scattering function to a single boundary return scattering function. Raytracing is still used, but refraction is not a factor.

The plots generated from the original model, SCATTER, have already been discussed in Chapter 3. Recall the power gain versus time plot of Figure 3.3 and the single spectrum plot of Figure 3.5. In the single spectrum plot, the surface and bottom contributions aopear at different Doppler shift values implying a different angle of backscattering from the surface than from the bottom. The degree of Doppler shifting of the surface and bottom returns will also be shown to be very important in the analysis of the multiple boundary return examples.

For the comparable RAYSCT example, all input parameters were kept the same as in the original model. The only input variables added to the revised model are the loss factors for surface and bottom reflections. For this example, raytracing is used to demonstrate multiple boundary returns, but as the velocity gradient has been set equal to zero, straight-line propagation results. The input parameters for the first RAYSCT scenario may be found in Appendix E.3.

Figure 4.1 contains the power gain versus time curves for the surface, volume, bottom, and combined total contributions to the scattering function. The additional surface and bottom boundary returns are seen to cause a slightly slower decay in the power gain curve as compared to the power gain curve of Figure 3.3. The individual surface and bottom contributions also decay more slowly than in Figure 3.3 because of the increased energy from the additional boundary returns. The volume reverberation, also, has a lower decay rate

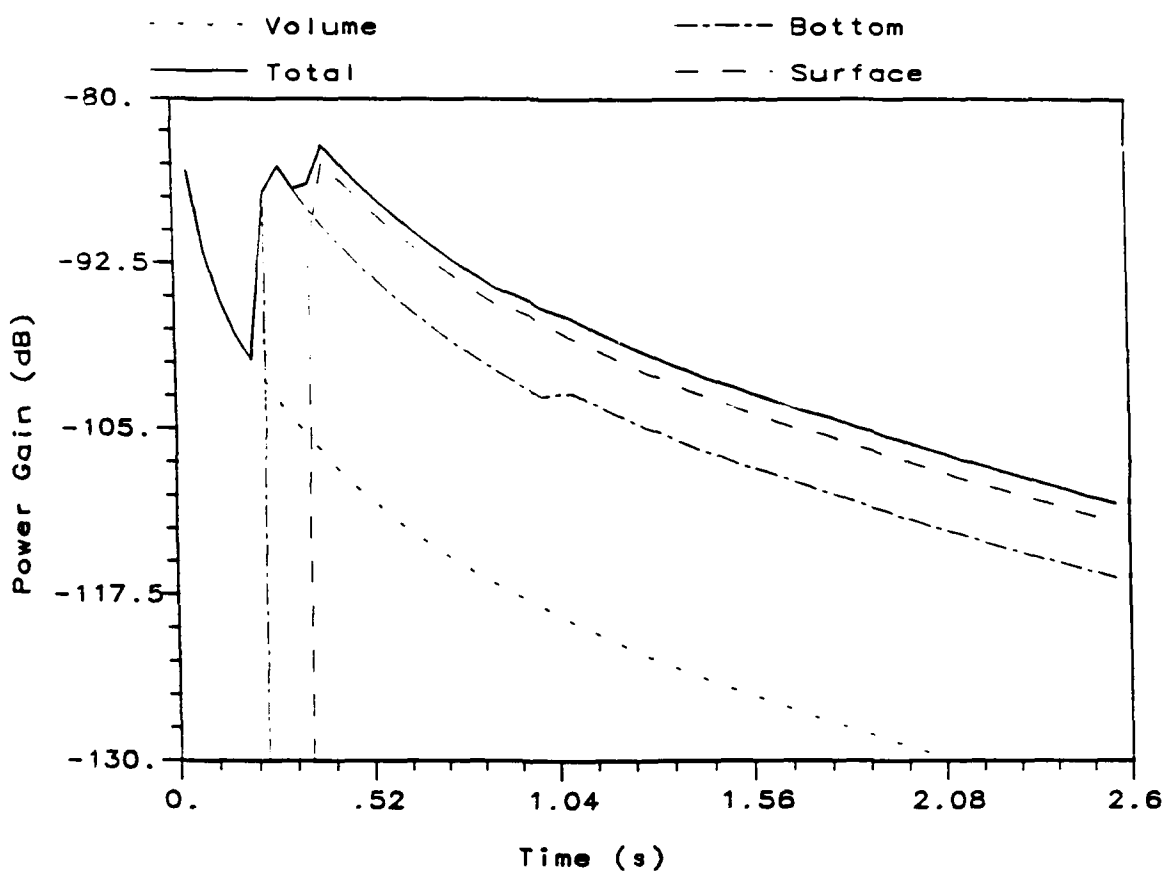

Figure 4.1 Output from RAYSCT. Power gain versus time plots for the surface, volume, bottom, and combined total. Ocean depth: 500 m.

associated with it. This is due to the additional volume reverberation originating after the occurrence of boundary returns.

It might be observed that the first occurrences of surface and bottom returns in Figure 4.1 appear at a slightly lower level than those in Figure 3.3. This is because the approximations for the ensonified areas of surface and bottom cells is more accurate in the revised model, RAYSCT. The width of the cell is approximated by the arc across the middle of the grid cell in RAYSCT (Figure 3.22), as opposed to the arc at the front (smaller end) of the grid cell as is assumed in SCATTER. The approximation in RAYSCT yields larger, but more accurately represented grid cells, which directly accounts for a slightly lower intensity than the approximation in SCATTER.

Figure 4.2 is a spectral density plot taken at a time of 1.74 seconds. The peak at zero Doppler shift is due to a combination of the first surface $(1-0)$ and the first bottom $(0-1)$ returns. These returns occur at or near zero Doppler because the time at which the spectrum was taken is such that the grazing angles of these returns at the boundaries are quite low. The next peak to the left, at approximately -60 Hz Doppler shift, is due to the next pair of surface $(1-2)$ and bottom $(2-1)$ returns. These returns are just approaching the zero Doppler point and appear in the same frequency region as each other. The next frequency peak in Figure 4.2, occurring at about -170 Hz Doppler shift, is solely the third bottom $(2-3)$ return. The third surface $(3-2)$ return with which it is paired, has not quite merged with it to the same frequency region. At this time ($t = 1.74$ seconds), the volume contribution may be observed at low levels between -100 Hz and $+30$ Hz Doppler shift.

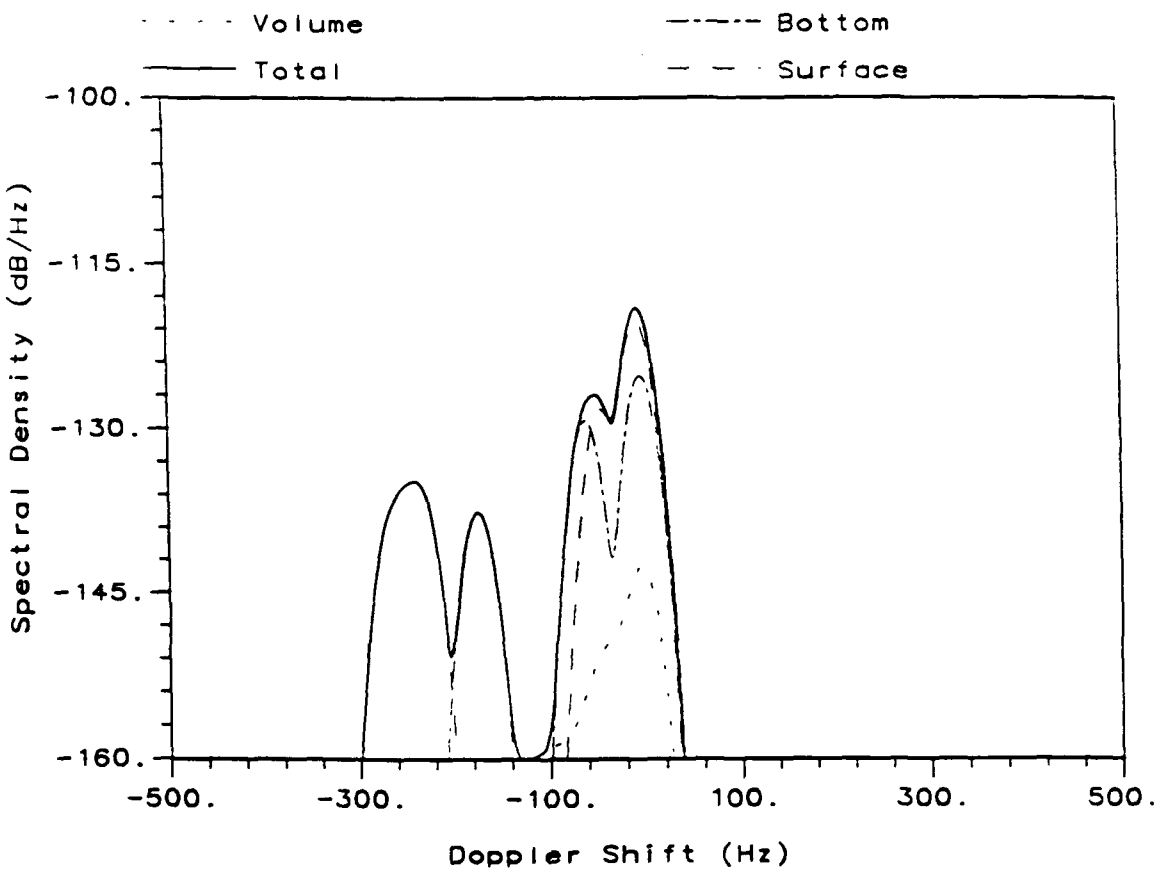

Figure 4.2 **Output from RAYSCT. Surface, volume, bottom and total contributions to the scattering function spectrum at a time of 1.74 s.**

4.3.2. Non-isovelocity Profile

Raytracing may have drastic effects on the scattering function. The scenario in the next example presented consists of a longer time interval than in the first set of examples. The source is situated one hundred meters from the surface at a 2000-meter ocean depth. The source has a velocity of five meters per second and all scattering elements have a mean velocity of zero. One set of plots has been generated by SCATTER. In this set, an isovelocity profile and no reflections at the boundaries have been assumed. A comparative set of plots has been generated by RAYSCT, the modified program. For these plots, the options of a non-isovelocity profile and the allowance of multiple boundary returns have been exercised.

A power gain versus time plot is shown in Figure 4.3 for the surface, volume, bottom, and total contributions to the scattering function for the isovelocity case, SCATTER. The input variables that were used are shown in Appendix *E*.4. The curves in Figure 4.3 are quite similar to the curves which appeared in Figure 3.3. The major difference is that, in Figure 4.3, the surface return, which has occurred almost immediately after transmitting, now precedes the bottom return. This bottom return, it can be seen from the figure, appears at a time equal to about 2.5 seconds. The times corresponding to the surface and bottom returns result directly from the situation of the source in the ocean; it is very close to the surface, and relatively far from the bottom. The surface reverberation seems to dominate for the entire range shown.

For the non-isovelocity case, the scattering function proves to be quite different. The sound velocity profile that was used is shown in Figure 4.4. This type of profile might be the result of a warm ocean surface suspended above a colder layer of water. Thus, the decrease in temperature, and also sound speed,

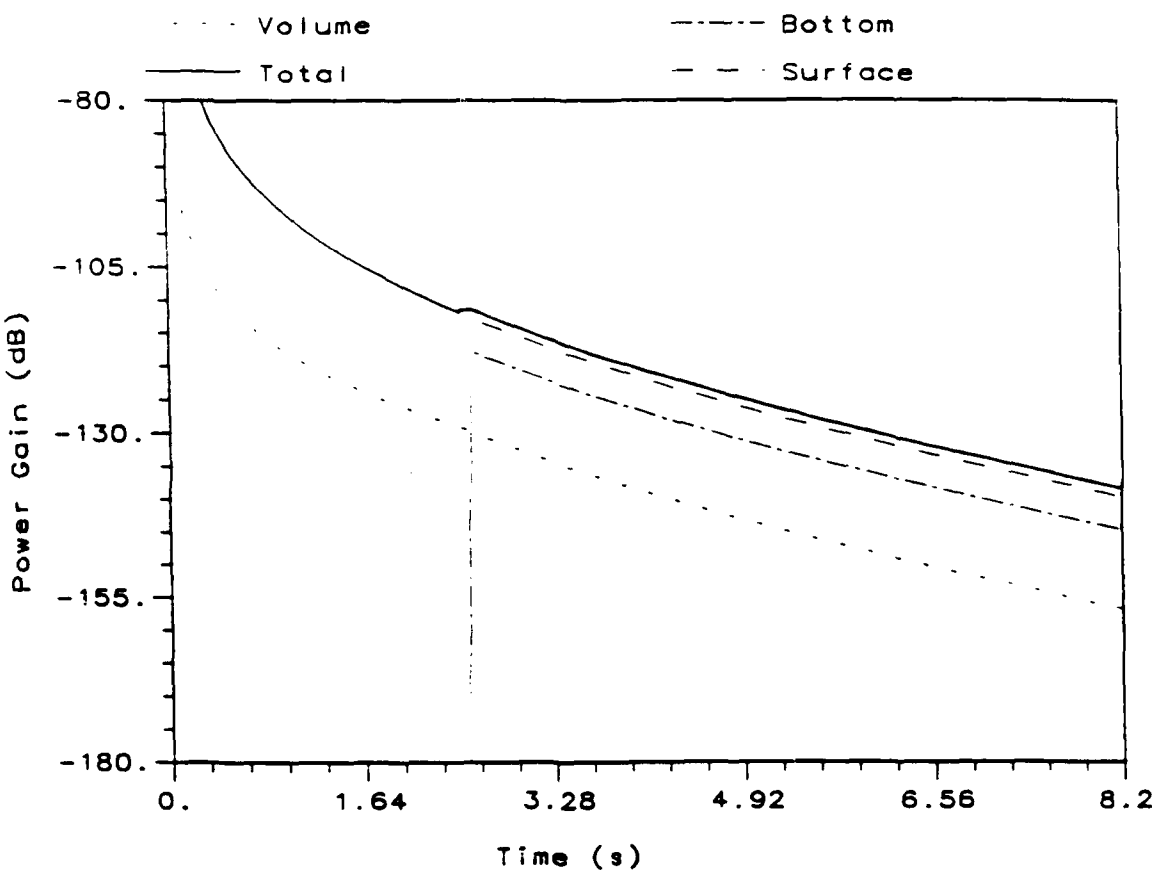

Figure 4.3 Output from SCATTER. Power gain versus time plots for the surface, volume, bottom and combined total. Ocean depth: 2000 m.

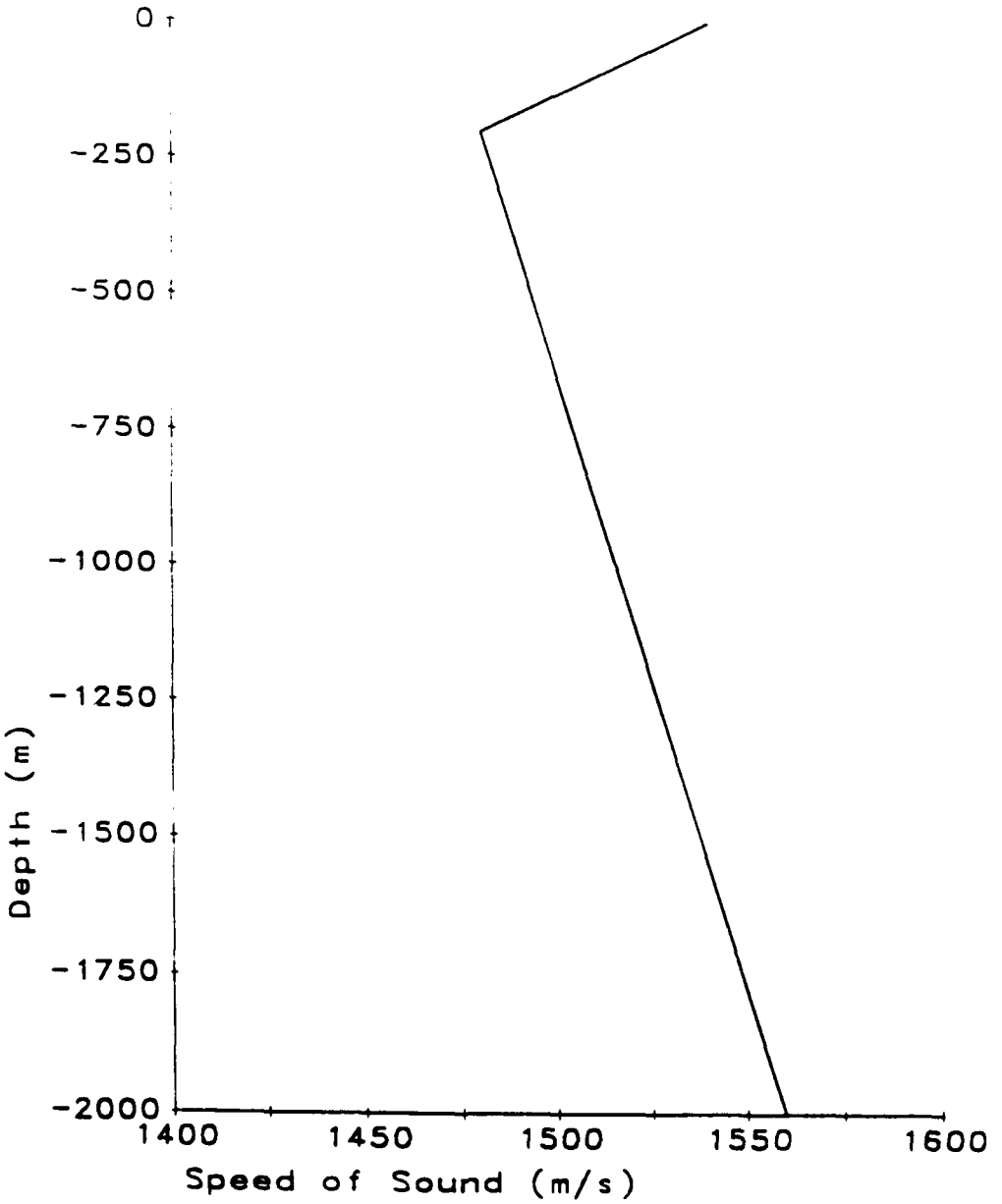

Figure 4.4 **Sound velocity profile.**

is evident to a depth of two hundred meters. The increase in the speed of sound with depth below two hundred meters would be due to the pressure increase with depth.

Power gain versus time plots for the surface, volume, bottom, and total contributions to the scattering function are shown in Figure 4.5. The input parameters that were used are shown in Appendix $E.5$. The surface reverberation has actually disappeared after a time of about 1.3 seconds. This occurs during the $(1-0)$ surface return. The ray diagram shown in Figure 4.6 explains this phenomenon. The rays have been traced for 2.5 seconds in two clusters of equispaced transmit angles: $9^\circ \leq \phi \leq 13^\circ$ in one half degree increments and $-88^\circ \leq \phi \leq -80^\circ$ in two degree increments. At the time at which the surface return vanishes, there is no possible ray solution to the surface; thus, there can be no surface reverberation. A critical ray, transmitted at 11.3 degrees, grazes the surface at a time of 0.66 seconds. Any ray transmitted at an angle higher in elevation than this critical angle, is reflected from the surface and yields volume reverberation. Any ray transmitted below this critical angle is refracted away from the surface and also yields volume reverberation. This refraction of energy away from the surface forms a shadow zone, a region in which the acoustic intensity is extremely weak compared to neighboring regions. The shadow zone, which is shown in Figure 4.6, begins at a time of 0.66 seconds. This shadow zone directly accounts for the loss in surface reverberation at a time of 1.3 seconds. Although the acoustic intensity is weak in a shadow zone, Figure 4.5 shows the model predicts that the surface return will vanish completely. This is because ray theory predicts zero intensity in a shadow zone.

Figure 4.5 also shows that the surface reverberation reappears at some later time. The surface return is rejuvenated, not through a direct path to the surface, but from a bottom reflection. Although the direct surface return has vanished,

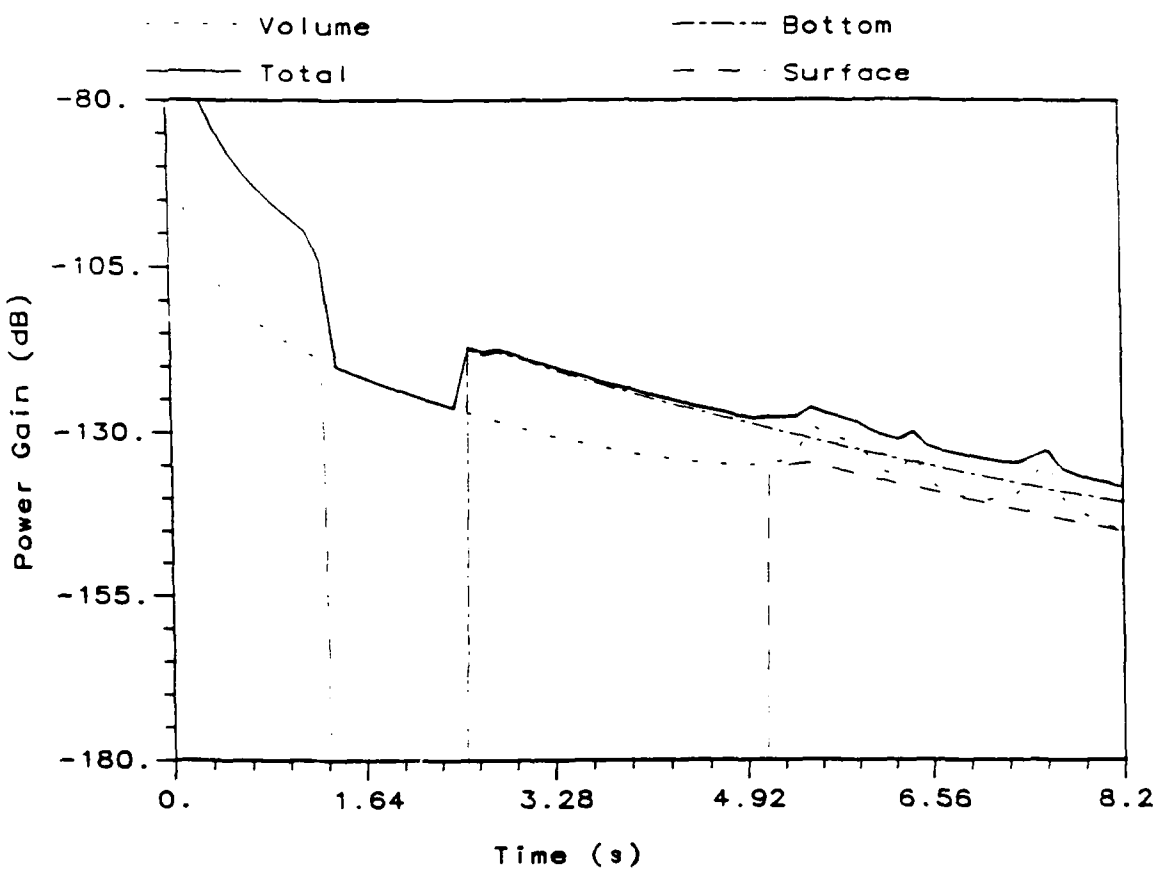

Figure 4.5 Output from RAYSCT. Power gain versus time plots for the surface, volume, bottom and combined total. Ocean depth: 2000 m.

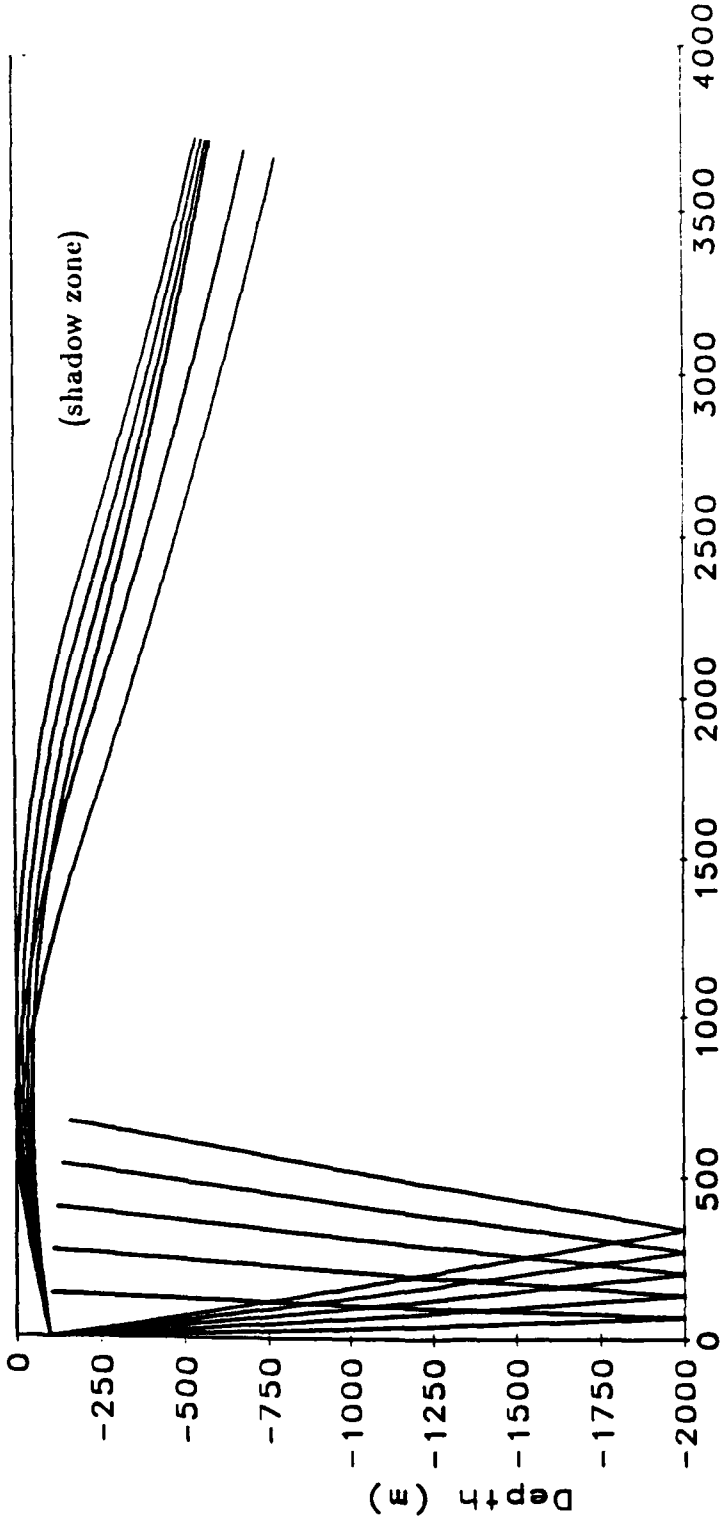

Figure 4.6 The ray diagram illustrates the emergence of a second surface return through a bottom reflection.

the somewhat attenuated $(1-2)$ source to bottom to surface return is very evident at a time of about 5.1 seconds. This surface return is weak since it has undergone two bottom reflections, one on the way to the scatterer, and one along the same path back to the source. In fact, the reverberation is dominated by the bottom contribution at this point.

Another peculiarity of Figure 4.5 may be observed in the volume component of the scattering function beyond the approximate 4.9 second mark. The power gain has increased rapidly and the curve has lost its smooth, continuous decay. For investigative purposes, a ray diagram of a portion of the volume has been generated as shown in Figure 4.7. The rays in the range of $-10° \leq \phi \leq +10°$ have been traced for 8 seconds. It can be seen that a strong caustic has formed at a distance of about 4000 meters. This would correspond to an approximate travel time of 5.3 seconds to the volume scattering elements and back to the receiver. The caustic region actually began at a distance of about 3500 meters and extends well beyond this. The volume contribution to the scattering function reflects this caustic. Additionally, the rays involved in the formation of the caustic have refracted away from the surface and the bottom, and therefore, have not experienced any reflection loss to these boundaries.

The increase in power gain due to the caustic may be explained as follows. The rays which vertically bound the cells involved in the caustic are shown to be converging in Figure 4.7, accounting for a very high intensity level at these cells. But, because the rays are very closely spaced, the volumes of these cells are small, accounting for relatively low backscattered levels. These low backscattered levels act to negate the high intensity levels incident on the volume scattering elements. The increased power gain shown in Figure 4.5 has, to this point, not yet been explained. It may not simply be attributed to a one-way focusing of energy on some localized region out in the field. The principle of acoustic reciprocity may

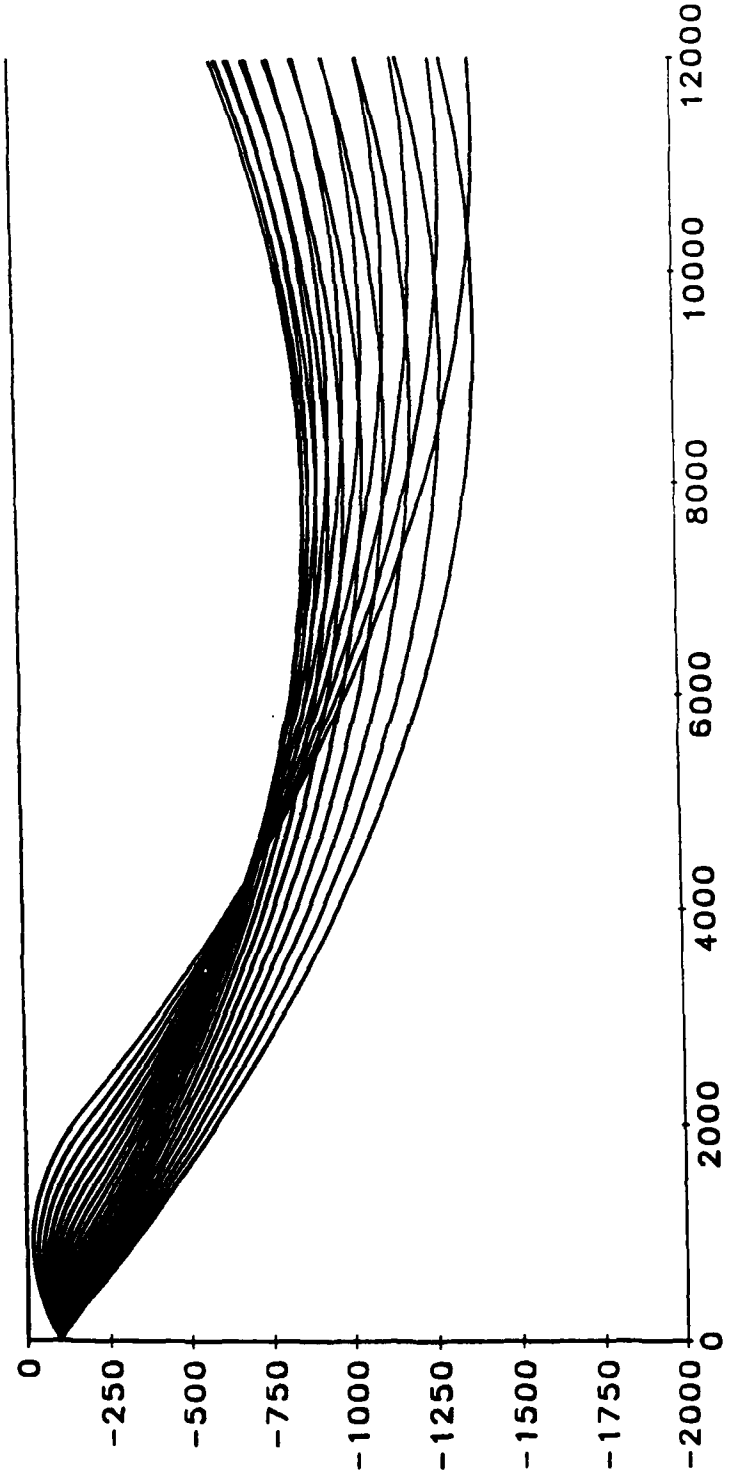

Figure 4.7 The ray diagram shows the existence of a strong caustic in the vicinity of 4000 m.

be used to shed some light on the problem. It states that, "if in an unchanging environment, the locations of a small source and a small receiver are interchanged, the received signal will remain the same" [6]. Utilizing this principle, it becomes clear that the backscattered sound from each cell involved in the caustic is focused back on the receiver in the same degree that the transmitted sound had been focused on the scatterer. It is this additional focusing of sound on the return path by many cells which is the cause for higher power gain levels at the receiver. Therefore, the rise in power gain that is shown in Figure 4.5 as the caustic is approached in time, should be expected.

Chapter 5

SUMMARY, CONCLUSIONS, AND RECOMMENDATIONS

5.1. Summary

Multiple boundary returns and non-isovelocity gradients can have significant effects on underwater acoustic reverberation originating from a moving pulsed source. An isovelocity reverberation model, which disallows surface and bottom boundary reflections has been modified to include raytracing and multiple boundary returns. The portion of the model which was revised is that used to compute the ocean scattering function which characterizes the received reverberation. It is independent of the transmitted pulse shape as well as its power level. Effects from the source and scatterer motion, the backscattering cross-section of the ocean elements, the acoustic beam effects, and the propagation losses are all considered in the determination of the scattering function.

In the modified scattering function computation, allowances for reflections from the air-water interface and the ocean bottom have been made. Reflection loss factors for surface and bottom reflections have been made input parameters to the revised model. Additionally, a depth-dependent sound velocity profile has been incorporated. As many as fifty depth-velocity pairs of points are allowed. The sound velocity profile has been assumed to consist of constant velocity gradient segments. The consequence of using such straight line segments is that the raypaths through any one horizontal stratification are arcs of circles.

A series of raytracing routines has been written to perform all raytracing functions required for the modification of the original scattering function program. The raytracing theory that has been used for the present model has been based on the theory from Clay and Medwin [2].

The raytracing routines have been written to perform two major functions. First, given a travel time, t, and an initial transmitted angle, ϕ_i, the final position of the ray is determined. The significance of this is that a constant time contour, over which to build a grid of cells, may be defined. In the original isovelocity model, the scattering functions from a spherical grid of cells are summed to obtain the total scattering function. A sphere is actually a constant distance contour. However, since the original model has assumed a constant sound speed, the sphere is also a constant time contour. When a non-isovelocity environment is introduced, the constant time contour no longer takes the shape of a sphere. The actual constant time contour is defined by the first raytracing function which yields the final position of a ray given the initial angle and the travel time. This raytracing routine also determines the final angle, path length, and absorption loss of the ray, as well as the numbers of surface and bottom reflections. Information from this routine is used to determine the reflection loss and the backscattering cross-section of any grid cell.

The second purpose of the raytracing package is to define all surface and bottom reverberation cells at a particular time. The original model has assumed that the only surface reverberation cells are those on the direct path from the source to the surface, and that the only bottom returns are on the direct path to the bottom. However, if the travel time is long enough, there may be a number of groups of both surface and bottom reverberation cells. In the raytracing routine in which the surface and bottom cells are defined, the travel time and the boundary of interest, either the surface or the bottom, are the input parameters. The angles, ϕ_i, of all rays which end at the boundary at the specified time are output from the routine. When the pulse length is known, this routine may be

used to determine all groups of transmit angles at the source which eventually yield surface or bottom reverberation cells. This routine is also used to determine the areas of the ensonified surface and bottom regions at a particular time.

The scattering function output from the original model assumed the form of either the power gain versus time or the spectral density of the scattering function for one particular time. The same convention is used for the output from the revised model, RAYSCT.

5.2. Conclusions

The inclusion of a non-isovelocity profile and multiple boundary returns to an isovelocity reverberation model has been shown to add a significant amount of detail to the scattering function of the ocean. Because of the allowance of reflections, the decay of the volume reverberation was not as rapid in the modified model. The additional surface and bottom returns have been shown in many cases to maintain the overall reverberation at a higher level in the revised model.

Even more pronounced differences have been shown in the frequency spectra of the scattering functions. When a source is in motion, a frequency offset is introduced for all scatterers that are off the axis of source motion. Thus, whenever a boundary return is observed for the first time on a scattering function versus time plot, it is maximally Doppler shifted, as its direction of arrival is ninety degrees off-axis of the source motion. For the cases that were presented, the multiple boundary returns were not shown to contribute enormously to the power gain curves, although, some significant differences were noted. However, the multiple boundary returns have been shown to contribute very significantly to the scattering function spectra.

When a non-isovelocity environment was introduced, the power gain curves, as well as the spectral density plots were sometimes observed to be extremely

different from the plots generated by the isovelocity model. In the example chosen, the surface reverberation went away completely after a certain length of time. This occurrence was shown, via raytracing diagrams, to be the result of a shadow zone at the surface. The surface component of the scattering function reappeared at a later time due to a different surface return. The path to the surface for the second return included a bottom reflection.

The particular example that was used to demonstrate ray effects did not show drastically different results than were expected for the bottom contribution to the scattering function. However, because the surface return had disappeared and then had returned at a lower level, the bottom component was seen to dominate the power gain versus time curve, even after the surface component had returned. This is an expected result because, although the surface backscattering coefficient had been input as a larger value than the bottom backscattering coefficient, the surface component had been attenuated during bottom reflection.

The volume reverberation from the non-isovelocity scenario has shown some very pronounced effects from a caustic region. The volume scattering function spectrum versus time was seen to increase at a time corresponding to the occurrence of the caustic. A ray diagram has been used to confirm the existence of this caustic. The increase in power gain was attributed to the focusing of backscattered energy from volume elements onto the receiver at the source location. The principle of acoustic reciprocity was used to point out that the focusing of energy is the same from a scattering element back to the receiver as it had been from the source to that scattering element. Therefore, the power gain in the case of a caustic was shown to be justifiably different from the power gain in an isovelocity scenario, in which spherical spreading exists along all paths both to and from all elements.

5.3. Recommendations for Further Work

In this effort, raytracing and multiple boundary returns have been introduced to an isovelocity reverberation model. Specular reflections, those in which the angle of reflection is equal to the angle of incidence, have been assumed. All reverberation has been assumed to result from backscattered energy only; the path from the scatterer back to the receiver is the same path as that from the source to the scatterer. This is referred to as the monostatic case. There are additional source to receiver paths which may exist, but they had been considered to be out of the scope of this effort. These reverberation paths, in which the return path is not the same as the path to the scattering element, may be referred to as bistatic returns. An example of such a return would be the raypath from the source to the surface, then to the bottom after a surface reflection, and finally back to the source from the bottom. This class of returns should be considered in the future. Some of the parameters of the model that would have to be examined if bistatic returns were to be incorporated are the Doppler shift, the grid cell depth, the bistatic scatterer radiation pattern and the acoustic beam effects. The Doppler due to a moving source would involve two factors: one resulting from the transmit angle and one resulting from the receive angle. The grid cell depth could no longer be defined as simply $\tau/2$, in seconds, because the energy would not be, in general, directly backscattered, but would be scattered at some other angle. The determination of the backscattering cross section should follow directly from the grid cell depth. Finally, the beam weighting factor would have to consist of a transmit beam attenuation at one angle, and a receive beam attenuation at some other angle.

Other work which would be beneficial to the model, would be the incorporation of frequency and grazing angle dependent scattering coefficients and

reflection loss factors. The FORTRAN computer code, which was written in this present effort, has been left open so that such modifications can be made.

Finally, the model should be tested for validity by running some comparisons to in-water data. For this to be done, actual acoustic beam patterns would have to be used, a transmit signal envelope and power level would have to be known, as well as some detailed information on the particular environment used. This would include an accurate sound velocity profile, the wind speed, the bottom type, the sea state, and the existence of any moving current layers. The revised model's performance on the prediction of reverberation from caustics and shadow zones should also be verified.

APPENDIX A

DOPPLER SHIFT CALCULATIONS

A.1. Source and Receiver Motion

Let V represent the source velocity. The Doppler, resulting at an angle, γ, from the axis of source motion, is related to the component of the source velocity in that direction. This component, v, is equal to $V \cos\gamma$.

During a pulse of duration, τ seconds, and frequency, f_o, there exist N cycles. The following relation holds:

$$f_o = \frac{N}{\tau} . \tag{A.1}$$

The length of the pulse is $c\tau$ in meters, where c is the speed of sound in meters per second. Consider the leading edge of a pulse, transmitted at a time, t_o, from a moving source, at some point, x_o. By the time the trailing edge is transmitted, the leading edge will have traveled a distance of $c\tau$ from its point of origin, x_o. The source, itself, however, will have traveled a distance of $v\tau$, where $v = V \cos\gamma$. The length of the transmitted pulse in the water is the difference between the leading and trailing edges of the pulse,

$$c\tau_D = c\tau - v\tau = (c - v)\tau \tag{A.2}$$

where τ_D is the duration of the Doppler-shifted, transmitted pulse. From equation $A.2$,

$$\tau_D = \frac{(c - v)\tau}{c}. \tag{A.3}$$

The Doppler-shifted frequency may be represented as

$$f_D = \frac{N}{\tau_D}. \tag{A.4}$$

Substitution of equation $A.3$ into $A.4$ yields

$$f_D = \frac{Nc}{(c - v)\tau} = f_o \left(\frac{c}{c - v}\right). \tag{A.5}$$

This may be rewritten as

$$f_D = f_o\left(\frac{1}{1-\frac{v}{c}}\right) = f_o\left(1+\frac{v}{c}+\frac{v^2}{c^2}+\cdots\right). \qquad (A.6)$$

For $v \ll c$, the higher ordered terms of the series in equation $A.6$ may be neglected, yielding

$$f_D = f_o\left(1+\frac{V}{c}\cos\gamma\right). \qquad (A.7)$$

For the case of a moving receiver, the same reasoning applies. If f_D returns to the receiver at the same angle, γ, off of the axis of receiver motion, then the received frequency, f_R, may be expressed as

$$f_R = f_D\left(1+\frac{V}{c}\cos\gamma\right) = f_o\left(1+\frac{V}{c}\cos\gamma\right)^2. \qquad (A.8)$$

Again, if the higher ordered terms are considered negligible, the received frequency becomes

$$f_R = f_o\left(1+\frac{2V}{c}\cos\gamma\right). \qquad (A.9)$$

A.2. Scatterer Motion

A somewhat different situation arises when the transmitted signal is backscattered from some moving point, x_s. The pulse, of frequency, f_o, begins with a length of $c\tau$ before backscattering. Consider a scatterer, moving with a velocity, U, at some angle, γ, from the direction of the approaching pulse. The component of the scatterer velocity in the direction of the pulse, u, is equal to $U\cos\gamma$.

At some time, t_o, the leading edge of the pulse reaches the scattering point, x_s. As the pulse folds back over itself, the trailing edge reaches the new scatterer position, x_s', in some time Δt, after the front of the pulse had reached the scatterer. The distance traveled by the trailing edge in the time, Δt, is

$$\Delta x_1 = c\Delta t. \qquad (A.10)$$

See Figure *A*.1. The leading edge of the pulse is labeled, L, and the trailing edge, T. In the same amount of time, $\triangle t$ the scatterer has moved from x_s to x_s', a distance of

$$\triangle x_2 = u\triangle t. \tag{A.11}$$

From the figure, it can be seen that the original pulse length, $c\tau$, is equal to the sum of $\triangle x_1$ and $\triangle x_2$.

$$c\tau = c\triangle t + u\triangle t = (c+u)\triangle t. \tag{A.12}$$

The length after backscattering, $c\tau_D$, is the difference between the leading and trailing edges of the pulse after $\triangle t$ has passed. The distance of the leading edge of the pulse from the original point, x_s, at time, $\triangle t$, is

$$x_L = c\triangle t, \tag{A.13}$$

and the distance of the trailing edge from the same point, is

$$x_T = u\triangle t. \tag{A.14}$$

The difference in these distances is the Doppler-shifted pulse length.

$$c\tau_D = c\triangle t - u\triangle t = (c-u)\triangle t. \tag{A.15}$$

From equation *A*.12,

$$\triangle t = \frac{c\tau}{(c+u)}. \tag{A.16}$$

Whereas, from equation *A*.15,

$$\triangle t = \frac{c\tau_D}{(c-u)}. \tag{A.17}$$

Equating equations *A*.16 and *A*.17,

$$\tau_D = \frac{\tau(c-u)}{(c+u)}. \tag{A.18}$$

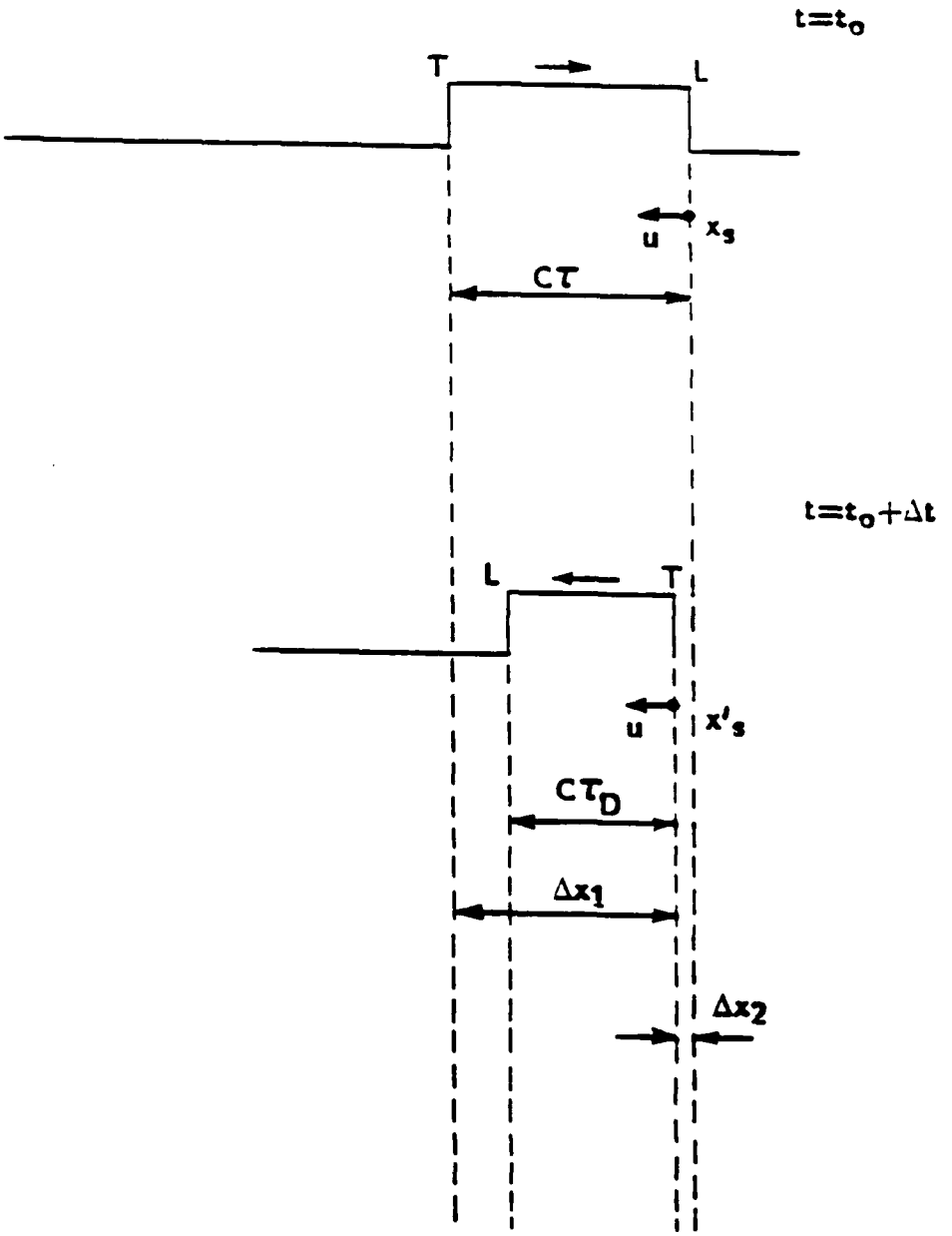

Figure A.1 The length of a pulse decreases as it is backscattered from an approaching scatterer.

Incorporating equations $A.1$ and $A.4$ into $A.18$, the backscattered, Doppler-shifted frequency may be expressed as

$$f_D = f_o \left(\frac{c+u}{c-u} \right) = f_o \left(\frac{c+u}{c\left(1-\frac{u}{c}\right)} \right). \qquad (A.19)$$

This may be rewritten as

$$f_D = \left(1+\frac{u}{c}\right)\left(\frac{1}{1-\frac{u}{c}}\right) = f_o \left(1+\frac{u}{c}\right)\left(1+\frac{u}{c}+\frac{u^2}{c^2}+\cdots\right). \qquad (A.20)$$

Finally, if $u \ll c$, the higher ordered terms may be neglected and the following result obtained:

$$f_D = f_o \left(1+\frac{2U}{c}\cos\gamma\right). \qquad (A.21)$$

APPENDIX B

SAMPLE CLASS OF RAYS

K = 1

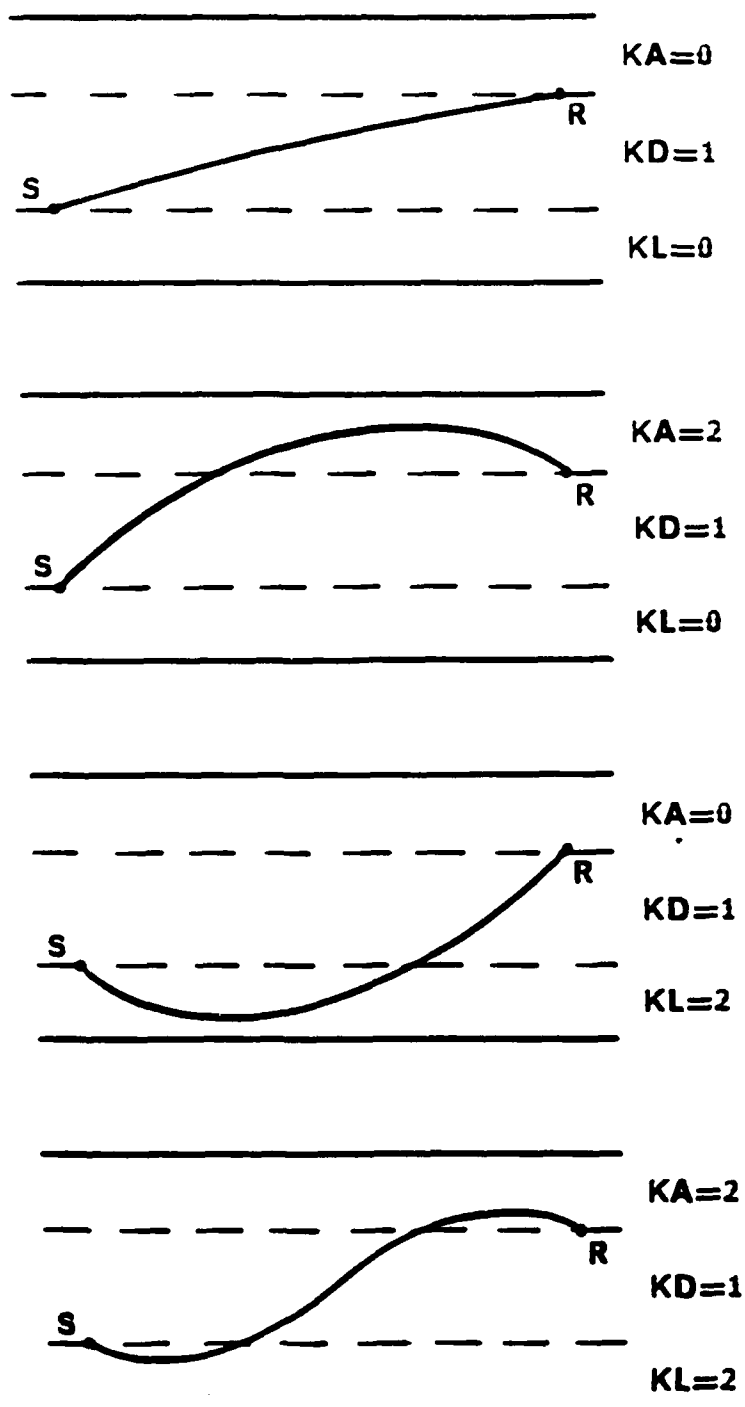

APPENDIX C

LIST OF INPUT VARIABLES

VS	source speed
VD	source depth
$DOCEAN$	ocean depth
$ALPHA$	absorption coefficient
SS	sound speed
$SSCAT$	surface scattering coefficient
$SSIG$	standard deviation of surface scatterer speed distribution
$SWTHE$	surface wave vector of motion
SWS	surface wave speed
$SWSIG$	standard deviation of surface wave speed distribution
$RATIO$	power ratio of surface wave to surface scattering component
$VSCAT$	volume scattering coefficient
$VSIG$	standard deviation of volume scatterer speed distribution
$BSCAT$	bottom scattering coefficient
$BSIG$	standard deviation of bottom scatterer speed distribution
NCL	number of current layers
$CTHICK(I)$	thickness of current layer, I
$CTHE(I)$	direction of motion of current layer, I
$CS(I)$	speed of current layer, I

FREQ	carrier frequency
TPLL	pulse length
TTHE	transmit beam vector in azimuth
TPHI	transmit beam vector in elevation
RTHE	receive beam vector in azimuth
RPHI	receive beam vector in elevation
BPINC	beam pattern file angular increment
NBP	number of beam pattern points
FS	baseband sampling rate
NFFT	number of bins across bandwidth
DELTHE	grid cell width in azimuth
TSTHE	total spread of grid azimuth centered on receive beam axis
DELPHI	grid cell height in elevation
TSPHI	total spread of grid elevation centered on receive beam axis
RB	range beginning
RE	range ending
RI	range increment
OUTCN1	scattered spectrum or total power flag
OUTCN2	surface, volume, bottom, total, or all four flag

APPENDIX D

ISOVELOCITY MODEL SUBROUTINES

D.1. Initialization Subroutines

D.1.1. INRVMD

Subroutine INRVMD simply reads into SCATTER the input parameters from the direct access file created back in INPUT. If it is desired, these input parameters may be displayed. There is also the option in this subroutine to use two-dimensional beam pattern weightings, as opposed to the assumed circularly symmetric ones created in BEAMS.

D.1.2. INITRM

Subroutine INITRM prepares the input parameters for use in program SCATTER. It is called once each time SCATTER is run. In this subroutine, the backscattering coefficients are converted from decibels to linear units; the standard deviation of scatterer speed distributions are converted from meters per second to hertz; and all angles are converted from degrees to radians. The variables defining the grid are initialized and the arrays for the scattering function accumulations are initialized to zero. Also, the output file for use in TRANSMIT is defined, and a header, a list of constants, is written to this output file.

D.2. Determination of Surface, Volume, or Bottom Reverberation

D.2.1. VANGLE

Subroutine VANGLE is called once for each range. Here, the vertical angles from the source to the surface and to the bottom at both the front and the back of the grid cell depth are calculated. The front of the cell is defined as the distance corresponding to the range and the back of the cell corresponds to the range plus the grid cell depth. Since this model does not consider any reflections

from the surface or the bottom, the first vertical cell in the grid is at the surface where the range (in meters) reaches the surface. If the current range is such that the surface is not yet reached by the pulse, then the first vertical cell appears straight upward from the source, or at $\phi = +90°$. A similar situation exists for the bottom with the last vertical cell. If the bottom is farther from the source than the current range, then the last vertical cell appears straight downward at $\phi = -90°$. Subroutine VANGLE utilizes subroutine TOTANG to determine the total number of vertical angular increments, or rows, in the grid. First found are the numbers of rows of cells pertaining to each, surface, volume, and bottom reverberation. The sum of these three is equal to the total number of rows in the grid.

D.2.2. INITDO

Program SCATTER has the option of computing either surface, volume, bottom, or total reverberation. It may also compute all four. It will have been predetermined (in program INPUT) exactly which type of reverberation is being sought. Subroutine INITDO sets the "do loop" parameters for the number of rows of cells to be considered. For example, if only surface reverberation is of interest, then the reverberant power gain from only those rows of grid cells which fall on the surface is to be accumulated. If, on the other hand, the total reverberation spectrum is desired, then the power gain from all rows of cells is to be accumulated. Subroutine INITDO prescribes the first and last rows of cells over which to accumulate the reverberation power gain.

D.3. Beam Patterns - Subroutine BPATRM

The total reverberation level from each cell is weighted by both the transmitting and receiving beams. As was stated earlier, these beams may each be steered in any direction through the specification of a steering vector, (θ, ϕ),

where θ is the azimuthal angle and ϕ is the elevation angle. Subroutine BPATRM computes the beam weightings for each cell by interpolating between the beam pattern points that had been input. Adjustments are made for the steering vectors for each beam and the transmit and receive beam pattern weightings are multiplied together to obtain a composite weighting at the receiver for that cell.

D.4. Frequency Spreading and Shifting Routines

D.4.1. ZPDF

Program SCATTER accumulates the reverberation power gain by beginning with a row of cells, computing the sonar equation for each cell in that row, and then proceeding to the next row to be processed. As it is structured, SCATTER steps through all surface reverberation cells first, then volume, then bottom. Subroutine ZPDF is called only for the first row of cells involved in each type of reverberation. Thus, it is called once for the surface, once for the volume, and once for the bottom.

The actual function of subroutine ZPDF is to calculate the quantized and truncated zero mean Gaussian scatterer velocity distribution. The probability density function defining the random scatterer motion is assumed to be a Gaussian curve shaped by the standard deviation, σ. The standard deviations of the surface, volume, and bottom scatterer speed distributions, which had been converted from m/s to Hz are input variables to INPUT. These parameters are what determine the amount of frequency spreading which occurs at each backscattering element. A standard deviation of 0.0 would denote that the scattering element has no motion at all, and that the backscattered spectral distribution would be identical to the incident spectral distribution.

D.4.2. DOPP

Subroutine DOPP calculates two Doppler shift components for each cell and adds a third. First of all, the Doppler due to source motion relative to the cell is determined. Secondly, the Doppler attributed to the mean scatterer speed relative to a stationary source is found. Additionally, a frequency offset, such that a stationary scatterer on the source axis has zero Doppler shift, is introduced. These three components are added to obtain one net Doppler shift value for each cell.

Subroutine DOPP also serves a secondary purpose. Included in REVMOD is the capability to account for Doppler shift resulting from the presence of current layers. Up to eight layers are allowed. Some volume cells may fall on the border of two or more current layers. In order to obtain a better representation of the Doppler for these cells, a current split loop has been set up in DOPP. This divides a volume cell into two or more portions, depending on how many current layers that cell occupies. Each portion of the cell is weighted according to the ratio of its volume to the total cell volume and is processed individually for its Doppler shift and frequency spreading contributions.

D.4.3. CNVOL1

Once the Doppler shift has been determined or a cell, the backscattered energy spectrum is shifted by the Doppler frequency. This is accomplished by a convolution of the Gaussian density distribution at the scatterer with an impulse located at the Doppler shift value [27].

D.4.4. SWPDF

The backscattered spectrum from the surface is modeled as a combination of two phenomena. First of all, a scattering function, due to the roughness of the surface, is computed. Secondly, a surface wave contribution is introduced as a

fraction of the total surface scattering contribution. In addition to the surface scattering input variables, the surface wave speed and its standard deviation are input. Thus, the surface reverberation is a combination of the surface scattering component plus the surface wave component. Subroutine SWPDF accounts for this additional scattering due to surface waves. The probability density function for the surface waves is added to that for surface scatterer. The resulting composite probability density function is normalized so that each surface scattering cell is not taken into account twice.

D.4.5. WTSCAT

Subroutine WTSCAT weights the scatterer speed distribution by the sonar equation solution for each cell in a horizontal row. The incremental scattering function is adjusted for a $1Hz$ band by dividing by $\triangle f$, the width of a frequency bin, which is defined by the sampling frequency, f_s, divided by the number of FFT points, N. The scattering functions for the cells in an entire row are then accumulated.

D.4.6. RINIT2 / RINIT3

Subroutine RINIT2 is called at the completion of each rows of cells. The vertical angle, ϕ, is incremented to the center angle of the next row to be processed. The azimuthal angle, θ, is reinitialized to the center angle of the first azimuth. The surface, volume, and bottom components of the scattering function and total power gain are separated for individual inspection. These scattering function and power gain arrays are written to a direct access file for plotting or as input to other REVMOD program sections. At the end of each range, RINIT3 is called to reinitialize the arrays. The combined (surface + volume + bottom) scattering function and power gain levels are written to a direct access file.

APPENDIX E

INPUT PARAMETERS

E.1. Input Parameters for Figure 3.3

```
                    *** INPUT PARAMETERS ***

                PARAMETERS FROM REVINP DISK FILE

                        *** SOURCE ***

SOURCE  SPEED        5.0 M/S      SOURCE  DEPTH      300.0 M

                    *** ENVIRONMENT ***

SOUND SPEED     1500.0 M/S      ABSORPTION COEF.     0.0014 DB/M
OCEAN DEPTH      500.0 M

     SURFACE

SURFACE SCATTERING COEFFICIENT  -30.0000 (DB/M**2)
STANDARD DEVIATION OF SURF. SCAT. SPEED DIST.     0.1667 M/S
SURF. WAVE DIRECTION OF MOTION REL. TO SRC. HEADING       0.00 DEG
SURFACE WAVE SPEED       0.00 M/S
STAN. DEV. OF SURF. WAVE SPEED DISTR.      0.167 M/S
POWER RATIO OF SURF. WAVE TO SURF. SCAT. COMP.          1.000


     VOLUME

VOLUME SCATTERING COEFFICIENT      -80.0 DB/M**3
STANDARD DEVIATION OF VOL. SCAT. SPEED DISTR.       0.17 M/S

     BOTTOM

BOTTOM SCATTERING COEFFICIENT   -35.000 (DB/M**2)
STANDARD DEV. OF BOTTOM SCATTERING SPEED DISTR.       0.17 M/S

     CURRENTS

NUMBER OF CURRENT LAYERS        0
THICKNESS (M)        0.0   0.0   0.0   0.0   0.0   0.0   0.0   0.0
DIR. OF MOT. (DEG)   0.0   0.0   0.0   0.0   0.0   0.0   0.0   0.0
SPEED (M/S)          0.0   0.0   0.0   0.0   0.0   0.0   0.0   0.0

     TRANSMITTED SIGNAL

CARRIER FREQUENCY   45000.0 HZ
PULSE LENGTH 0.0500000 S
GRID CELL DEPTH (c*tau/2)       37.5M

                        *** BEAMS***

TRANSMIT BEAM VECTOR - THETA =      0.0       PHI =      0.0 DEG
RECEIVE BEAM VECTOR - THETA =      0.0       PHI =      0.0 DEG
BEAM PATTERN FILE ANGULAR INCREMENT     3.00 DEG
NUMBER BEAM PATTERN POINTS SPECIFIED OR PATTERN #    31

                    *** REVERBERATION MODEL ***

BASEBAND SAMPLING RATE BANDWIDTH  1000.0 HZ
# OF BINS IN BANDWIDTH       64
GRID CELL WIDTH IN AZIMUTH     2.00 DEG
TOTAL SPREAD OF GRID AZ. CENTERED ON REC. BEAM AXIS     10.0 DEG
GRID CELL HEIGHT IN ELEVATION     2.00 DEG
```

TOTAL SPREAD OF GRID EL. CENTERED ON REC. BEAM AXIS 180.0 DEG

*** OUTPUTS ***

NUMBER OF RANGES = 64 RANGE INCREMENT = 30.0 M
RANGE BEGINNING = 30.0 M RANGE ENDING = 1920.0 M
SCATTERING SPECTRUM VS. TOTAL POWER FLAG F
SURFACE,VOLUME,BOTTOM,TOTAL OR ALL FOUR FLAG 1

TRANSMIT BEAM PATTERN

0.1000E+01	0.1000E+01	0.1000E+01	0.1000E+01	0.1000E+01	0.1000E+01
0.1000E+01	0.1000E+01	0.1000E+01	0.1000E+01	0.1000E+01	0.1000E+01
0.1000E+01	0.1000E+01	0.1000E+01	0.1000E+01	0.1000E+01	0.1000E+01
0.1000E+01	0.1000E+01	0.1000E+01	0.1000E+01	0.1000E+01	0.1000E+01
0.1000E+01	0.1000E+01	0.1000E+01	0.1000E+01	0.1000E+01	0.1000E+01
0.1000E+01					

RECEIVE BEAM PATTERN

0.1000E+01	0.1000E+01	0.1000E+01	0.1000E+01	0.1000E+01	0.1000E+01
0.1000E+01	0.1000E+01	0.1000E+01	0.1000E+01	0.1000E+01	0.1000E+01
0.1000E+01	0.1000E+01	0.1000E+01	0.1000E+01	0.1000E+01	0.1000E+01
0.1000E+01	0.1000E+01	0.1000E+01	0.1000E+01	0.1000E+01	0.1000E+01
0.1000E+01	0.1000E+01	0.1000E+01	0.1000E+01	0.1000E+01	0.1000E+01
0.1000E+01					

E.2. Input Parameters for Figure 3.5

```
                    *** INPUT PARAMETERS ***

                PARAMETERS FROM REVINP DISK FILE

                        *** SOURCE ***

SOURCE  SPEED        5.0 M/S      SOURCE  DEPTH      300.0 M

                     *** ENVIRONMENT ***

SOUND SPEED     1500.0 M/S      ABSORPTION COEF.     0.0014 DB/M
OCEAN DEPTH      500.0 M

     SURFACE

SURFACE SCATTERING COEFFICIENT  -30.0000 (DB/M**2)
STANDARD DEVIATION OF SURF. SCAT. SPEED DIST.     0.1667 M/S
SURF. WAVE DIRECTION OF MOTION REL. TO SRC. HEADING       0.00 DEG
SURFACE WAVE SPEED       0.00 M/S
STAN. DEV. OF SURF. WAVE SPEED DISTR.      0.167 M/S
POWER RATIO OF SURF. WAVE TO SURF. SCAT. COMP.          1.000


     VOLUME

VOLUME SCATTERING COEFFICIENT      -80.0 DB/M**3
STANDARD DEVIATION OF VOL. SCAT. SPEED DISTR.       0.17 M/S

     BOTTOM

BOTTOM SCATTERING COEFFICIENT   -35.000 (DB/M**2)
STANDARD DEV. OF BOTTOM SCATTERING SPEED DISTR.       0.17 M/S

     CURRENTS

NUMBER OF CURRENT LAYERS          0
THICKNESS (M)          0.0   0.0   0.0   0.0   0.0   0.0   0.0   0.0
DIR. OF MOT. (DEG)     0.0   0.0   0.0   0.0   0.0   0.0   0.0   0.0
SPEED (M/S)            0.0   0.0   0.0   0.0   0.0   0.0   0.0   0.0

     TRANSMITTED SIGNAL

CARRIER FREQUENCY   45000.0 HZ
PULSE LENGTH 0.0500000 S
GRID CELL DEPTH (c*tau/2)       37.5M

                        *** BEAMS***

TRANSMIT BEAM VECTOR - THETA =      0.0       PHI =      0.0 DEG
RECEIVE BEAM VECTOR - THETA =      0.0       PHI =      0.0 DEG
BEAM PATTERN FILE ANGULAR INCREMENT     3.00 DEG
NUMBER BEAM PATTERN POINTS SPECIFIED OR PATTERN #    31

                  *** REVERBERATION MODEL ***

BASEBAND SAMPLING RATE BANDWIDTH  1000.0 HZ
# OF BINS IN BANDWIDTH       64
GRID CELL WIDTH IN AZIMUTH     2.00 DEG
TOTAL SPREAD OF GRID AZ. CENTERED ON REC. BEAM AXIS     10.0 DEG
GRID CELL HEIGHT IN ELEVATION     2.00 DEG
```

TOTAL SPREAD OF GRID EL. CENTERED ON REC. BEAM AXIS 180.0 DEG

*** OUTPUTS ***

NUMBER OF RANGES = 1 RANGE INCREMENT = 360.0 M
RANGE BEGINNING = 360.0 M RANGE ENDING = 360.0 M
SCATTERING SPECTRUM VS. TOTAL POWER FLAG T
SURFACE,VOLUME,BOTTOM,TOTAL OR ALL FOUR FLAG T

TRANSMIT BEAM PATTERN

0.1000E+01 0.1000E+01 0.1000E+01 0.1000E+01 0.1000E+01 0.1000E+01
0.1000E+01 0.1000E+01 0.1000E+01 0.1000E+01 0.1000E+01 0.1000E+01
0.1000E+01 0.1000E+01 0.1000E+01 0.1000E+01 0.1000E+01 0.1000E+01
0.1000E+01 0.1000E+01 0.1000E+01 0.1000E+01 0.1000E+01 0.1000E+01
0.1000E+01 0.1000E+01 0.1000E+01 0.1000E+01 0.1000E+01 0.1000E+01
0.1000E+01

RECEIVE BEAM PATTERN

0.1000E+01 0.1000E+01 0.1000E+01 0.1000E+01 0.1000E+01 0.1000E+01
0.1000E+01 0.1000E+01 0.1000E+01 0.1000E+01 0.1000E+01 0.1000E+01
0.1000E+01 0.1000E+01 0.1000E+01 0.1000E+01 0.1000E+01 0.1000E+01
0.1000E+01 0.1000E+01 0.1000E+01 0.1000E+01 0.1000E+01 0.1000E+01
0.1000E+01 0.1000E+01 0.1000E+01 0.1000E+01 0.1000E+01 0.1000E+01
0.1000E+01

E.3. Input Parameters for Figure 4.1 and 4.2

```
                    *** INPUT PARAMETERS ***

                PARAMETERS FROM REVINP DISK FILE

                        *** SOURCE ***

SOURCE SPEED        5.0 M/S      SOURCE DEPTH      300.0 M

                      *** ENVIRONMENT ***

SOUND SPEED AT SOURCE     1500.0 M/S      ABSORPTION COEF. VARIES WITH SVP
OCEAN DEPTH      500.0 M
NUMBER OF BOUNCES BOUNCES  6 EA., SURF. AND BOT.

     SURFACE

SURFACE SCATTERING COEFFICIENT  -30.0000 (DB/M**2)
STANDARD DEVIATION OF SURF. SCAT. SPEED DIST.     0.1667 M/S
SURF. WAVE DIRECTION OF MOTION REL. TO VEH. HEADING       0.00 DEG
SURFACE WAVE SPEED       0.00 M/S
STAN. DEV. OF SURF. WAVE SPEED DISTR.      0.167 M/S
POWER RATIO OF SURF. WAVE TO SURF. SCAT. COMP.      1.000
LOSS PER SURFACE BOUNCE     -2.000 dB


     VOLUME

VOLUME SCATTERING COEFFICIENT      -80.0 DB/M**3
STANDARD DEVIATION OF VOL. SCAT. SPEED DISTR.       0.17 M/S

     BOTTOM

BOTTOM SCATTERING COEFFICIENT   -35.000 (DB/M**2)
STANDARD DEV. OF BOTTOM SCATTERING SPEED DISTR.       0.17 M/S
LOSS PER BOTTOM BOUNCE     -4.000 dB

     CURRENTS

NUMBER OF CURRENT LAYERS         0
THICKNESS (M)        0.0   0.0   0.0   0.0   0.0   0.0   0.0   0.0
DIR. OF MOT. (DEG)   0.0   0.0   0.0   0.0   0.0   0.0   0.0   0.0
SPEED (M/S)          0.0   0.0   0.0   0.0   0.0   0.0   0.0   0.0

     TRANSMITTED SIGNAL

CARRIER FREQUENCY    45000.0 HZ
PULSE LENGTH 0.500000 S
GRID CELL DEPTH WILL BE CALCULATED IN REVSCT


                        *** BEAMS***

TRANSMIT BEAM VECTOR - THETA =      0.0       PHI =      0.0 DEG
RECEIVE BEAM VECTOR - THETA =      0.0       PHI =      0.0 DEG
BEAM PATTERN FILE ANGULAR INCREMENT     3.00 DEG
NUMBER BEAM PATTERN POINTS SPECIFIED OR PATTERN #    31


                  *** REVERBERATION MODEL ***

BASEBAND SAMPLING RATE BANDWIDTH  1000.0 HZ
# OF BINS IN BANDWIDTH       64
```

```
GRID CELL WIDTH IN AZIMUTH     2.00 DEG
TOTAL SPREAD OF GRID AZ. CENTERED ON REC. BEAM AXIS     10.0 DEG
GRID CELL HEIGHT IN ELEVATION     2.00 DEG
TOTAL SPREAD OF GRID EL. CENTERED ON REC. BEAM AXIS    180.0 DEG

                          *** OUTPUTS ***

NUMBER OF RANGES =       64      RANGE INCREMENT =      0.040 S
RANGE BEGINNING =        0.040 S       RANGE ENDING =        2.560 S
SCATTERING SPECTRUM VS. TOTAL POWER FLAG    F
SURFACE,VOLUME,BOTTOM,TOTAL OR ALL FOUR FLAG     1


   TRANSMIT BEAM PATTERN
0.1000E+01  0.1000E+01  0.1000E+01  0.1000E+01  0.1000E+01  0.1000E+01
0.1000E+01  0.1000E+01  0.1000E+01  0.1000E+01  0.1000E+01  0.1000E+01
0.1000E+01  0.1000E+01  0.1000E+01  0.1000E+01  0.1000E+01  0.1000E+01
0.1000E+01  0.1000E+01  0.1000E+01  0.1000E+01  0.1000E+01  0.1000E+01
0.1000E+01  0.1000E+01  0.1000E+01  0.1000E+01  0.1000E+01  0.1000E+01
0.1000E+01

   RECEIVE BEAM PATTERN
0.1000E+01  0.1000E+01  0.1000E+01  0.1000E+01  0.1000E+01  0.1000E+01
0.1000E+01  0.1000E+01  0.1000E+01  0.1000E+01  0.1000E+01  0.1000E+01
0.1000E+01  0.1000E+01  0.1000E+01  0.1000E+01  0.1000E+01  0.1000E+01
0.1000E+01  0.1000E+01  0.1000E+01  0.1000E+01  0.1000E+01  0.1000E+01
0.1000E+01  0.1000E+01  0.1000E+01  0.1000E+01  0.1000E+01  0.1000E+01
0.1000E+01
```

NUMDEP	DEPTH	SPEED	ISOCT	-INV.GRAD.	ALPHA
1	500.00	1500.00	1500.00	0.00	0.1400E-02
2	300.00	1500.00	1500.00	0.00	0.1400E-02
3	0.00	1500.00	0.00	0.00	0.1400E-02

E.4. Input Parameters for Figure 4.3

```
                    *** INPUT PARAMETERS ***

                PARAMETERS FROM REVINP DISK FILE

                        *** SOURCE ***

SOURCE  SPEED        5.0 M/S      SOURCE  DEPTH      100.0 M

                     *** ENVIRONMENT ***

SOUND SPEED     1500.0 M/S      ABSORPTION COEF.     0.0014 DB/M
OCEAN DEPTH     2000.0 M

     SURFACE

SURFACE SCATTERING COEFFICIENT  -30.0000 (DB/M**2)
STANDARD DEVIATION OF SURF. SCAT. SPEED DIST.     0.1667 M/S
SURF. WAVE DIRECTION OF MOTION REL. TO SRC. HEADING      0.00 DEG
SURFACE WAVE SPEED       0.00 M/S
STAN. DEV. OF SURF. WAVE SPEED DISTR.      0.167 M/S
POWER RATIO OF SURF. WAVE TO SURF. SCAT. COMP.          1.000


     VOLUME

VOLUME SCATTERING COEFFICIENT      -80.0 DB/M**3
STANDARD DEVIATION OF VOL. SCAT. SPEED DISTR.       0.17 M/S

     BOTTOM

BOTTOM SCATTERING COEFFICIENT   -35.000 (DB/M**2)
STANDARD DEV. OF BOTTOM SCATTERING SPEED DISTR.       0.17 M/S

     CURRENTS

NUMBER OF CURRENT LAYERS          0
THICKNESS (M)          0.0   0.0   0.0   0.0   0.0   0.0   0.0   0.0
DIR. OF MOT. (DEG)     0.0   0.0   0.0   0.0   0.0   0.0   0.0   0.0
SPEED (M/S)            0.0   0.0   0.0   0.0   0.0   0.0   0.0   0.0

     TRANSMITTED SIGNAL

CARRIER FREQUENCY   45000.0 HZ
PULSE LENGTH 0.0500000 S
GRID CELL DEPTH (c*tau/2)       37.5M

                        *** BEAMS***

TRANSMIT BEAM VECTOR - THETA =      0.0       PHI =      0.0 DEG
RECEIVE BEAM VECTOR - THETA =      0.0       PHI =      0.0 DEG
BEAM PATTERN FILE ANGULAR INCREMENT     3.00 DEG
NUMBER BEAM PATTERN POINTS SPECIFIED OR PATTERN #    31

                  *** REVERBERATION MODEL ***

BASEBAND SAMPLING RATE BANDWIDTH  1000.0 HZ
# OF BINS IN BANDWIDTH       64
GRID CELL WIDTH IN AZIMUTH     2.00 DEG
TOTAL SPREAD OF GRID AZ. CENTERED ON REC. BEAM AXIS     10.0 DEG
GRID CELL HEIGHT IN ELEVATION     2.00 DEG
```

TOTAL SPREAD OF GRID EL. CENTERED ON REC. BEAM AXIS 180.0 DEG

*** OUTPUTS ***

NUMBER OF RANGES = 64 RANGE INCREMENT = 96.0 M
RANGE BEGINNING = 96.0 M RANGE ENDING = 6144.0 M
SCATTERING SPECTRUM VS. TOTAL POWER FLAG T
SURFACE,VOLUME,BOTTOM,TOTAL OR ALL FOUR FLAG 1

TRANSMIT BEAM PATTERN

0.1000E+01	0.1000E+01	0.1000E+01	0.1000E+01	0.1000E+01	0.1000E+01
0.1000E+01	0.1000E+01	0.1000E+01	0.1000E+01	0.1000E+01	0.1000E+01
0.1000E+01	0.1000E+01	0.1000E+01	0.1000E+01	0.1000E+01	0.1000E+01
0.1000E+01	0.1000E+01	0.1000E+01	0.1000E+01	0.1000E+01	0.1000E+01
0.1000E+01	0.1000E+01	0.1000E+01	0.1000E+01	0.1000E+01	0.1000E+01
0.1000E+01					

RECEIVE BEAM PATTERN

0.1000E+01	0.1000E+01	0.1000E+01	0.1000E+01	0.1000E+01	0.1000E+01
0.1000E+01	0.1000E+01	0.1000E+01	0.1000E+01	0.1000E+01	0.1000E+01
0.1000E+01	0.1000E+01	0.1000E+01	0.1000E+01	0.1000E+01	0.1000E+01
0.1000E+01	0.1000E+01	0.1000E+01	0.1000E+01	0.1000E+01	0.1000E+01
0.1000E+01	0.1000E+01	0.1000E+01	0.1000E+01	0.1000E+01	0.1000E+01
0.1000E+01					

E.5. Input Parameters for Figure 4.5

```
                    *** INPUT PARAMETERS ***

                PARAMETERS FROM REVINP DISK FILE

                        *** SOURCE ***

SOURCE SPEED        5.0 M/S      SOURCE DEPTH      100.0 M

                      *** ENVIRONMENT ***

SOUND SPEED AT SOURCE     1510.0 M/S      ABSORPTION COEF. VARIES WITH SVP
OCEAN DEPTH     2000.0 M
NUMBER OF BOUNCES BOUNCES  6 EA., SURF. AND BOT.

     SURFACE

SURFACE SCATTERING COEFFICIENT  -30.0000 (DB/M**2)
STANDARD DEVIATION OF SURF. SCAT. SPEED DIST.     0.1667 M/S
SURF. WAVE DIRECTION OF MOTION REL. TO VEH. HEADING       0.00 DEG
SURFACE WAVE SPEED       0.00 M/S
STAN. DEV. OF SURF. WAVE SPEED DISTR.      0.167 M/S
POWER RATIO OF SURF. WAVE TO SURF. SCAT. COMP.      1.000
LOSS PER SURFACE BOUNCE     -2.000 dB


     VOLUME

VOLUME SCATTERING COEFFICIENT      -80.0 DB/M**3
STANDARD DEVIATION OF VOL. SCAT. SPEED DISTR.       0.17 M/S

     BOTTOM

BOTTOM SCATTERING COEFFICIENT   -35.000 (DB/M**2)
STANDARD DEV. OF BOTTOM SCATTERING SPEED DISTR.       0.17 M/S
LOSS PER BOTTOM BOUNCE     -4.000 dB

     CURRENTS

NUMBER OF CURRENT LAYERS         0
THICKNESS (M)        0.0   0.0   0.0   0.0   0.0   0.0   0.0   0.0
DIR. OF MOT. (DEG)   0.0   0.0   0.0   0.0   0.0   0.0   0.0   0.0
SPEED (M/S)          0.0   0.0   0.0   0.0   0.0   0.0   0.0   0.0

     TRANSMITTED SIGNAL

CARRIER FREQUENCY   45000.0 HZ
PULSE LENGTH 0.0500000 S
GRID CELL DEPTH WILL BE CALCULATED IN REVSCT


                        *** BEAMS***

TRANSMIT BEAM VECTOR - THETA =      0.0       PHI =      0.0 DEG
RECEIVE BEAM VECTOR - THETA =      0.0       PHI =      0.0 DEG
BEAM PATTERN FILE ANGULAR INCREMENT     3.00 DEG
NUMBER BEAM PATTERN POINTS SPECIFIED OR PATTERN #    31


                  *** REVERBERATION MODEL ***

BASEBAND SAMPLING RATE BANDWIDTH  1000.0 HZ
# OF BINS IN BANDWIDTH       64
```

GRID CELL WIDTH IN AZIMUTH 2.00 DEG
TOTAL SPREAD OF GRID AZ. CENTERED ON REC. BEAM AXIS 10.0 DEG
GRID CELL HEIGHT IN ELEVATION 2.00 DEG
TOTAL SPREAD OF GRID EL. CENTERED ON REC. BEAM AXIS 180.0 DEG

*** OUTPUTS ***

NUMBER OF RANGES = 64 RANGE INCREMENT = 0.128 S
RANGE BEGINNING = 0.128 S RANGE ENDING = 8.192 S
SCATTERING SPECTRUM VS. TOTAL POWER FLAG T
SURFACE,VOLUME,BOTTOM,TOTAL OR ALL FOUR FLAG 1

TRANSMIT BEAM PATTERN

0.1000E+01	0.1000E+01	0.1000E+01	0.1000E+01	0.1000E+01	0.1000E+01
0.1000E+01	0.1000E+01	0.1000E+01	0.1000E+01	0.1000E+01	0.1000E+01
0.1000E+01	0.1000E+01	0.1000E+01	0.1000E+01	0.1000E+01	0.1000E+01
0.1000E+01	0.1000E+01	0.1000E+01	0.1000E+01	0.1000E+01	0.1000E+01
0.1000E+01	0.1000E+01	0.1000E+01	0.1000E+01	0.1000E+01	0.1000E+01
0.1000E+01					

RECEIVE BEAM PATTERN

0.1000E+01	0.1000E+01	0.1000E+01	0.1000E+01	0.1000E+01	0.1000E+01
0.1000E+01	0.1000E+01	0.1000E+01	0.1000E+01	0.1000E+01	0.1000E+01
0.1000E+01	0.1000E+01	0.1000E+01	0.1000E+01	0.1000E+01	0.1000E+01
0.1000E+01	0.1000E+01	0.1000E+01	0.1000E+01	0.1000E+01	0.1000E+01
0.1000E+01	0.1000E+01	0.1000E+01	0.1000E+01	0.1000E+01	0.1000E+01
0.1000E+01					

NUMDEP	DEPTH	SPEED	ISOCT	-INV.GRAD.	ALPHA
1	2000.00	1560.00	0.00	-22.50	0.1400E-02
2	200.00	1480.00	0.00	3.33	0.1400E-02
3	100.00	1510.00	0.00	3.33	0.1400E-02
4	0.00	1540.00	0.00	0.00	0.1400E-02

APPENDIX F

CONSTANT FACTOR IN DOPPLER EQUATIONS

The Doppler shift equation for a moving source has been defined as

$$f_D = f_o \left(1 + \frac{2v}{c} \cos\gamma\right), \tag{F.1}$$

where f_o is the original frequency, v is the source velocity, c is the speed of sound, and γ is the angle at which the Doppler is realized. In an isovelocity environment, the incident angle, γ_s, at a scatterer, is identical to the angle, γ, at the source. Therefore, the Doppler equation for a moving scatterer is

$$f_D = f_o \left(1 + \frac{2u}{c} \cos\gamma\right). \tag{F.2}$$

The difference in the Doppler-shifted frequency from the original is

$$\triangle f = \frac{2f_o v}{c} \cos\gamma \tag{F.3}$$

for source motion, and

$$\triangle f = \frac{2f_o u}{c} \cos\gamma \tag{F.4}$$

for scatterer motion. To simplify the calculations, the constant factor,

$$\frac{2f_o}{c} \cos\gamma, \tag{F.5}$$

is used in program SCATTER for Doppler due to either source or scatterer motion.

When a non-isovelocity environment is present, this simplification might not seem valid, although it is. In general, in a non-isovelocity scenario, the angle, γ, at the source is not equal to the angle, γ_s, at the scatterer. Nor is the speed of sound at the source equal to the speed of sound at the scatterer. However, there is a relation between the angles and speeds of sound from one point to another. This relation has been introduced as Snell's law, and it states that

$$\frac{\sin\gamma'}{c} = \frac{\sin\gamma'_s}{c_s}, \tag{F.6}$$

where c is the speed of sound at the source and c_s is the speed of sound at the scatterer. The angles, γ' and γ'_s, are the angles at the source and the scatterer, respectively. These angles, however, must be measured with the convention of zero degrees being straight downward, so that Snell's law applies. That is to say that zero degrees must be perpendicular to the horizontally stratified layers. To convert the angles, γ' and γ'_s, to the actual angles in SCATTER, γ and γ_s, a shift of ninety degrees must be introduced. Snell's law may now be expressed as

$$\frac{\sin\gamma + 90}{c} = \frac{\sin\gamma_s + 90}{c_s}. \qquad (F.7)$$

This simplifies to

$$\frac{\cos\gamma}{c} = \frac{\cos\gamma_s}{c_s}. \qquad (F.8)$$

Therefore, when the Doppler shift at a scattering element is determined, the factor

$$\frac{2f_o}{c}\cos\gamma, \qquad (F.9)$$

is a constant, whether it is measured at the source or at the scatterer.

APPENDIX G

HIERARCHY CHART FOR RAYSCT

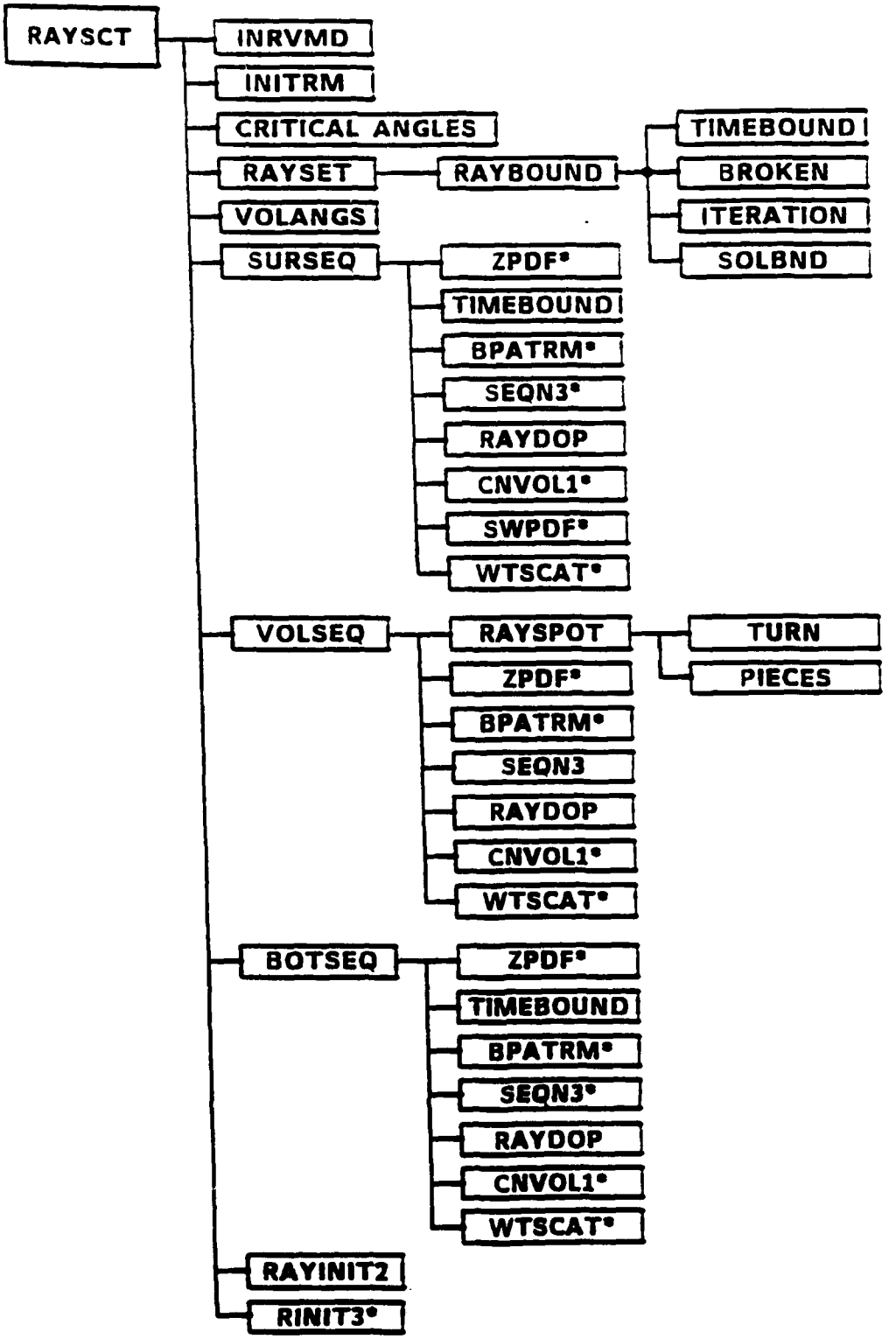

APPENDIX H

RAYTRACING SUBROUTINE FLOWCHARTS

H.1. CRITICAL ANGLES

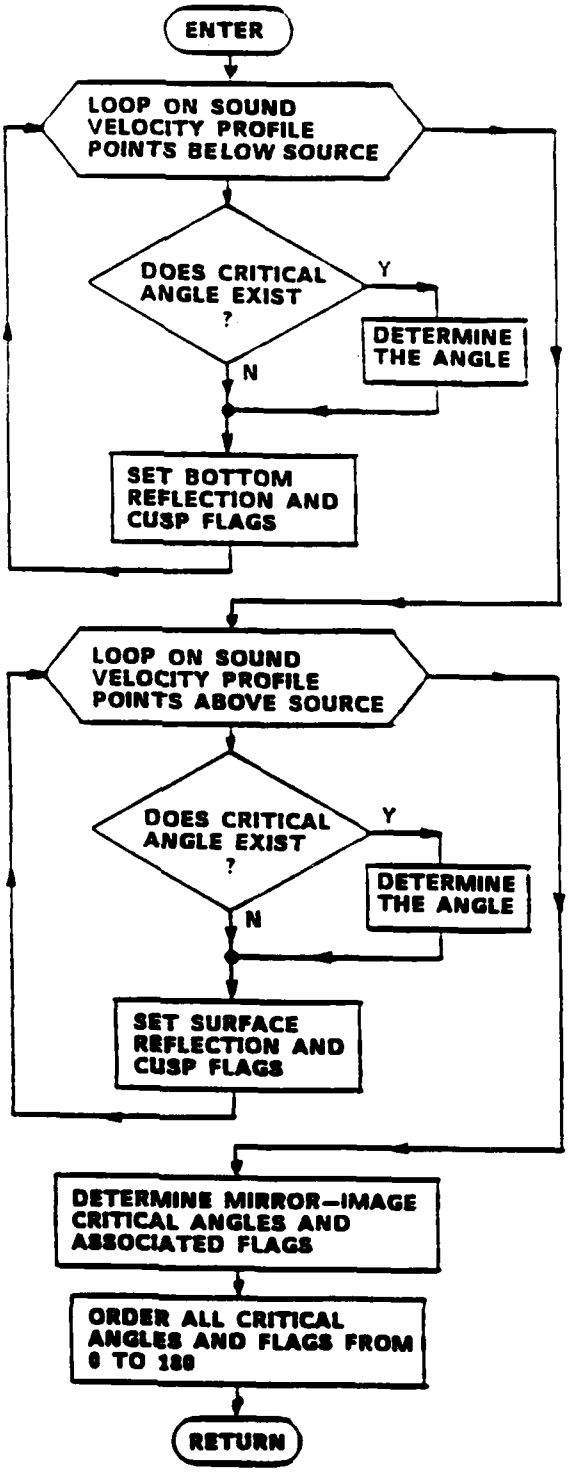

H.2. RAYSET

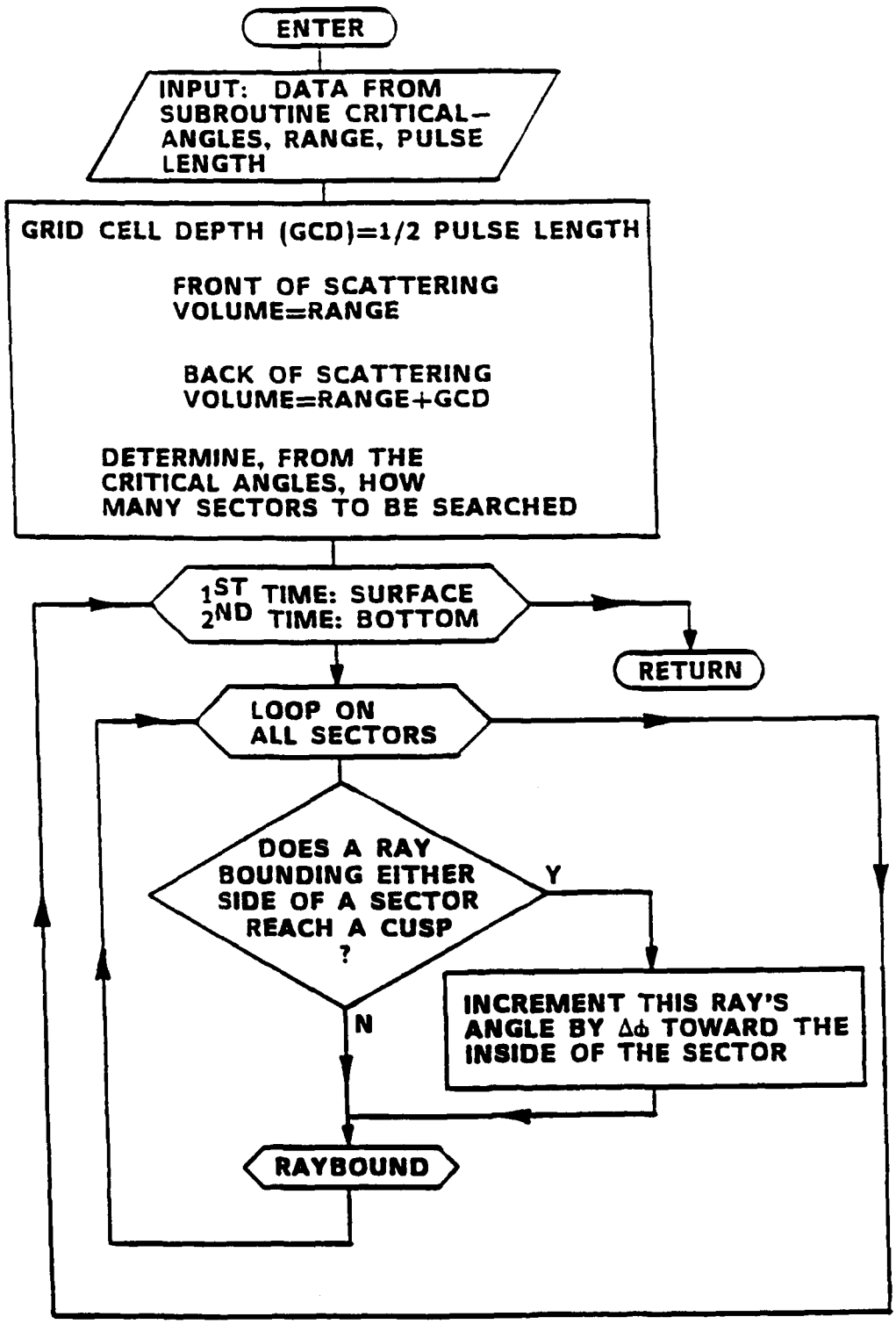
ENTER
INPUT: DATA FROM SUBROUTINE CRITICAL-ANGLES, RANGE, PULSE LENGTH
GRID CELL DEPTH (GCD)=1/2 PULSE LENGTH
FRONT OF SCATTERING VOLUME=RANGE
BACK OF SCATTERING VOLUME=RANGE+GCD
DETERMINE, FROM THE CRITICAL ANGLES, HOW MANY SECTORS TO BE SEARCHED
1ST TIME: SURFACE
2ND TIME: BOTTOM
RETURN
LOOP ON ALL SECTORS
DOES A RAY BOUNDING EITHER SIDE OF A SECTOR REACH A CUSP ?
Y
N
INCREMENT THIS RAY'S ANGLE BY Δϕ TOWARD THE INSIDE OF THE SECTOR
RAYBOUND

H.3. RAYBOUND

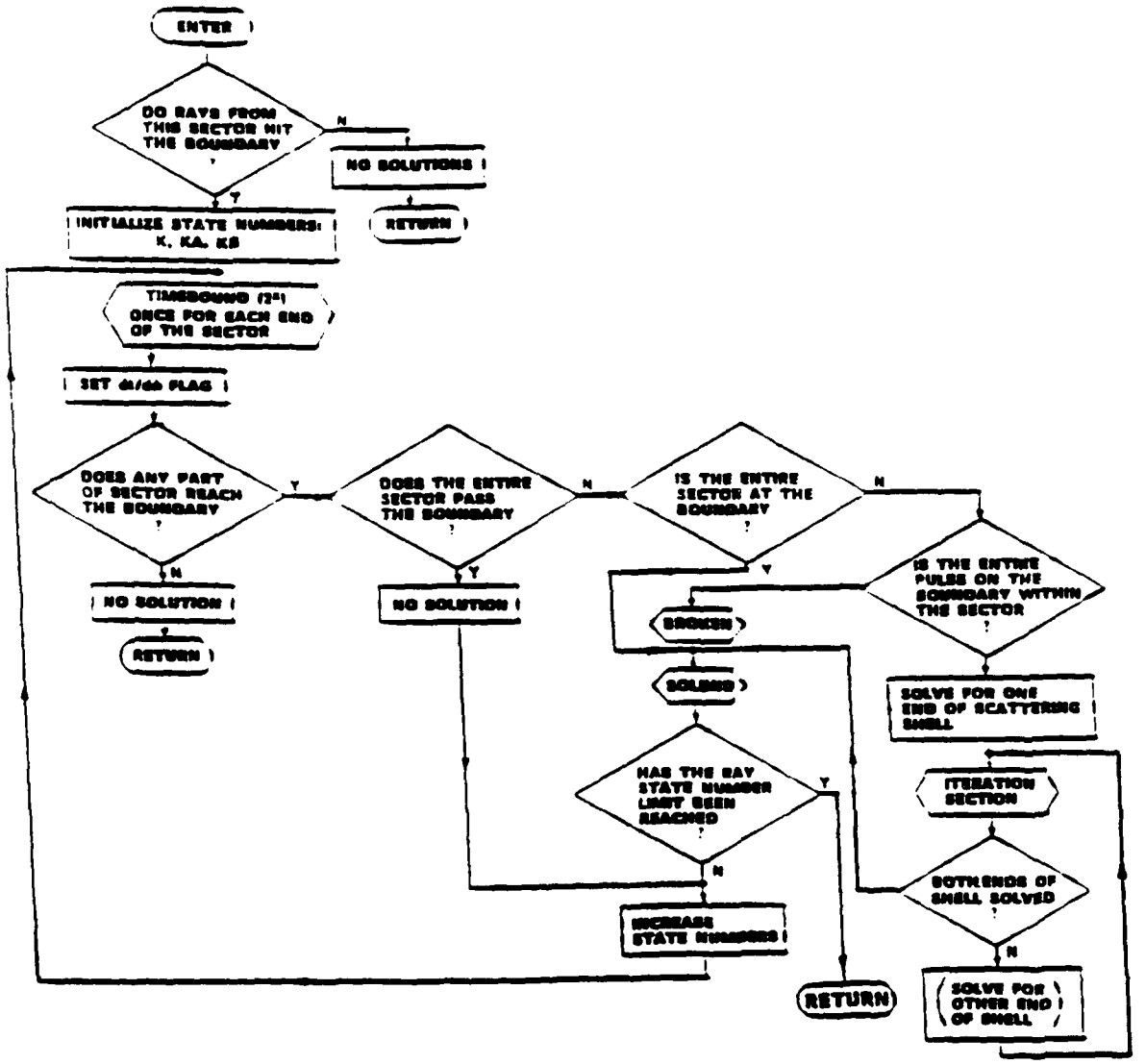
ENTER
DO RAYS FROM THIS SECTOR HIT THE BOUNDARY
N
NO SOLUTIONS
RETURN
Y
INITIALIZE STATE NUMBERS: K, KA, KB
TIMEBOUND (2*I) ONCE FOR EACH END OF THE SECTOR
SET da/db FLAG
DOES ANY PART OF SECTOR REACH THE BOUNDARY
Y
DOES THE ENTIRE SECTOR PASS THE BOUNDARY
N
IS THE ENTIRE SECTOR AT THE BOUNDARY
N
N
NO SOLUTION
RETURN
NO SOLUTION
Y
Y
IS THE ENTIRE PULSE ON THE BOUNDARY WITHIN THE SECTOR
BROKEN
SOLVED
SOLVE FOR ONE END OF SCATTERING SHELL
HAS THE RAY STATE NUMBER LIMIT BEEN REACHED
Y
ITERATION SECTION
N
BOTH ENDS OF SHELL SOLVED
INCREASE STATE NUMBERS
RETURN
N
SOLVE FOR OTHER END OF SHELL

H.4. TIMEBOUND

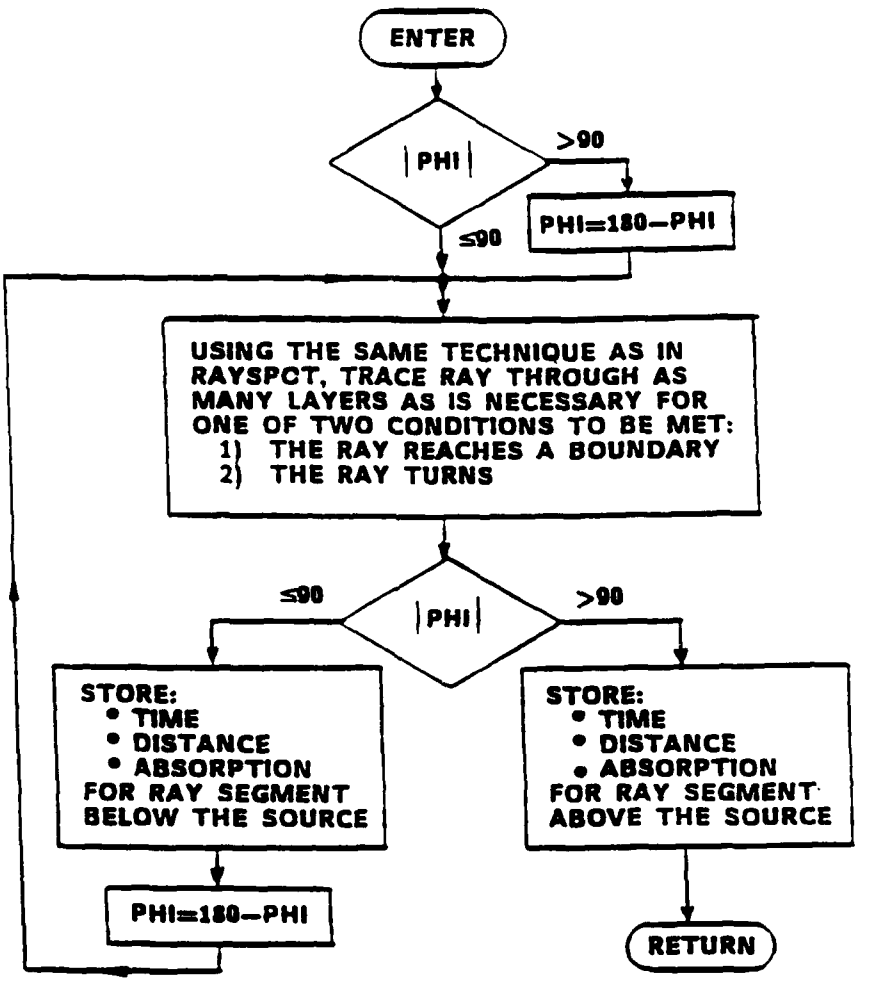

H.5. BROKEN

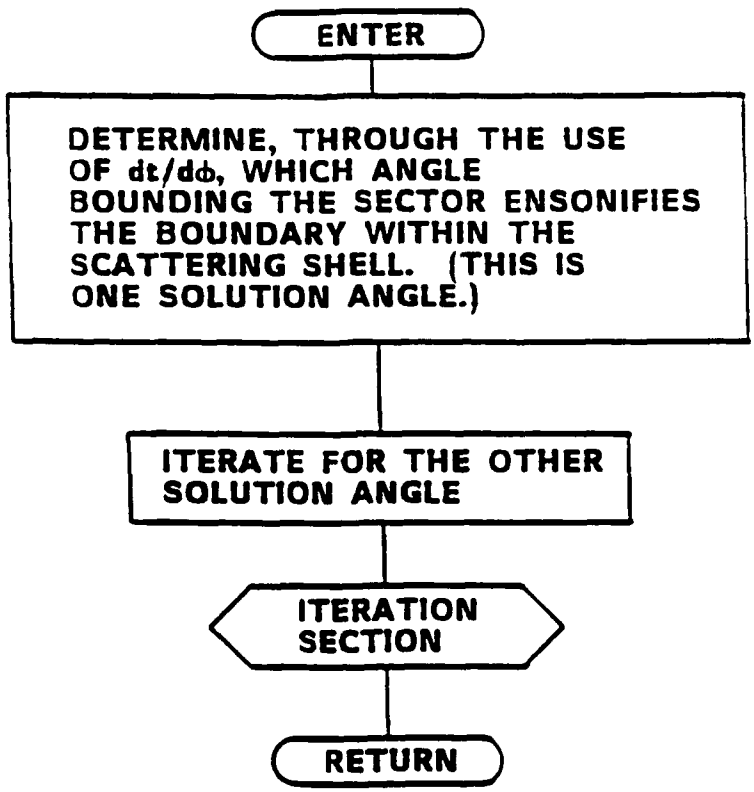
ENTER
DETERMINE, THROUGH THE USE OF dt/dϕ, WHICH ANGLE BOUNDING THE SECTOR ENSONIFIES THE BOUNDARY WITHIN THE SCATTERING SHELL. (THIS IS ONE SOLUTION ANGLE.)
ITERATE FOR THE OTHER SOLUTION ANGLE
ITERATION SECTION
RETURN

H.6. ITERATION SECTION

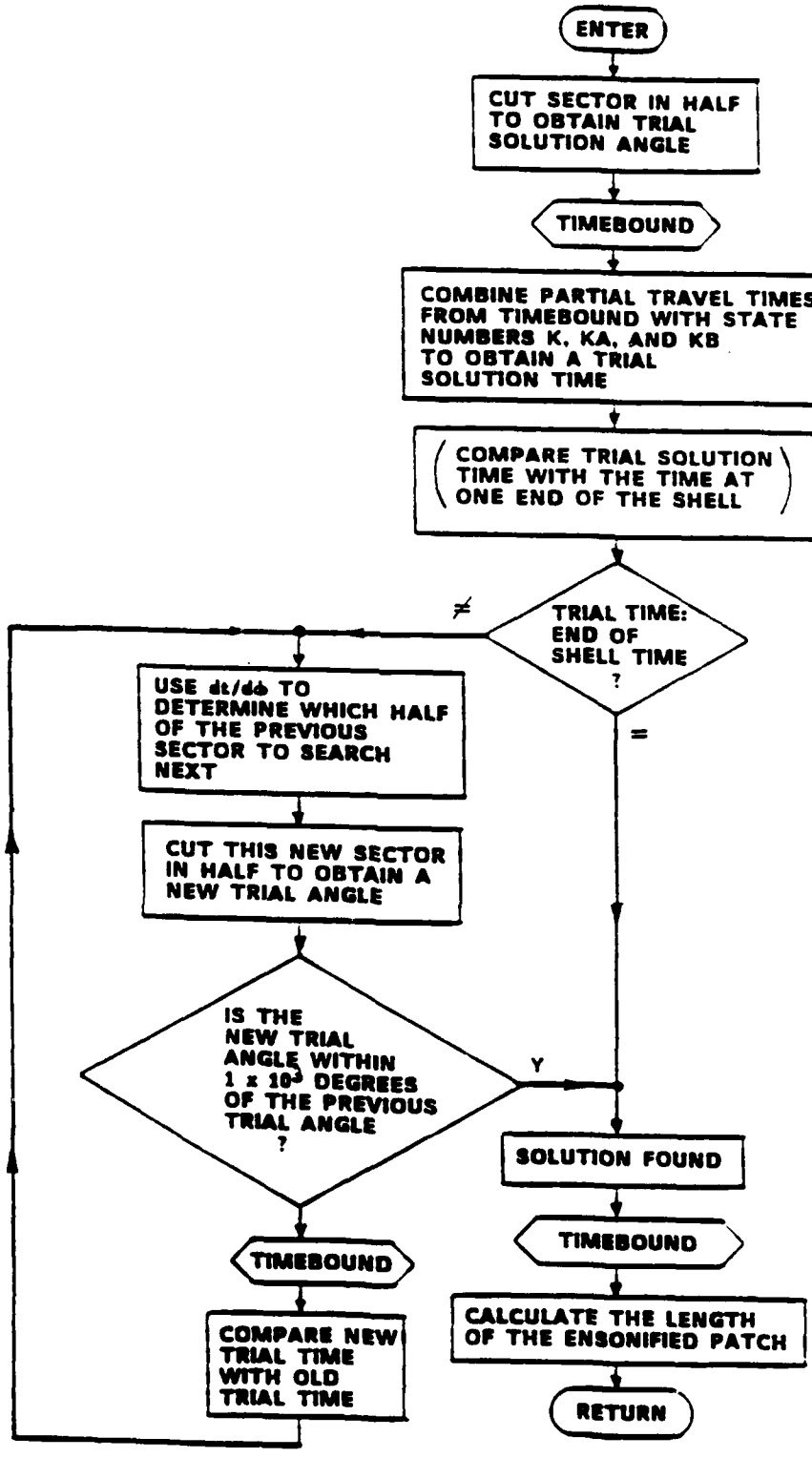

H.7. SOLBND

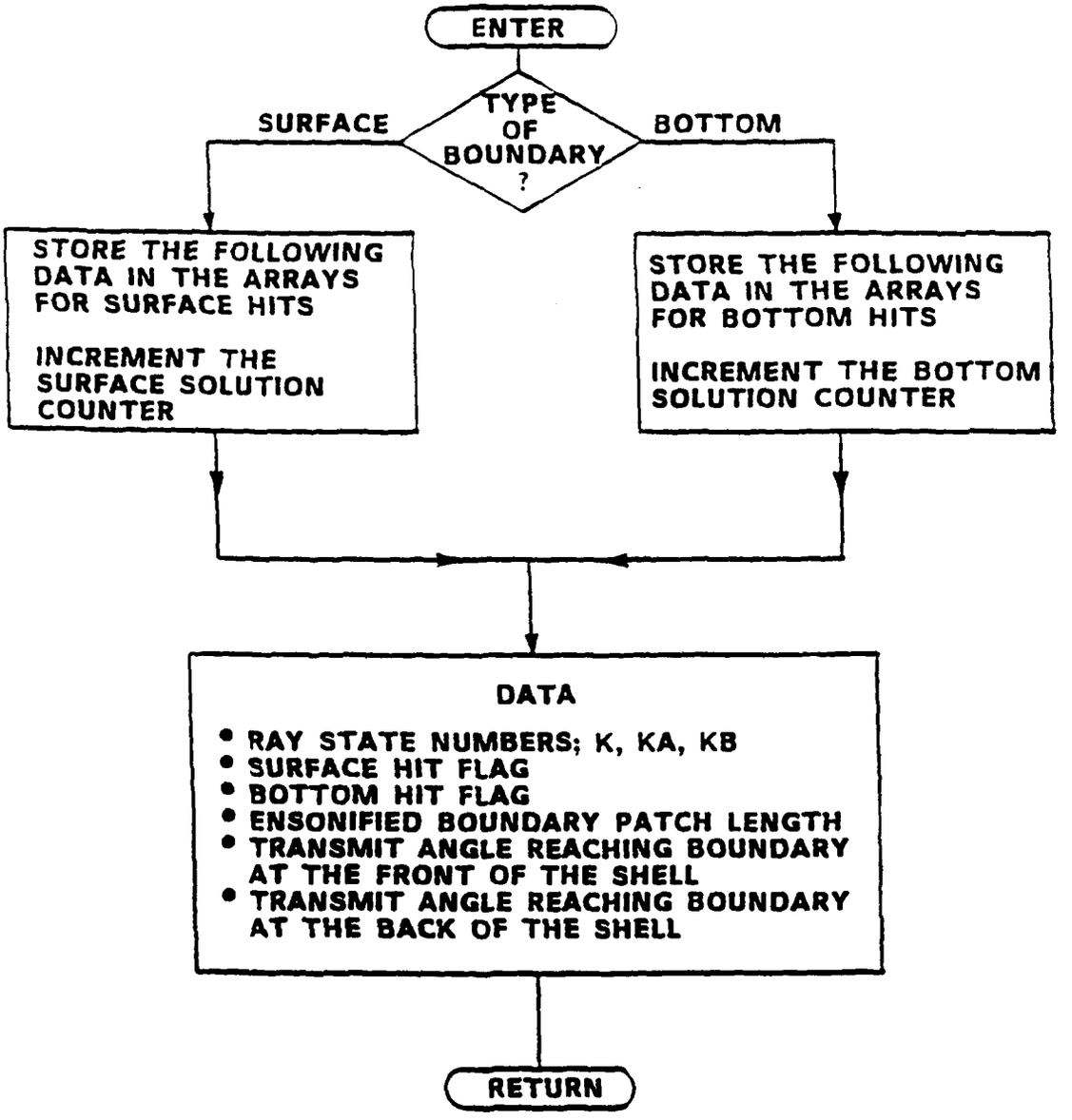
ENTER
TYPE OF BOUNDARY ?
SURFACE
BOTTOM
STORE THE FOLLOWING DATA IN THE ARRAYS FOR SURFACE HITS
INCREMENT THE SURFACE SOLUTION COUNTER
STORE THE FOLLOWING DATA IN THE ARRAYS FOR BOTTOM HITS
INCREMENT THE BOTTOM SOLUTION COUNTER
DATA
• RAY STATE NUMBERS; K, KA, KB
• SURFACE HIT FLAG
• BOTTOM HIT FLAG
• ENSONIFIED BOUNDARY PATCH LENGTH
• TRANSMIT ANGLE REACHING BOUNDARY AT THE FRONT OF THE SHELL
• TRANSMIT ANGLE REACHING BOUNDARY AT THE BACK OF THE SHELL
RETURN

H.8. VOLANGS

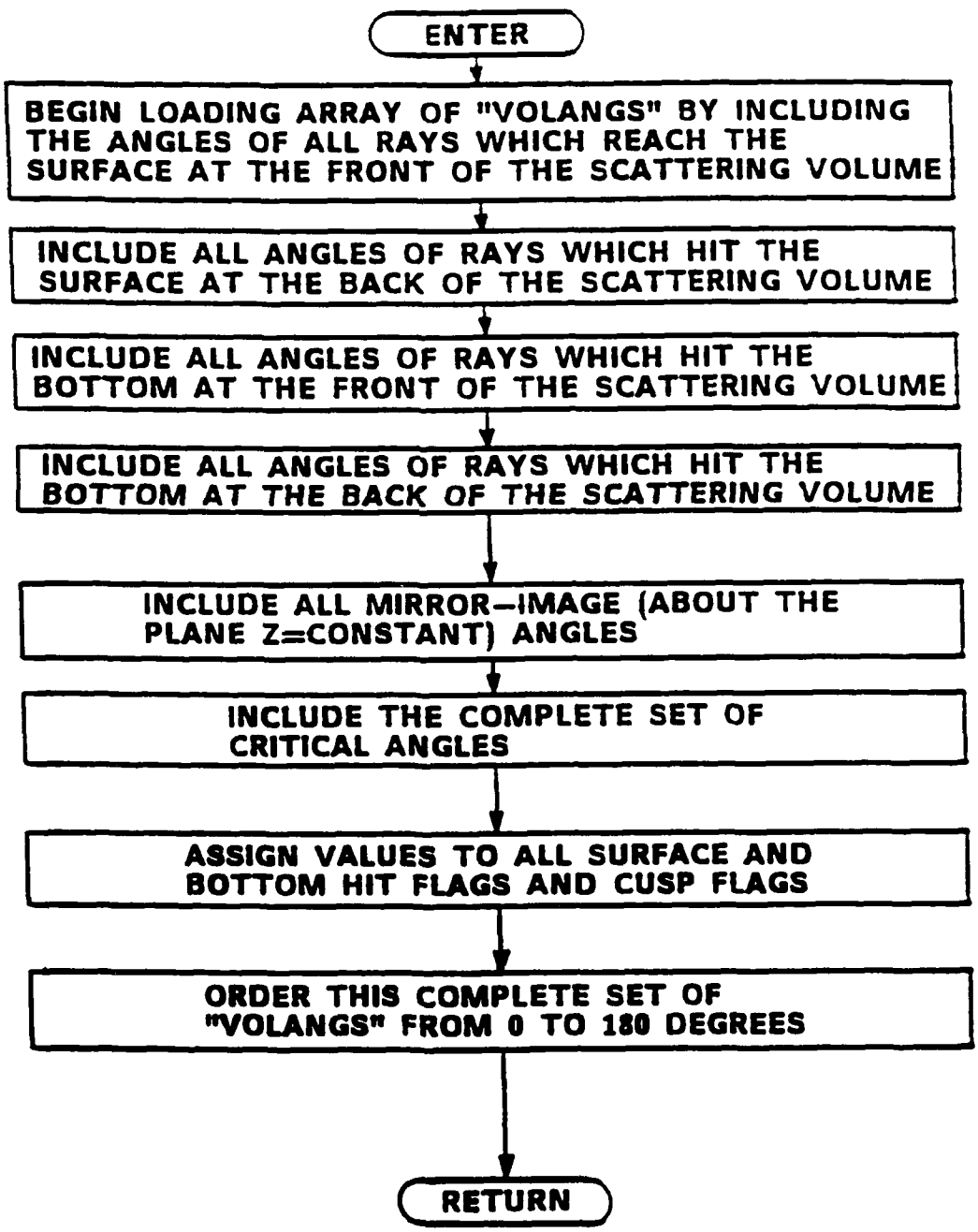
ENTER
BEGIN LOADING ARRAY OF "VOLANGS" BY INCLUDING THE ANGLES OF ALL RAYS WHICH REACH THE SURFACE AT THE FRONT OF THE SCATTERING VOLUME
INCLUDE ALL ANGLES OF RAYS WHICH HIT THE SURFACE AT THE BACK OF THE SCATTERING VOLUME
INCLUDE ALL ANGLES OF RAYS WHICH HIT THE BOTTOM AT THE FRONT OF THE SCATTERING VOLUME
INCLUDE ALL ANGLES OF RAYS WHICH HIT THE BOTTOM AT THE BACK OF THE SCATTERING VOLUME
INCLUDE ALL MIRROR-IMAGE (ABOUT THE PLANE Z=CONSTANT) ANGLES
INCLUDE THE COMPLETE SET OF CRITICAL ANGLES
ASSIGN VALUES TO ALL SURFACE AND BOTTOM HIT FLAGS AND CUSP FLAGS
ORDER THIS COMPLETE SET OF "VOLANGS" FROM 0 TO 180 DEGREES
RETURN

H.9. SURSEQ

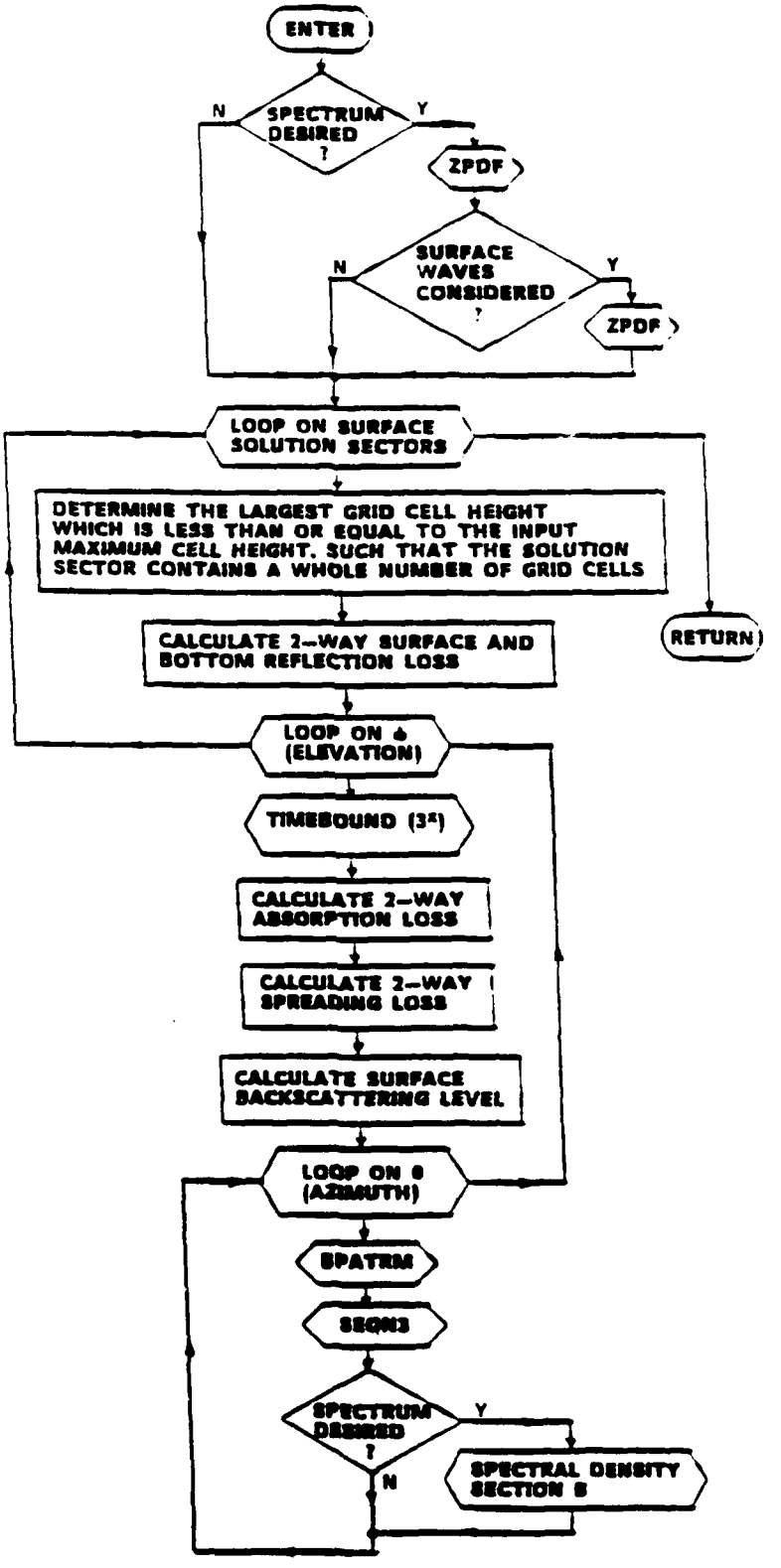
ENTER
SPECTRUM DESIRED ?
N
Y
ZPDF
SURFACE WAVES CONSIDERED ?
N
Y
ZPDF
LOOP ON SURFACE SOLUTION SECTORS
DETERMINE THE LARGEST GRID CELL HEIGHT WHICH IS LESS THAN OR EQUAL TO THE INPUT MAXIMUM CELL HEIGHT, SUCH THAT THE SOLUTION SECTOR CONTAINS A WHOLE NUMBER OF GRID CELLS
CALCULATE 2-WAY SURFACE AND BOTTOM REFLECTION LOSS
RETURN
LOOP ON φ (ELEVATION)
TIMEBOUND (3ˣ)
CALCULATE 2-WAY ABSORPTION LOSS
CALCULATE 2-WAY SPREADING LOSS
CALCULATE SURFACE BACKSCATTERING LEVEL
LOOP ON θ (AZIMUTH)
SPATRM
SEQN3
SPECTRUM DESIRED ?
Y
N
SPECTRAL DENSITY SECTION S

H.10. SPECTRAL DENSITY SECTION B

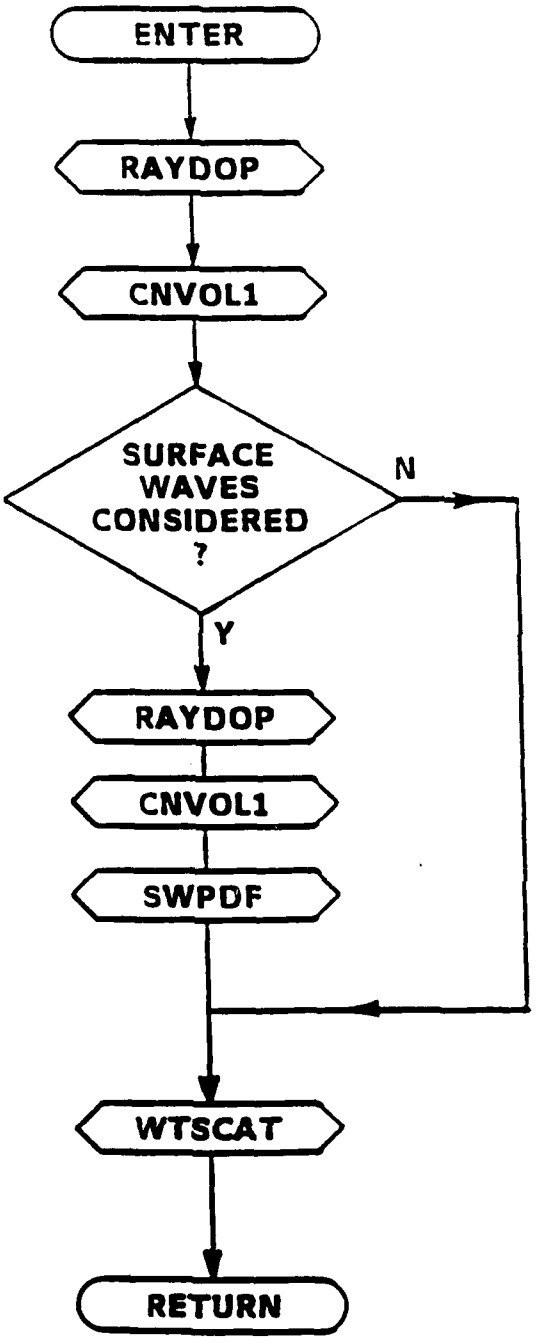

H.11. VOLSEQ

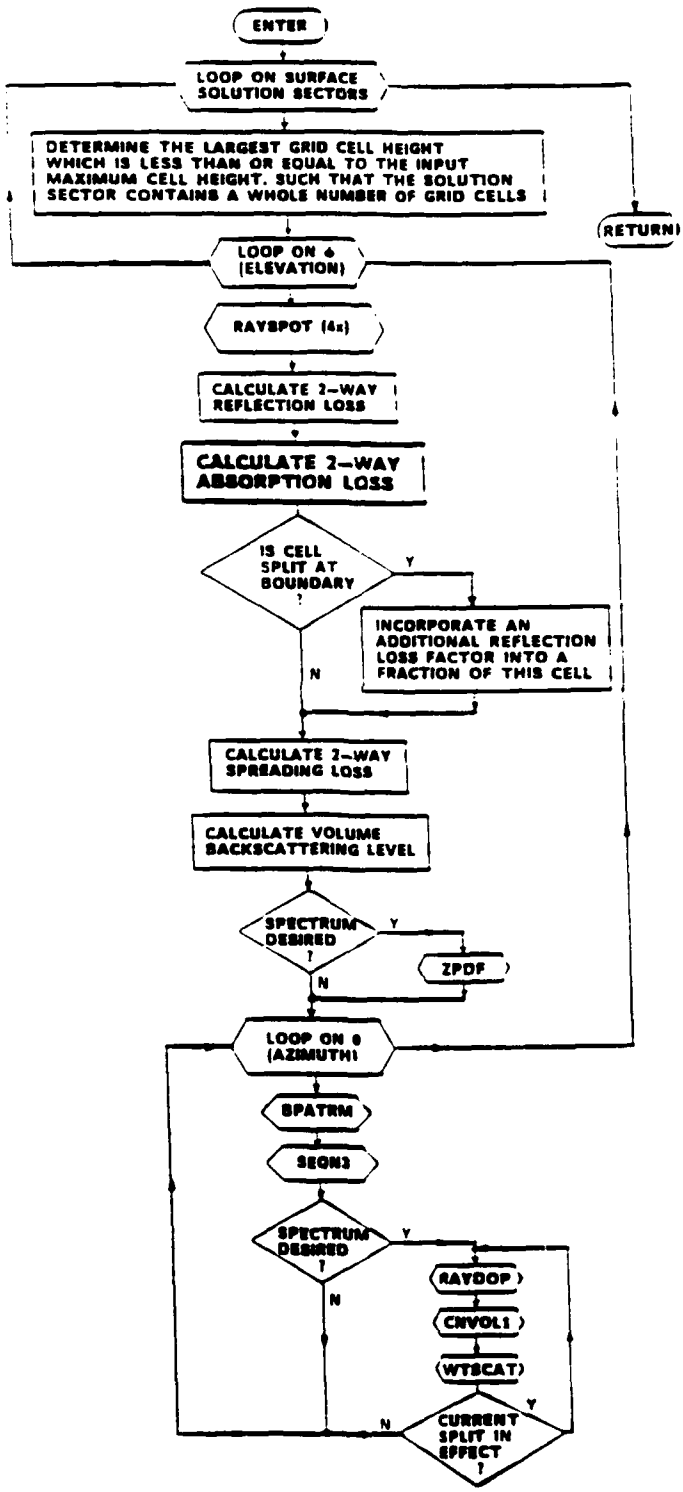
ENTER
LOOP ON SURFACE SOLUTION SECTORS
DETERMINE THE LARGEST GRID CELL HEIGHT WHICH IS LESS THAN OR EQUAL TO THE INPUT MAXIMUM CELL HEIGHT, SUCH THAT THE SOLUTION SECTOR CONTAINS A WHOLE NUMBER OF GRID CELLS
RETURN
LOOP ON φ (ELEVATION)
RAYSPOT (4π)
CALCULATE 2-WAY REFLECTION LOSS
CALCULATE 2-WAY ABSORPTION LOSS
IS CELL SPLIT AT BOUNDARY ?
Y
N
INCORPORATE AN ADDITIONAL REFLECTION LOSS FACTOR INTO A FRACTION OF THIS CELL
CALCULATE 2-WAY SPREADING LOSS
CALCULATE VOLUME BACKSCATTERING LEVEL
SPECTRUM DESIRED ?
Y
N
ZPDF
LOOP ON θ (AZIMUTH)
SPATRM
SEGN3
SPECTRUM DESIRED ?
Y
N
RAYDOP
CNVOL1
WTSCAT
CURRENT SPLIT IN EFFECT ?
Y
N

H.12. BOTSEQ

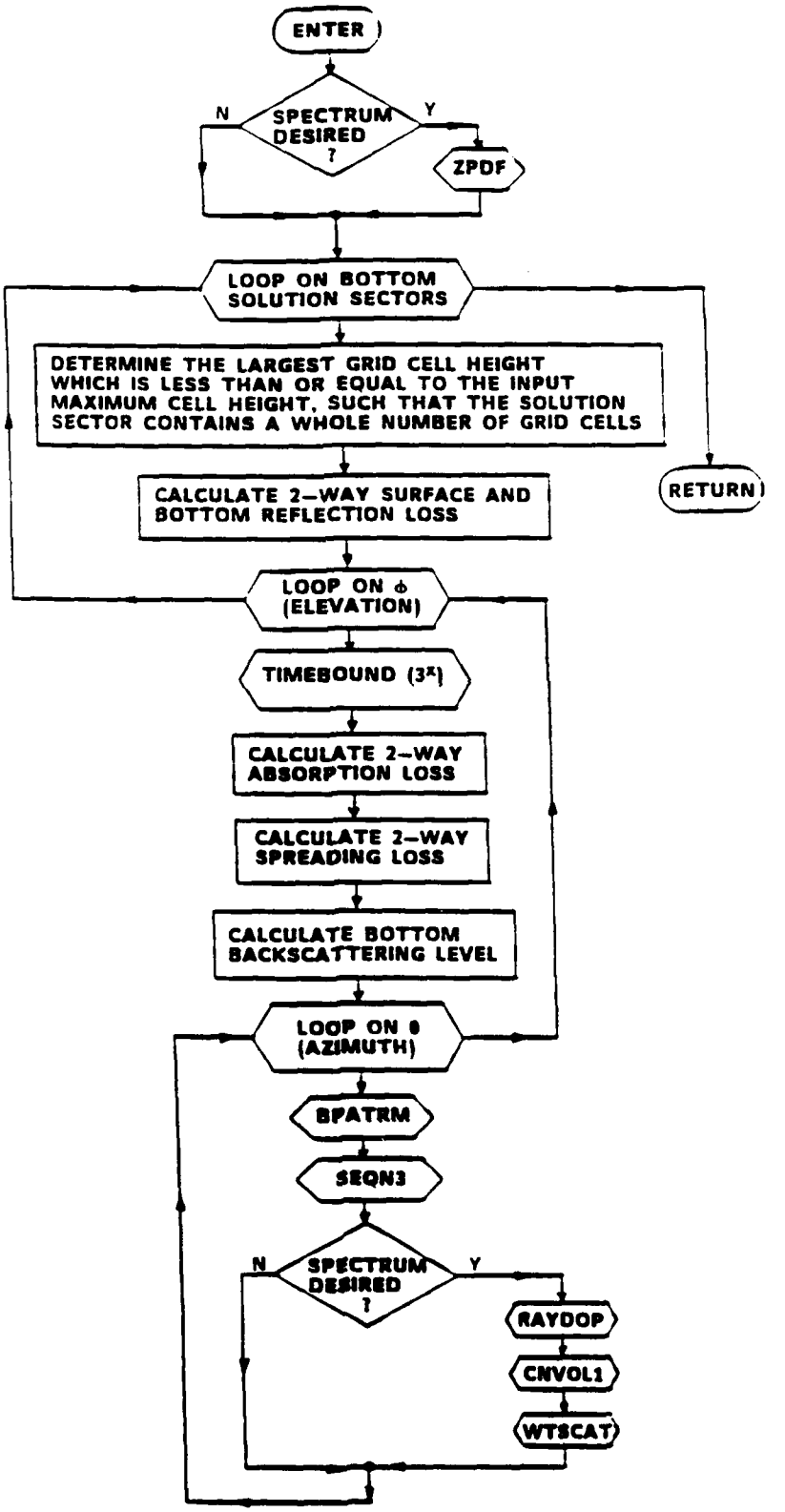
ENTER
SPECTRUM DESIRED ?
N
Y
ZPDF
LOOP ON BOTTOM SOLUTION SECTORS
DETERMINE THE LARGEST GRID CELL HEIGHT WHICH IS LESS THAN OR EQUAL TO THE INPUT MAXIMUM CELL HEIGHT, SUCH THAT THE SOLUTION SECTOR CONTAINS A WHOLE NUMBER OF GRID CELLS
CALCULATE 2-WAY SURFACE AND BOTTOM REFLECTION LOSS
RETURN
LOOP ON ϕ (ELEVATION)
TIMEBOUND (3^X)
CALCULATE 2-WAY ABSORPTION LOSS
CALCULATE 2-WAY SPREADING LOSS
CALCULATE BOTTOM BACKSCATTERING LEVEL
LOOP ON θ (AZIMUTH)
BPATRM
SEQN3
SPECTRUM DESIRED ?
N
Y
RAYDOP
CNVOL1
WTSCAT

H.13. RAYDOP

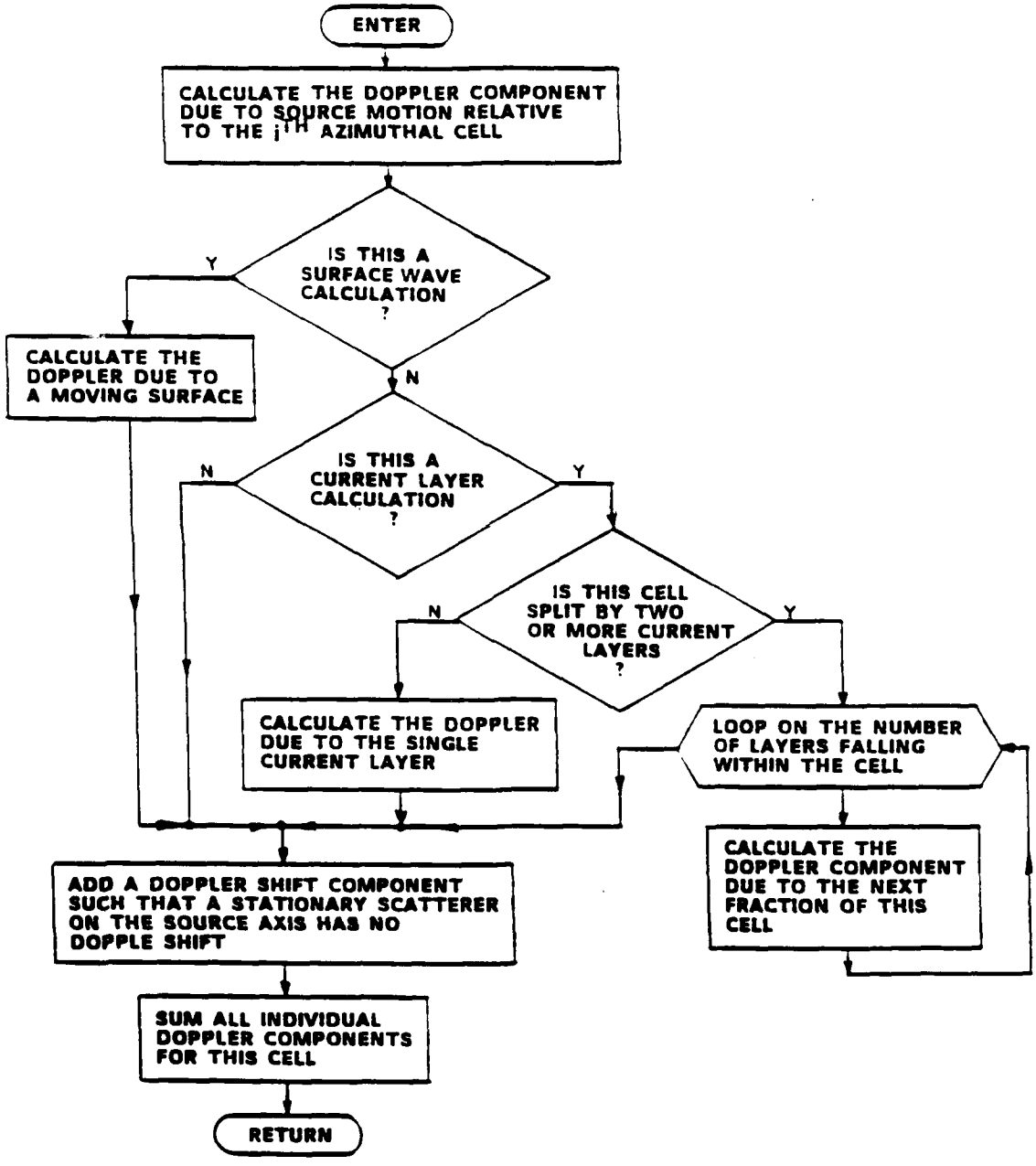
ENTER
CALCULATE THE DOPPLER COMPONENT DUE TO SOURCE MOTION RELATIVE TO THE i TH AZIMUTHAL CELL
IS THIS A SURFACE WAVE CALCULATION ?
Y
N
CALCULATE THE DOPPLER DUE TO A MOVING SURFACE
IS THIS A CURRENT LAYER CALCULATION ?
N
Y
IS THIS CELL SPLIT BY TWO OR MORE CURRENT LAYERS ?
N
Y
CALCULATE THE DOPPLER DUE TO THE SINGLE CURRENT LAYER
LOOP ON THE NUMBER OF LAYERS FALLING WITHIN THE CELL
CALCULATE THE DOPPLER COMPONENT DUE TO THE NEXT FRACTION OF THIS CELL
ADD A DOPPLER SHIFT COMPONENT SUCH THAT A STATIONARY SCATTERER ON THE SOURCE AXIS HAS NO DOPPLE SHIFT
SUM ALL INDIVIDUAL DOPPLER COMPONENTS FOR THIS CELL
RETURN

H.14. RAYSPOT

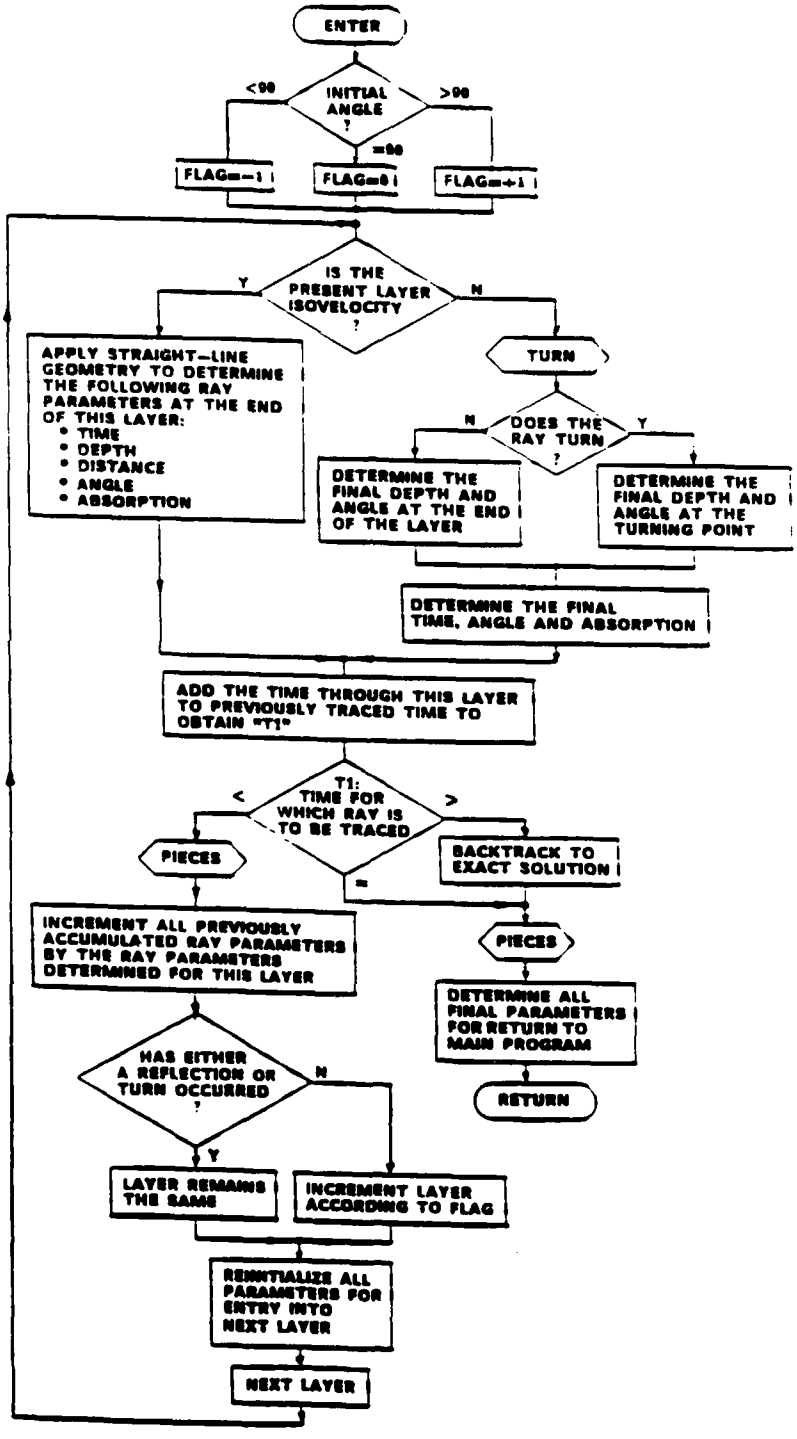
ENTER
INITIAL ANGLE ?
<90
=90
>90
FLAG=-1
FLAG=0
FLAG=+1
IS THE PRESENT LAYER ISOVELOCITY ?
Y
N
APPLY STRAIGHT-LINE GEOMETRY TO DETERMINE THE FOLLOWING RAY PARAMETERS AT THE END OF THIS LAYER:
• TIME
• DEPTH
• DISTANCE
• ANGLE
• ABSORPTION
TURN
DOES THE RAY TURN ?
N
Y
DETERMINE THE FINAL DEPTH AND ANGLE AT THE END OF THE LAYER
DETERMINE THE FINAL DEPTH AND ANGLE AT THE TURNING POINT
DETERMINE THE FINAL TIME, ANGLE AND ABSORPTION
ADD THE TIME THROUGH THIS LAYER TO PREVIOUSLY TRACED TIME TO OBTAIN "T1"
T1: TIME FOR WHICH RAY IS TO BE TRACED
<
=
>
PIECES
BACKTRACK TO EXACT SOLUTION
INCREMENT ALL PREVIOUSLY ACCUMULATED RAY PARAMETERS BY THE RAY PARAMETERS DETERMINED FOR THIS LAYER
PIECES
DETERMINE ALL FINAL PARAMETERS FOR RETURN TO MAIN PROGRAM
RETURN
HAS EITHER A REFLECTION OR TURN OCCURRED ?
N
Y
LAYER REMAINS THE SAME
INCREMENT LAYER ACCORDING TO FLAG
REINITIALIZE ALL PARAMETERS FOR ENTRY INTO NEXT LAYER
NEXT LAYER

H.15. TURN

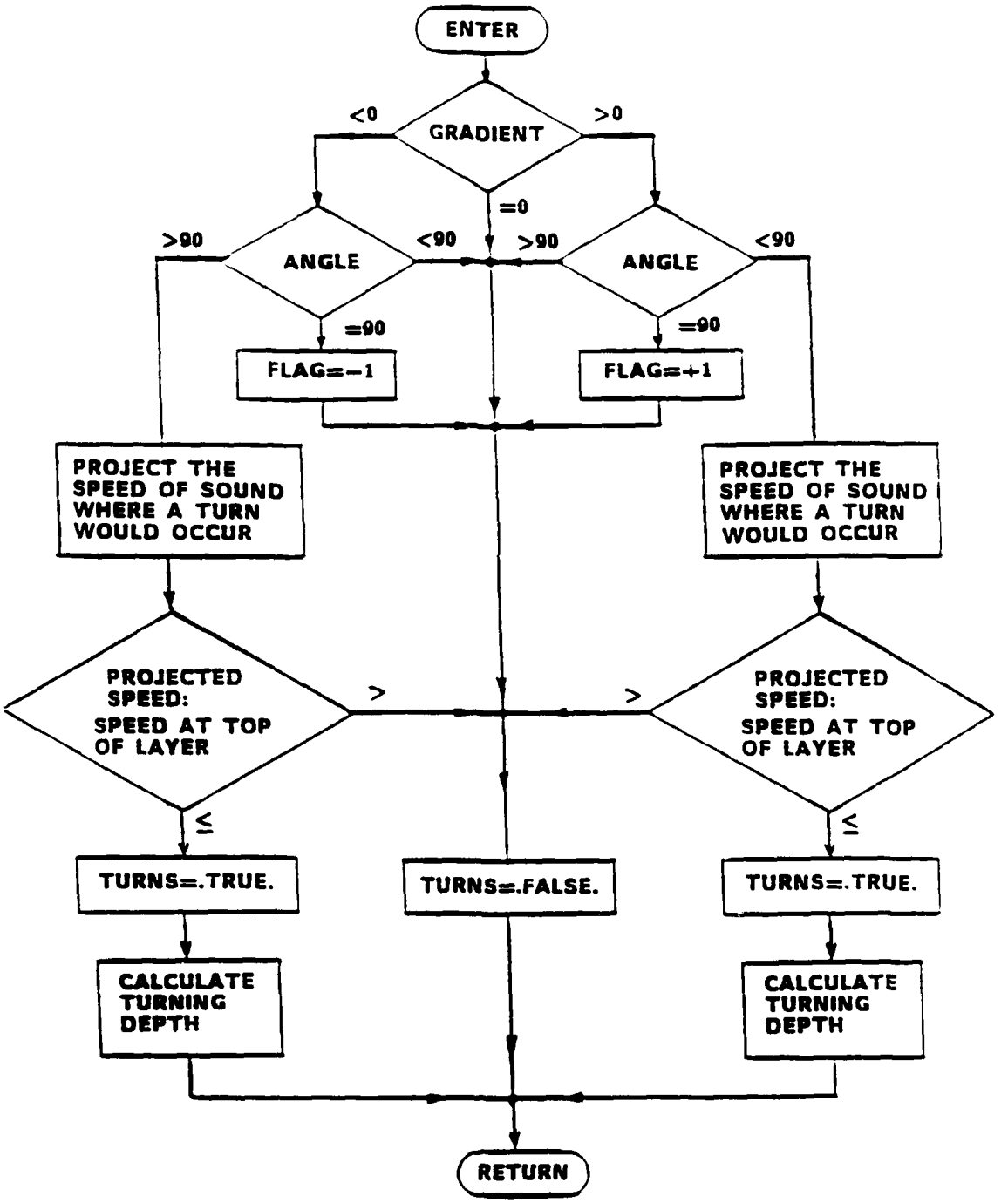
ENTER
GRADIENT
<0
>0
=0
ANGLE
>90
<90
=90
FLAG=-1
FLAG=+1
PROJECT THE SPEED OF SOUND WHERE A TURN WOULD OCCUR
PROJECTED SPEED:
SPEED AT TOP OF LAYER
>
≤
TURNS=.TRUE.
TURNS=.FALSE.
CALCULATE TURNING DEPTH
RETURN

H.16. PIECES

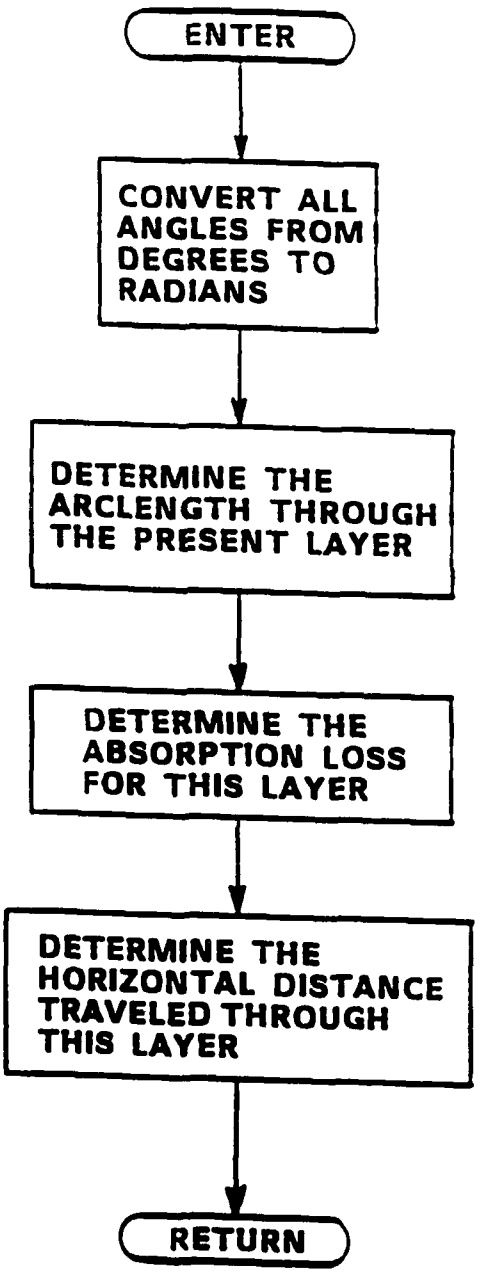
ENTER
CONVERT ALL ANGLES FROM DEGREES TO RADIANS
DETERMINE THE ARCLENGTH THROUGH THE PRESENT LAYER
DETERMINE THE ABSORPTION LOSS FOR THIS LAYER
DETERMINE THE HORIZONTAL DISTANCE TRAVELED THROUGH THIS LAYER
RETURN

REFERENCES

1. W. S. Hodgkiss, "An Oceanic Reverberation Model," *IEEE Journal of Oceanic Engineering*, volume OE-9 No. (April 1984).

2. C. S. Clay and H. Medwin, *Acoustical Oceanography*, Wiley (1977).

3. A. V. Oppenheim, *Applications of Digital Signal Processing*, Prentice Hall (1978).

4. H. L. Van Trees, *Detection, Estimation, and Modulation Theory part III*, Wiley (1971).

5. J. S. Bendat and A. G. Piersol, *Random Data, Analysis and Measurement Procedures*, Wiley (1986).

6. L.E. Kinsler, A. R. Frey, A. B. Coppens, and J. V. Sanders, *Fundamentals of Acoustics*, Wiley (1982).

7. A. D. Pierce, *Acoustics: An Introduction to its Physical Principles and Applications*, McGraw-Hill (1981).

8. C. B. Officer, *The Theory of Sound Transmission*, McGraw-Hill (1958).

9. R. J. Urick, *Principles of Underwater Sound*, McGraw-Hill (1983).

10. C. E. Tschiegg and E. E. Hays, "Transistorized Velocimeter for Measuring the Speed of Sound in the Sea," *Journal of the Acoustical Society of America* 31 pp. 1038-1039 (1959).

11. W. D. Wilson,"Equation for the Speed of Sound in Sea Water," *Journal of the Acoustical Society of America* 32 p. 1357 (1960).

12. W. D. Wilson, "Speed of Sound as a Function of Temperature, Pressure, and Salinity," *Journal of the Acoustical Society of America*, 32, p. 641-644 (1960).

13. W. D. Wilson, "Extrapolation for the Speed of Sound in Sea Water," *Journal of the Acoustical Society of America* 34, p. 866 (1962).

14. M. W. Roeckel, Personal Communication (1987).

15. G. Neumann and W. S. Pierson, Jr., *Principles of Physical Oceanography*, Prentice Hall (1966).

16. L. M. Lyamshev, "A Question in Connection with the Principle of Reciprocity in Acoustics," *Soviet Physics Doklady*, pp. 406-409 (January 18, 1959).

17. W. P. Mason, *Physical Acoustics, volume II, part A*, Academic Press, New York, NY (1965).

18. F. H. Fisher and V. P. Simmons, "Sound Absorption in Sea Water," *Journal of the Acoustical Society of America* 62, pp. 558-564 (1977).

19. R. J. Urick and R. M. Hoover, "Backscattering of sound from the Sea Surface: Its Measurements, Causes, and Applications to the Prediction of Reverberation Levels," *Journal of the Acoustical Society of America* 28, pp. 1038-1042 (1956).

20. G. R. Garrison, S. R. Murphy, and D. S. Potter, "Measurements of the Backscattering of Underwater Sound from the Sea Surface," *Journal of the Acoustical Society of America* 32, pp. 104-111 (1960).

21. Albers, *Underwater Acoustics Handbook II*, The Pennsylvania State University Press (1965).

22. K. V. MacKenzie, "Reflection of Sound from Coastal Bottoms," *Journal of the Acoustical Society of America* 32, pp. 100-104 (1960).

23. R. J. Urick, "The Backscattering of Sound from a Harbor Bottom," *Journal of the Acoustical Society of America* 26, pp. 231-235 (1954).

24. C. M. McKinney and C. D. Anderson, "Measurement of Backscattering of Sound from the Ocean Bottom," *Journal of the Acoustical Society of America* 36, pp. 158-163 (1963).

25. E. L. Hamilton, G. Shumway, H. W. Menard, and C. J. Shipek, "Acoustic and Other Physical Properties of Shallow Water Sediments off San Diego," *Journal of the Acoustical Society of America* 28, pp. 1-15 (1956).

26. W. S. Hodgkiss, "Reverberation Model: I. Technical Description and Users' Guide," University of California, San Diego, Marine Physical Laboratory of the Scripps Institution of Oceanography, Technical Memorandum 319 (July 31, 1980).

27. W. S. Hodgkiss, "Reverberation Model: II. Software Description," University of California, San Diego, Marine Physical Laboratory of the Scripps Institution of Oceanography, Technical Memorandum 320 (July 31, 1980).